Università di Catania

Department of Biomedical and Biotechnological Sciences Ph.D. in Biotechnology

Curriculum in Biomedical and preclinical sciences

XXXIV Cycle

DAMIANO CALCAGNO

Ubiquitin Proteasome system modulation, a novel strategy to control the amyloidogenic pathway involved in Alzheimer's disease.

PhD Thesis

Tutor: *Prof. Vincenzo G. Nicoletti*

Coordinator: *Prof. Vito De Pinto*

ACADEMIC YEARS 2018/2021

SUMMARY

1. ABSTRACT

Alzheimer's disease (AD), a diffuse form of dementia among the elderly, represents an increasing worldwide problem with no effective solution until today. The etiology of AD is considered complex, while many studies claim that metabolic and vascular dysfunctions are implicated in its progression. One of the prominent features of AD is the extracellular accumulation of amyloid beta (Aβ) peptide, the major protein component of senile plaques in AD brains: the misfolding and aggregation of Aβ exerts cytotoxic effect leading to progressive memory and cognition impairment in AD patients. For this reason, Aβ clearance systems such as the Ubiquitin Proteasome System (UPS), autophagy/lysosome pathway, and metalloproteases are crucial for maintaining physiological status.

This research plan aimed to study the molecular mechanisms that are responsible for the pathological development of AD, focusing attention on the pathways that drive the UPS system. This cell machinery is the main control of cellular proteome homeostasis; thereby its failure has been strongly associated with all amyloidogenic-based neurodegenerative diseases where specific aggregation-prone proteins typically accumulate.

In our experiments, Aβ has shown to have a relatively significant affinity for Ub, forming 1:1 protein-protein complexes; moreover, water-soluble fragment Aβ 1–16 significantly inhibits Ub chain growth in tube tests. ELISA experiments confirmed non-covalent interactions between Ub and the Aβ peptide in the presence of whole-cell extracts from differentiated SH-SY5Y neuroblastoma cells.

In the present study, the regulation of 20S Proteasome activity was evaluated in neuronal cell cultures (SH-S5Y5) throughout a new real-time procedure based on fluorescent measurements of the chymotrypsin-like protease activity. In this way, we screened some proteasome modulators to characterize its molecular basis, identify new potential drugs to be applied in recovering the altered Aβ homeostasis and hence develop innovative therapeutic strategies against AD and related neurodegenerative disease.

2. KEYWORDS AND ABBREVIATIONS

Keywords: Alzheimer′s disease; proteasome; proteostasis; redox unbalance; amyloidogenesis; 20S inhibitors; proteasome activators; protein turnover; neurodegenerative diseases; cancer; *Brassica Oleracea*, polyubiquitin;

List of abbreviations:

AD	Alzheimer Disease
ATP	Adenosine Triphosphate
Aβ	Amyloid Beta Peptide
BTZ	Bortezomib
CFZ	Carfilzomib
C-L	Caspase-like
CPZ	Chlorpromazine
CT-L	Chymotrypsin-like
ELISA	Enzyme-linked immunosorbent assay
GLS	Glucosinolates
IDE	Insulin Degrading Enzyme
MTT	3-(4,5-dimethylthiazol-2-yl)-2,5-diphenyltetrazolium bromide
NFTs	Neurofibrillary tangles
PD	Parkinson Disease
PI	Proteasome Inhibitor
R110	Rhodamine 110 fluorochrome
SDS	Sodium dodecyl sulfate
SPR	Surface Plasmon Resonance
T-L	Trypsin-like
UB	Ubiquitin
UPS	Ubiquitin Proteasome System

3. AFFILIATIONS

Laboratory of Neurobiology, Department of Biomedical and Biotechnological Science (BIOMETEC), University of Catania, Via S. Sofia, 89, 95123 Catania, Italy.

Collaborations:

Institute of Biostructures and Bioimages (National Research Council) IBB-CNR, Catania, Italy.

Prof. Ferdinando Branca e Dott.ssa Maria Concetta Di Bella, Department of Agriculture, Food and Environment, University of Catania, Catania, 95123, Italy;

Prof. Salvatore Guccione, Department of Pharmaceutical Sciences, University of Catania, Catania, Italy

Prof. Giuseppe Lanza, Department of Surgery and Medical-Surgery Specialties, University of Catania, Via Santa Sofia 78, 95123 Catania, Italy

Prof. Giuseppe Grasso,
Dipartimento di Scienze Chimiche, Università di Catania, V.le Andrea Doria 6, 95125 Catania, Italy; Italy;

4. INTRODUCTION

4.1. Alzheimer's Disease Scenario

Alzheimer's disease (AD) is one of the most diffused neurodegenerative pathologies, in which patients are affected by memory loss, cognitive impairment, mood and behavior changes, and difficulties in daily activities. Alois Alzheimer discovered AD in 1901 when he described the presence of neurofibrillary tangles (NFTs) and amyloid fibrils in a 51 years old woman's brain, affected by senile dementia and presenting all previously mentioned symptoms.

Senile plaques were called improperly "amyloids" because fibrils resembled the shape of starch when the crude iodine-staining technique is used (Grasso et al., 2017). These plaques are constituted for the most part by amyloid beta peptide (Aβ) aggregates, in particular, the isoform $A\beta_{1-42}$ (more toxic) and the isoform $A\beta_{1-40}$, both characterized by an N-terminus hydrophilic portion (1-28) and a C-terminus hydrophobic moiety (29-40/42) (Holtzman et al., 2011). Amyloid accumulation and aggregation are not specific to AD but are also present in several other diffused neuropathologies like Parkinson's disease (PD), Huntington's disease, and amyotrophic lateral sclerosis (ALS).

In all the above-mentioned diseases, the accumulation and the consequent aggregation of specific peptides cause progressive impairment of the central nervous system that leads to death. Therefore, it is clear that the imbalance in the clearance of these peptides gives rise to an altered cellular proteostasis, assuming a central role in neuropathological development (Balch et al., 2008). The ubiquitin-proteasome system (UPS) and the autophagy/lysosome pathway play a primary role in protein clearance: in particular, the former is indicated for soluble misfolded proteins, while the latter is capable to digest proteinaceous aggregates (Ciechanover et al., 2015). Another protective factor against peptide aggregation is the action of intracellular molecular chaperons that help misfolded proteins to refold in the native conformation (Hartl et al. 2011) and the activity of metalloproteases in the extracellular matrix (Malgieri & Grasso, 2014).

AD is a sporadic event for most cases, where age is the major risk factor, whereas a little portion of affected people is the result of genetic disorders. Several exogenous factors could increase the AD incidence, including traumatic brain damage, obesity, smoking, diabetes, cholesterol and lead, mercury, or aluminum exposure (Faller et al., 2013). Among genetic risk

factors, amyloid precursor protein (APP) and presenilin gene mutations (Jack et al., 2010) [**Errore. Il segnalibro non è definito.**] have to be considered. Presenilin is a component of g-secretase, responsible for the "not-amyloidogenic" cleavage of APP; for this reason, when presenilin is mutated, an overproduction of amyloid beta peptides occurs. Moreover, the homozygotic presence of the isoform ApoE4 of cholesterol transporter apolipoprotein (ApoE), increases the incidence of sporadic AD by 15 times (La Ferla et al., 2007).

Several trials for possible pharmacological therapies have been done during these years, but poor or no results have been achieved; current treatments are mainly symptoms relieving, and after one year at best, they become ineffective. The most diffused drugs for AD treatments to improve cognitive symptoms are based on *N*-methyl-*D*-aspartate (NMDA) receptor antagonists (*memantine*) or acetylcholinesterase inhibitors such as *donepezil* (Faller et al., 2013).

AD affects more than 30 million people overall and this number grows very fast day-by-day (100 million people affected expected in 2050). The healthcare system, consequently, is going under pressure and scientific research is always very active to find out an alternative and winning strategy to defeat this pathology (Faller et al., 2013).

AD brains present specific features, such as loss of neurons and synapses in the cerebral cortex and in particular in the hippocampus, responsible for memory and cognition. This brings patients to a condition of senile dementia that excludes them progressively from the outer world. Other hallmarks are oxidized biomolecules due to increased oxidative stress, impaired energy metabolism and glucose uptake, altered levels of metals like zinc, copper, iron, and calcium, high presence of homocysteine, and abnormal expression of metallothioneins (Faller et al., 2013).

Two precise peculiarities in AD pathophysiology are extracellular amyloid plaques and neurofibrillary tangles consisting of twisted strands of hyper-phosphorylated τ-proteins that in normal conditions play an active role in the structural integrity of microtubules, whereas in AD lose their original function causing neurodegeneration (Jack et al., 2010).

4.2 Alzheimer's Disease Pathogenesis

Deposits of amyloid plaques are not a unique hallmark of AD brains. Indeed, amyloid deposits are found in 20-40% of unaffected elderly people's post-mortem brains. This fact indicates that the "amyloid cascade hypothesis" is not satisfactory to give a complete explanation of the AD pathological development (Wilquet & De Strooper, 2004). For this reason, during the last decade, besides this hypothesis, other theories have emerged such as the "metal ion hypothesis" and the "oxidative stress hypothesis"; all these theories are not in competition to one another but most probably they all contribute toward a more comprehensive explanation of AD.

The former hypothesis highlights the role of Amyloid beta peptides that aggregate and accumulate in neuronal tissue resulting in amyloid plaques deposit. The plaques are constituted of insoluble fibrils that are the final product of a pathway in which Aβ monomers begin to self-assemble to form oligomers, nuclei, protofibrils, protofilaments, and finally mature fibrils (Smith et al., 2007).

Aβ derives from APP, a type 1 transmembrane protein ubiquitously expressed and located both in outer cellular membranes and in organelles membranes such as mitochondria (La Ferla et al., 2007). Even if the main biological function of APP has not been yet identified, it exerts several different potential biochemical activities including regulation of intracellular calcium, cell growth, cell adhesion, axonal transport of vesicles, and metal ion homeostasis (Smith et al., 2007). APP can be cleaved in two possible ways, the so-called amyloidogenic and non-amyloidogenic ones. The latter is carried out by a group of proteases named α-secretases. These peptidases are mainly membrane zinc proteases and belong to the ADAM family (a disintegrin and metalloprotease family). When they cleave APP, sAPPα, a non-toxic peptide released outside the cell is produced (Wilquet & De Strooper, 2004; Nunan & Small, 2000; Seals & Courtneidge, 2003). On the contrary, if the enzyme involved in the APP cleavage is the β-secretase, and, in particular, the aspartyl protease BACE1 (β–site APP cleaving enzyme1), amyloidogenic peptides are produced (Sinha et al., 1999; Vassar et al.,1999). Indeed, after BACE1, another enzyme complex, the γ-secretase, cleaves the initial product leading to the formation of the two variants of Aβ, $A\beta_{1\text{-}40}$ and $A\beta_{1\text{–}42}$, respectively with 40 and 42 amino acid residues (Lovell, 2009).

In healthy brains, Aβ biosynthesis and clearance are balanced to maintain a safe amount of protein and to prevent amyloid aggregation. Several degradation pathways, besides the

generic proteostatic system (UPS, autophagy/lysosome pathway, chaperons, metalloproteases), also exist. One of the most important proteases, able to degrade Aβ monomers and oligomers, is neprilysin (Kanemitsu et al., 2003); other proteases are insulin degrading enzyme (IDE), angiotensin converting enzyme, matrix metalloprotease-2 (MMP-2), and matrix metalloprotease-9 (MMP-9) (Yin et al., 2006).

Aβ distribution in the human body is not homogeneous: in the soluble fraction, e.g. in the cerebrospinal fluid (CSF) the $A\beta_{1-42}/A\beta_{1-40}$ ratio is about 1/9, while in the amyloid plaques this ratio can reach about 1/2, indicating a greater propensity of $A\beta_{1-42}$ to aggregate (Kuperstein et al., 2010). For this reason, $A\beta_{1-42}$ is considered more toxic than $A\beta_{1-40}$, probably due to the two additional hydrophobic amino acids (Yoshiike et al., 2001).

The toxicity is also given by the aggregation states of the peptides, indeed oligomers are considered the toxic species, whereas the extracellular deposits are not directly toxic (Haas & Selkoe, 2007). Many experimental pieces of evidence support this theory: for example, oligomers may damage directly neurons and lead to cellular death (Carter & Lippa, 2001); they may impair electrochemical signaling (Walsh et al., 2002) through the formation of small membrane channels that disrupt the ion gradient, e.g. Ca^{2+} (Demuro et al., 2005).

Aβ oligomers also accumulate into mitochondria impairing the respiratory chain and bringing oxidative stress and neuronal death (Faller et al., 2013); furthermore, it is reported that oligomers, but not monomers, inhibit proteasome *in vitro* (Tseng et al., 2008). Aβ monomer is a highly flexible disordered structure that, in aqueous buffered solutions, assumes a random coil conformation (Hilbich et al., 1991), whereas in a hydrophobic environment (like an organic solvent, a detergent, or in the phospholipid bilayer) shows a high content of α-helicity (Coles et al., 1998). During aggregation, Aβ reorganizes itself in β-strand fibril structures (parallel and antiparallel) where the backbone N-H of one strand and the C=O of the neighbor strand form a hydrogen bonding network or collapse in amorphous aggregates (Crescenzi et al., 2002).

Amyloid aggregation is a complex and dynamic process influenced by thermodynamic and kinetic factors; furthermore, another pivotal factor is the critical concentration (C_c), that is the minimal monomeric Aβ concentration at equilibrium with amyloids that lead to fibrils formation (Smith et al., 2007). The critical concentration for $A\beta_{1-40}$, in phosphate buffered saline (PBS) at 37 °C, varies between 0.7 μM and 1 μM (O'Nuallain et al., 2005); this means that at any lower peptide concentration than C_c no aggregation is observed. In addition, amyloidogenicity depends on environmental conditions such as solvent nature (Shen & Murphy, 1995), ionic strength (Campos-Ramirez et al., 2017), temperature (Gursky &

Aleshkov, 2000) and pH: amyloid fibrils maturation becomes faster as the ionic strength of the solution increases; furthermore high temperature and low pH values determine higher aggregation rates (Su & Chang, 2001).

4.3 Ubiquitin Proteasome system involvement in diseases

4.3.1 Ubiquitin Proteasome system overview

Ubiquitin Proteasome System (UPS) is one of the most relevant proteostatic control apparatus in eukaryotic cells, permitting a fine regulation of protein turnover and maintaining a physiological status in biochemical processes (G.R. Tundo et al., 2020). As a matter of fact, through its protein degrading ability it is implied in several biological activities, namely: 1) cell cycle control; 2) cell death programming; 3) nucleic acids repair; 4) neural network development, 5) environmental stress response; 6) phlogosis induction; 7) immune regulation (Glickman & Ciechanover, 2002). Due to its importance, when UPS is impaired or dysregulated, there is a high probability to develop severe neuro-degenerative disorders or initiating tumorigenesis (G.R. Tundo et al., 2020).

The UPS is a multifactorial complex devoted to protein degradation through specific enzymatic reactions. At first, ubiquitin, a 76-aminoacid signal polypeptide, is covalently attached to a target protein by a process called ubiquitination; then 26S Proteasome, a 2500kDa enzymatic machinery, recognizes and unfold tagged substrates thanks to its regulatory particle (19S) while the catalytic moiety, the core particle (20S), collects and hydrolyzes the polypeptide via different proteasic activities. In detail, the UPS action starts with ubiquitination following these organized steps: 1) ATP-dependent formation of a high energy thiol-ester bond between a ubiquitin-activating enzyme (E1) and ubiquitin; 2) ubiquitin transfer via a trans-esterification reaction to a ubiquitin-conjugating enzyme (E2); 3) substrate specific mono-ubiquitination or poly-ubiquitination (usually 4 UB molecules) by a ubiquitin-ligase (E3) (Ciechanover, 2013).

Next, peculiar subunits of 19S recognize ubiquitinated proteins, unfold them through an ATP-driven process together opening the 20S channel, remove poly-ubiquitin via de-ubiquitinase (DUB) activity and finally translocate the resulting unfolded chain to the 20S proteasome core particle where it is degraded to amino-acids or small peptides (Collins & Goldberg, 2017) (***Figure 1, Panel A***).

Nevertheless, a poly-ubiquitin tag is not the only signal to initiate a substrate degradation by the proteasome: mono-ubiquitinated or ubiquitin-free unfolded proteins are addressed to 20S proteolytic chamber as well, indicating other molecular triggers, probably based on a specific primary sequence or a peculiar conformational element (Kudriaeva & Belogurov, 2019).

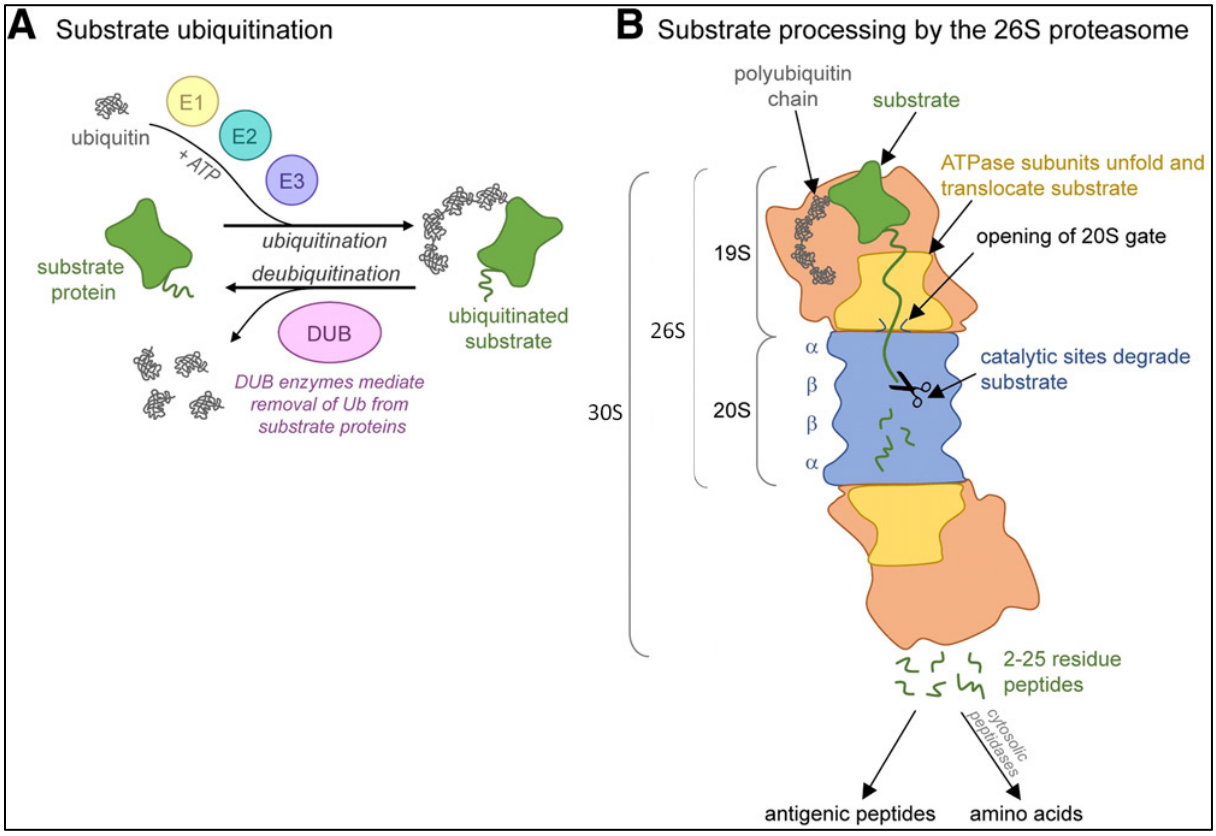

Figure 1. The ubiquitin proteasome system (UPS) pathway: (A) Ubiquitin conjugation system with tagging of substrates. (B) Poly-ubiquitinated substrates processing by the 26S proteasome with the release of peptides and aminoacids. *(*Figure reproduced and modified from *Thibaudeau & Smith, 2019)*

Under redox dyshomeostasis, 26S proteasome disassembles in 19S and 20S free moieties due to specific cysteine thiols oxidation (Martín Hugo et al., 2018); moreover, this oxidative environment temporary impairs the ubiquitinating activity of E1, E2, and E3 (Grune et al., 2011); there is, also, a higher cellular concentration of oxidized or misfolded proteins exposing hydrophobic residues: all these conditions favor a ubiquitin-independent degradation by the uncapped core particle which can collect and hydrolyze substrates with no involvement of the regulatory particles (G.R. Tundo et al., 2020).

This degradation fashion characterizes other peptides with high hydrophobic disordered portions, i.e. α-synuclein, tau protein, and amyloid-β peptide, exclusively when they are in monomeric form (Xiaobei Zhao and Jerry Yang, 2010).

4.3.2 Proteasome structure and arrangement

As described above, 26S proteasome is a complex multifactorial system made of several subunits able to maintain protein homeostasis through a well-arranged series of enzymatic reactions. The holoenzyme is denominated 26S when it is constituted by only one regulatory particle and one core particle, otherwise, it is described as the 30S if two regulatory particles and one core particle are assembled (Marshall & Viestra, 2019) (***Figure 1, Panel B***).

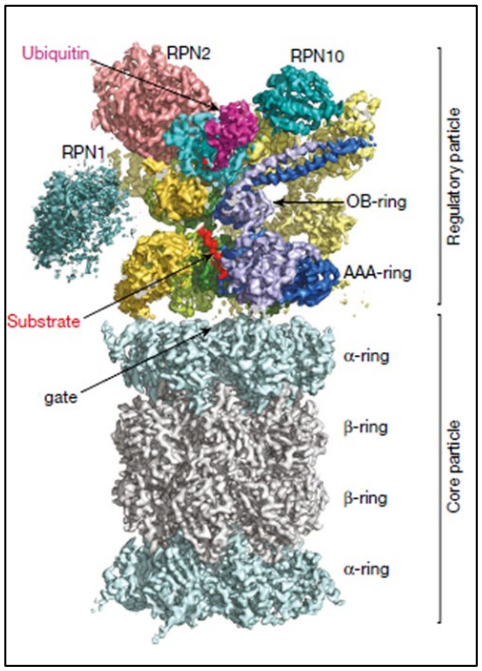

Figure 2. Cryo-EM density map of substrate-bound human 26S proteasome: in the upper part is located the 19S particle or regulatory particle forming the lid or cap; in the lower side, the 20S core particle is depicted. (Figure reproduced and modified from *Dong et al., 2018*)

The 19S regulatory particle (***Figure 2***) forms the so-called "cap" because it sterically occludes the 20S channel and actively regulates its opening via an ATP-dependent series of events. The upper part provides several ubiquitin-binding sites, residing on four non-ATPase subunits, namely Rpn1, Rpn2, Rpn10, and Rpn13 (G.R. Tundo et al., 2020). Once the ubiquitin-tagged substrates are recognized by intrinsic or extrinsic ubiquitin receptors, poly-ubiquitin chains are removed by Rpn11, a Zn^{2+} de-ubiquitinase, which hydrolyzes the isopeptide bond to recycle ubiquitin monomers (Yao & Cohen, 2002). The resulting polypeptide is then directed towards the ATPase hexameric motor ring formed by Rpt1, Rpt2, Rpt3, Rpt4, Rpt5, and Rpt6, able to unfold and translocate it into the inner catalytic core, using the chemical energy derived from ATP hydrolysis (De la Pena et al., 2018). Rpt2, Rpt3, and

Rpt5 are also involved in 20S channel opening: indeed, their conserved c-terminus HbYX motifs induce a conformational change in the adjacent N-terminus of 20S α-subunits that undergo tail displacement causing the gate widening (Smith et al., 2007).

As mentioned previously, the 20S open gate conformation is not always due to an ATP-dependent 19S involvement but sometimes can appear in particular cellular conditions, as redox unbalance, or after low concentration SDS treatment (e.g., 0,02%) during *in vitro* experiments (Bajorek & Glickman, 2004).

Moreover, 19S is not the only known regulatory particle involved in proteasome assembly and modulation: 11S/PA28 and PA200/Blm10, in particular circumstances, e.g. oxidative stress, can replace 19S particle to carry out, probably, the degradation of oxidized proteins in an ATP-independent fashion; however, due to the low amount of information about their biological role, more studies must be performed to further deepen it (Pickering and Davies, 2012).

Regarding the 20S proteasome structure, in detail, it is arranged in a barrel-like shape made of four piled up heptameric rings, two α-rings covering two inner β-rings, to form a central channel of 130Å in diameter and long 160Å (Baumeister et al., 1988; Borissenko & Groll, 2007) (***Figure 3***). The proteolytic chamber is defined by six active β-subunits: each β-ring includes three distinct active sites that show a common threonine protease activity due to a nucleophilic attack brought by the hydroxyl group of Thr1 at each N-terminus (Kisselev, Songyang, & Goldberg, 2000). As a matter of fact, inside the core particle, three different

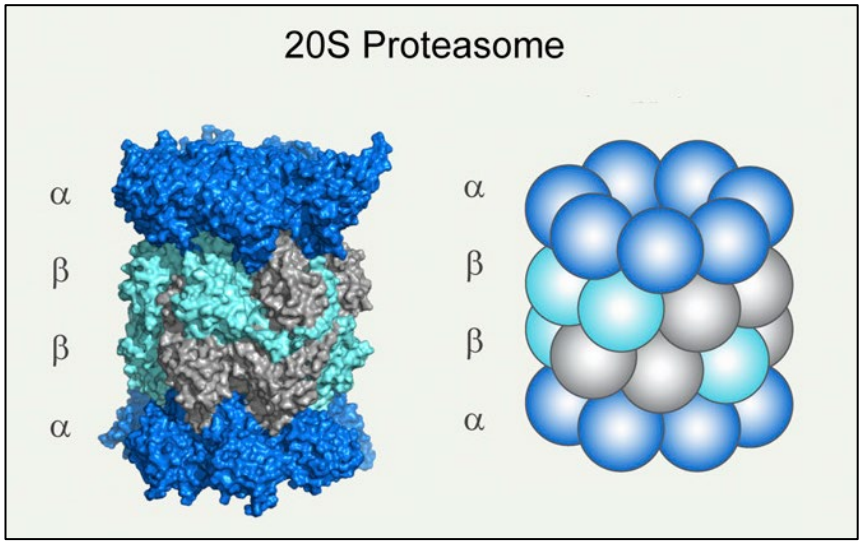

Figure 3. PDB Structure (4r3o) and cartoon representation of 20S proteasome (Figure reproduced and modified from *Thibaudeau & Smith, 2019*)

enzymatic activities occur, namely: chymotrypsin-like cut (β5 subunits), after hydrophobic amino acidic residues; trypsin-like cut (β2), after basic one, and caspase-like cut (β1), after acidic one (Groll & Huber, 2003).

In particular conditions, constitutive 20S particle (c-20S) is not the main proteasome isoform to perform altered peptides cleavage: as an example, immune cells (e.g. Hematopoietic cells, $CD8^+$ T cells) and immune tissues (e.g. Thymus) have their specialized proteasome, called immunoproteasome and thymoproteasome, respectively. Biologically, these alternative 20S forms, play a primary role in antigen processing for MCH class I presentation as reported in several studies (Blum, J. S. et al., 2013; Eggensperger & Tampé, 2015).

The molecular differences between these isoforms and the constitutive reside in specific subunits that are overexpressed according to tissues and cellular requirements: in immunoproteasome, β1, β2, and β5 of c-20S are displaced by induced subunits β1i, β2i, and β5i; in Thymus, where thymoproteasome is dominant, we find β1i, β2i, and a unique subunit, called β5t, that substitutes constitutive β5 to carry out its proteolytic function (Murata et al., 2018) (***Figure 4***). However, it is possible to induce, in the majority of non-immune cells, the expression of immunoproteasome subunits through treatment with specific cytokines such as interferon-γ, interferon-α, interferon-β or tumor necrosis factor (TNF) (Aki, M. et al., 1994; Shin, E. C. et al., 2006).

Alternative subunits are preferably embedded in the core rings due to a higher affinity compared to the constitutive ones: this characteristic allows a more reactive response to immunogenic stimuli or inflammatory insults (Heink et al., 2005).

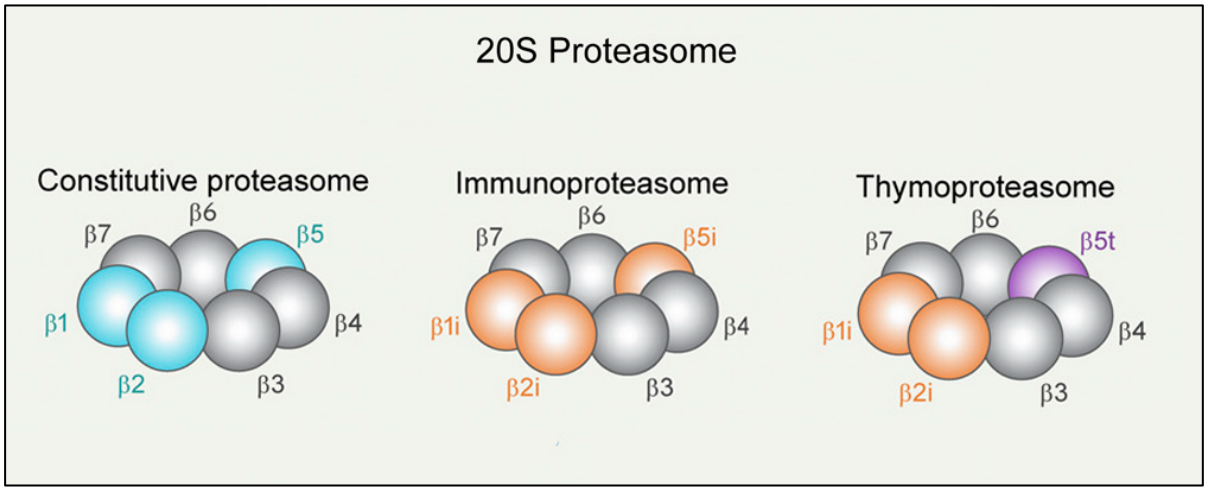

Figure 4. Different β-subunit combinations found in tissue-specific proteasomes of the β-ring of 20S proteasome (Figure reproduced and modified from *Thibaudeau & Smith, 2019*)

4.3.3 UPS role in cancer

Nowadays, despite all research work done in this direction, cancer progression modulation and stoppage is still very challenging target to reach. Classical tumor hallmarks are related to peculiar biomolecular and biochemical features such as 1) genomic instability with a high frequency of DNA mutations (deletions, inversions, large portion duplications, chromosomes aneuploidy, and translocations); 2) high proliferation rate due to an altered cellular signaling and a metabolic reprogramming; 3) high capacity of spreading and dissemination through tissues via enhanced angiogenic processes (Hanahan & Weinberg, 2000).

Besides these canonical hallmarks, proteostasis unbalance is pushing forward as a novel tumor hallmark: the quality control of protein synthesis, folding, and degradation are markedly impaired in cancerous cell lines (Carvalho et al., 2016); nevertheless, cells are not destined to the apoptotic pathway as normal ones, but they can survive and proliferate overcoming the proteotoxic environment and adapting their metabolism to stressful conditions (acidosis, hypoxia, and starvation) thanks to a protein network rearrangement (G.R. Tundo et al., 2020). Moreover, several preclinical reports show that proteasome levels and activity are altered in numerous solid tumors (lung, pancreas, thyroid, head, and neck, etc.), as in hematological ones (Adams, 2003; Roeten, Cloos & Jahnsen, 2018).

A crucial aspect in carcinogenesis is the broken equilibrium between oncoproteins and oncosuppressors caused by a deregulated proteasome activity (Chang & Ding, 2018). Furthermore, the cell cycle control plays a central role as well in tumor proliferation and diffusion: for this reason, a regulated proteasome-mediated degradation of cyclin-dependent kinase (Cdk) and cyclin-dependent kinase inhibitors (CdkIs) is fundamental to maintain cellular homeostasis (Diehl & Ponugoti, 2010). Among these pivotal factors, whose levels finely influences cancer pathogenesis, the most studied and characterized are the following: 1) NF-kB, a transcriptional factor involved in promoting tumorigenesis in specific human malignances blocking the apoptotic processes (Baldwin, 2001; Aggarwal, 2004); p53, a nuclear transcriptional factor with pro-apoptotic activity (Gupta et al., 2019); p21 and p27 CdkIs, whose expression guarantees cell cycle arrest in normal conditions while their degradation favors high proliferative rate in cancer cells (Abbas e Dutta, 2009).

Taken together, all these notions about UPS involvement in cancer progression/regression open to the idea that proteasome can be considered as a promising target to block to prevent cancer development.

4.3.4 20S proteasome inhibitors

Proteasome inhibitors (PI) were originally developed as an anti-inflammatory drug and used in the treatment of cancer-related cachexia. In 1990, Bortezomib (BTZ), or PS-341, was introduced for this purpose but surprisingly preclinical evidence reported that this PI showed an effective anti-cancer activity, especially towards Multiple Myeloma that underwent apoptosis and lost its invasive capacity (Mitch & Goldberg, 1996). For this reason, in 2003, U.S. Food and Drug Administration (FDA) approved BTZ administration as anti-cancer therapy while the European Medicines Agency (EMA) made it one year later (Dou, Q.P. et al., 2014).

A lot of scientists, at first, were doubtful about the use of PI as cancer treatment, just because proteasome is fundamental machinery for cellular homeostasis; but after the pre-clinical and clinical reports, they assumed that PI is a very useful weapon against cancer cells for the reason that the latter is more sensitive than normal cells due to their higher protein trafficking for rapid proliferation and metastatic spreading (Almond & Cohen, 2002; Chen et al., 2011).

BTZ belongs to peptide boronates (***Figure 5***), with a boronic acid residue in its structure and binds reversibly the chymotrypsin-like (CT-L) β5 subunit of 20S particle with high affinity, while caspase-like (C-L) and trypsin-like (T-L) activity, as well, are inhibited with lower affinity (Buac et al., 2013). This inhibition, from a biochemical point of view, is toxic towards malignant cells: indeed, the impairment of the NF-kB pathway and the stabilization of p53 induces apoptosis in cancerous cells raising the levels of Bcl-2 and NOXA, two known pro-apoptotic proteins. Moreover, after BTZ treatment, angiogenesis is slowed down because vascular endothelial growth factor receptors (VEGFRs) levels are decreased (Hideshima et al., 2003).

Unfortunately, after prolonged cycles of BTZ treatment, patients develop drug resistance and side effects, such as peripheral neuropathy. Indeed, tumors don't respond anymore to BTZ because cells activate several resistance mechanisms; among these, of particular relevance, we cite the mutations of the active site of β5 subunits that lead to an altered docking of the PI, losing its impairing effect (Barrio et al., 2019).

To overcome these drawbacks, new molecules with fewer side effects (highly specific for 20S CT-L) and less drug-resistance induction were synthesized: the promising Carfilzomib (CFZ) (***Figure 5***) is a second-generation, irreversible, tetrapeptide epoxyketone class CT-L inhibitor with minimal cross-reactivity to other proteases (Dou, Q.P. et al., 2014). CFZ was approved as an anticancer agent in 2012 by FDA and in 2015 by EMA and it is administered

especially in relapsed multiple myeloma (RMM) patients, rising their survival rate. Compared to BTZ, CFZ is more effective and reduces the onset of side effects due to its higher specificity and better pharmacokinetics, even if few cases of drug resistance were reported too (Shah et al., 2018; Ao et al., 2012).

Among other innovative PI we report: 1) ixazomib, the first oral reversible inhibitor that belongs to peptide boronates, approved in 2015 by FDA (Chauhan, Catley, et al., 2005); 2) oprozomib, an irreversible epoxyketone inhibitor, orally administered under preclinical investigation (Zhou et al., 2009); 3) marizomib (Salinosporamide A), the main nonpeptide irreversible PI, derived from the microbial fermentation of *Salinospora tropica*, an aquatic actinomycete (Potts & Lam, 2010) (***Figure 5***).

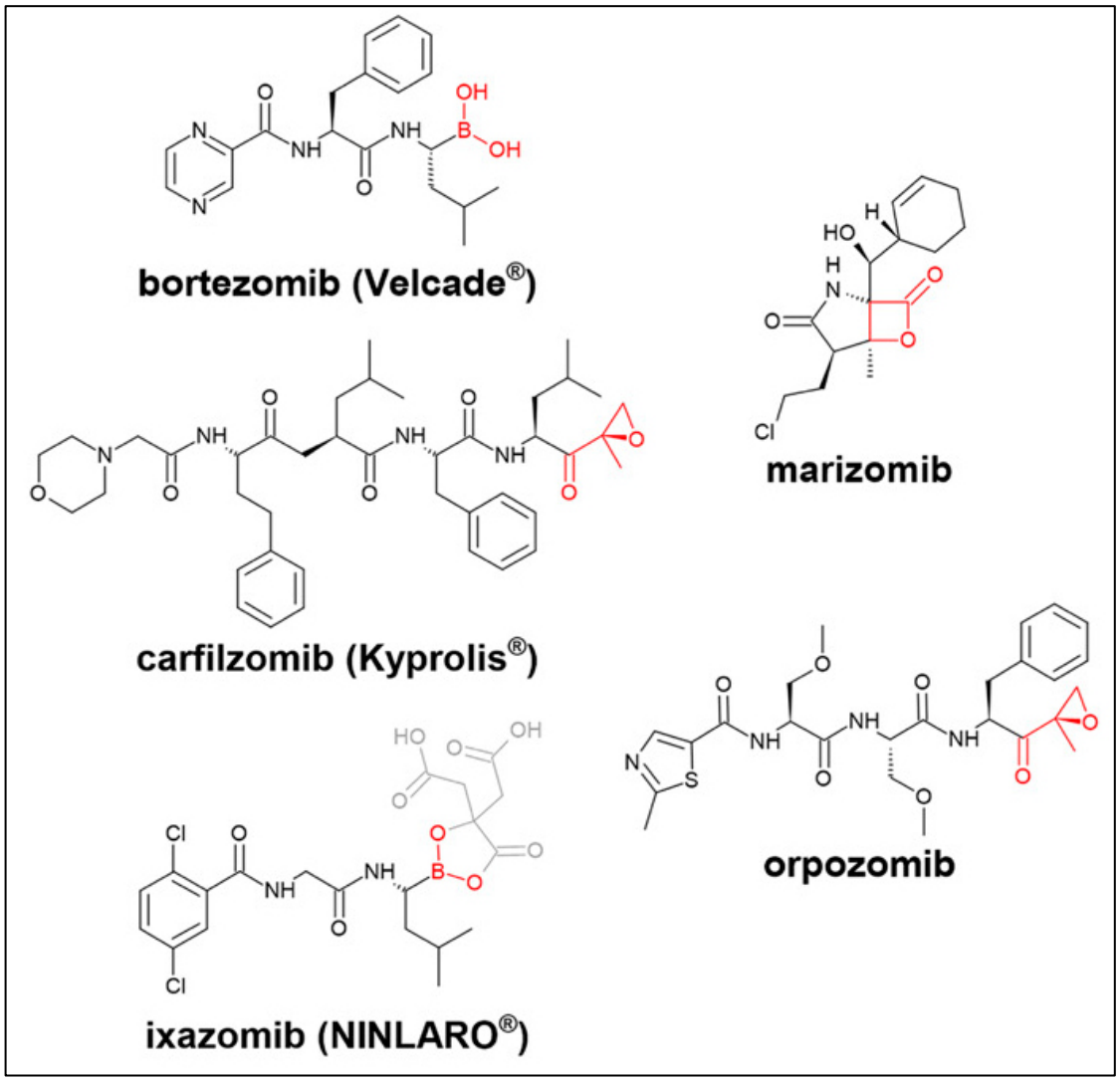

Figure 5. Chemical structures of FDA-approved proteasome inhibitors (PI) or in clinical trials (Figure reproduced and modified from *Thibaudeau & Smith, 2019*)

4.3.5 UPS role in neurodegenerative pathologies

Nowadays, neurodegenerative diseases spreading is becoming more and more consistent determining a big challenge for medics and researchers to avoid a social and economic drama. Indeed, etiopathogeneses of neurodegenerative disorders are still unclear and considered a matter of debate: Alzheimer's disease (AD), Parkinson's disease (PD) and Huntington disease (HD), amyotrophic lateral sclerosis (ALS), and Creutzfeldt-Jakob disease (CJD) are the most diffused pathologies. All of them are characterized by a common hallmark, the presence of aggregation-prone proteins, in particular, amyloid-β and tau protein in AD, α-synuclein in PD, huntingtin in HD, 43kDa TAR DNA-binding protein (TDP-43) in ALS, and prion protein in CJD (McAlary et al., 2019).

Misfolded and aggregated polypeptides are strictly related to a deep disequilibrium in protein homeostasis leading to neurotoxicity in altered tissues (Bredesen, Rao & Mehlen, 2006). UPS has a primary regulative role in the neurological process such as memory, synapses signaling, calcium efflux/influx, and long-term synaptic plasticity (Bingol & Schuman, 2004).

In neurodegenerative conditions, UPS is severely compromised by the aggregation and accumulation of toxic aggregated proteins that affect, in particular, the 20S proteasome degradation. Indeed, as reported previously, soluble amyloid oligomers are the most toxic isoform among all the aggregated species and present the peculiar characteristic to be recognized by the antibody A11, which is capable to ligate indiscriminately soluble oligomers of α-synuclein, amyloid-β and huntingtin exhibiting a common 3D conformation; these species, via a nanomolar affinity interaction with specific α-subunits of the outer ring, can induce an allosteric modification that stabilizes a close-gate status in 20S proteasome (Thibaudeau et al., 2018) (***Figure 6***).

Going in-depth regarding AD, its pathogenesis is strongly related to proteasome derangement: 20S plays a fundamental role in degrading monomeric amyloid beta and avoids its accumulation and aggregation, but, at the same time, the interaction between toxic Aβ oligomers and 20S core particle brings to a conformational change in the latter that blocks its proteasic activities; it is not still clear, in pathological conditions, whether the initial event is the amyloid cascade with oligomers production or, vice versa, a reduced proteasome efficiency before Aβ accumulation, aggregation and its consequent toxicity (G.R. Tundo et al., 2020). Furthermore, in AD, hyperphosphorylated tau aggregated species can impair

proteasome, thus increasing ubiquitinated protein levels and accumulating on synaptic junctions (Tai et al., 2012; Myeku et al., 2016).

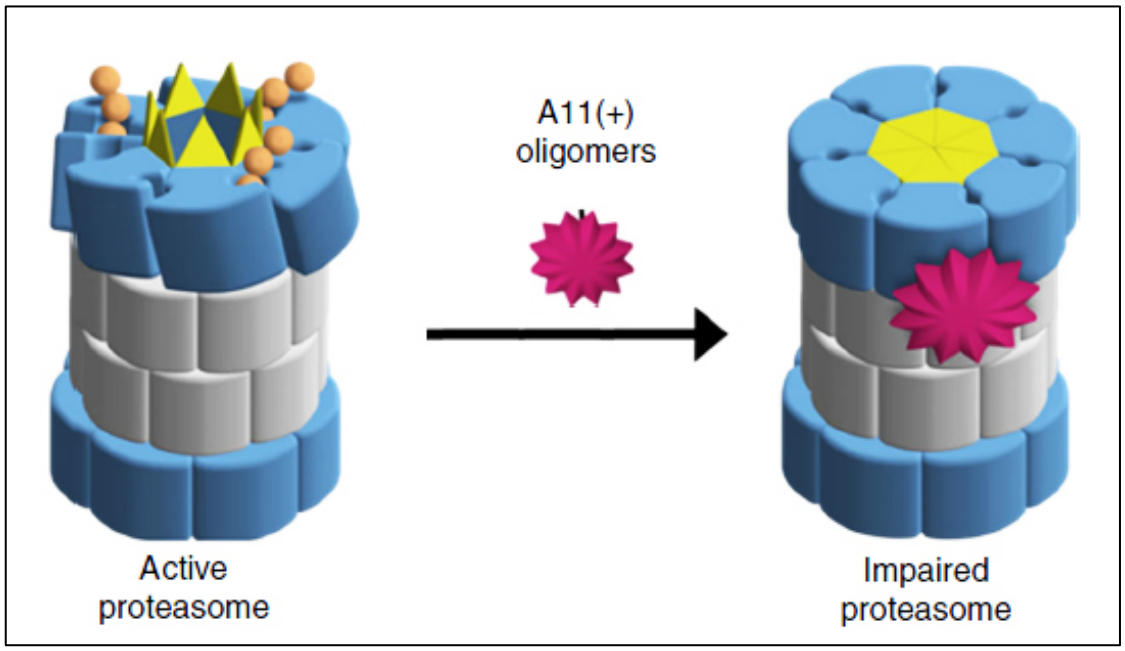

Figure 6. Amyloid oligomers, reactive to A11 antibody (A11+), induce an allosteric conformational change in 20S Proteasome stabilizing the closed-gate status and impairing enzymatic reactions (Figure reproduced and modified from *Thibaudeau et al., 2018*)

While the constitutive proteasome activity decreases in AD, the immunoproteasome, conversely, is overexpressed in astrocytes (Keller, Hanni & Markesbery, 2000) and in the neuroglia that encircles amyloid plaques of diseased mice: here, it was observed that the use of a PI (YU102) suppressed the excretion of inflammatory cytokines from glial cells recovering the cognitive functions of mice (Yeo et al., 2019).

In Parkinson's disease, moreover, the UPS is deeply involved in Lewis body formation, through the "aggresome" development, a structure made of poly-ubiquitinated proteins, α-synuclein precipitates and random misfolded polypeptides. Also in this case the nature of aggresome is strongly debated: is it a protective event to sequester toxic aggregates or an initial pathogenic process that deregulates physiological processes (Raiss et al., 2016)? This question is still unsolved in all neurodegenerative diseases interested by aggregation-prone proteins and, to provide a satisfying answer, a lot of research work is needed urgently.

Another aspect relates indissolubly PD to UPS dysfunction: PD peculiar hereditary mutations reside on genes that are translated in proteins all involved in UPS communication or ubiquitin-conjugating enzymes, such as Parkin (PARK2 gene), a-synuclein (SNCA gene), PINK or PTEN-induced putative kinase 1(PARK6 gene) or ubiquitin carboxyhydroxylase L1 (UCH-L1 gene) (G.R. Tundo et al., 2020).

Proteasome, hence, is emerging day by day as a new rising target to explore to progressively slow down and finally defeat AD, PD, and the other main neurodegenerative disorders characterized by amyloid cascade and consequent deregulation of UPS.

4.3.6 UPS Positive Modulators

All these previous notions present a picture where UPS and in particular proteasomal degradation machinery suffer under protein dyshomeostasis: proteasome impairment, due to aggregated species, in addition to redox imbalance and metal ions dysregulation, are responsible for unavoidable neuronal cell death.

To overcome this condition and avoid the onset of pathologic events new strategies have been developed to recover deregulated UPS or to reclaim a functional 20S proteasome after its inhibition. Among these strategies, proteasome subunits phosphorylation (Myeku & Duff, 2018) and positive UPS modulators have been implemented to enhance proteasome activities. The selection and development of these positive enhancer molecules is not a simple step to take because once a particular drug or a natural compound showed an agonist activity in vitro, only in rare cases do they reflect the same benefits in more physiological conditions (Trader DJ et al., 2017).

As we discuss before, HbYX motifs are part of ATPase hexameric motor subunits of the 19S proteasome and are directly involved in opening the 20S core gate through a series of molecular interactions; according to this, to find out new promising biochemical tools to retrieve UPS functionality, HbYX moiety was introduced into synthetic peptides: it was seen that these modified peptides enhance proteasome degradation *in vitro* (Karpowicz et al., 2015; Lau & Dunn, 2018). Surprisingly, *in cell* experiments have shown that the addition of this motif into a proline- and arginine-rich peptide (PR11), a known 20S inhibitor, can convert it into a 20S activator (Gizynska et al., 2019).

Another class of UPS positive modulators of natural origin is the phytochemical compounds extracted from vegetables and fruits. These peculiar compounds are very attractive as pharmacological treatments against neurodegenerative disorders thanks to their detoxifying, antioxidant, anti-inflammatory and antiaging properties (Naoi et al., 2019). The majority of these molecules, curiously, have a dual behavior depending on the applied dose, exhibiting an activating faculty if low concentrated or an inhibiting property if high

concentrated (G.R. Tundo et al., 2020). Among natural molecules able to modulate the proteasome activity, the most studied are, namely: curcumin, derived from curcuma, that induce proteasome activity in keratinocytes at low concentration (1μM) (Murakami, 2013; Cuanalo-Contreras & Moreno-Gonzalez, 2019); quercetin, a very diffused flavonoid, able to reduce Aβ toxicity through the activation of proteasome activity in a *Caenorhabtidis elegans* model of AD (Chondrogianni et al., 2010); resveratrol, effective in recovering protein homeostasis in an AD mouse model and in *C. elegans* model (Regitz et al., 2016); oleuropein, a polyphenol derived from fruits and leafs of *Olea europaea*, inducing all three proteasome enzymatic activities (CT-L, C-L, T-L) in human fibroblast (Katsiki et al., 2007); betulinic acid, a lipid involved in proteasome-mediated neurotrophic effect in a murine vascular dementia model where levels of brain-derived neurotrophic factor (BDNF) are increased (Kaundal et al., 2018); 18α-glycyrrhetinic acid (18α-GA), derived from licorice, capable of increasing lifespan of *C. elegans* and induce neuroprotection in human and murine cell models (Papaevgeniou et al., 2016) and, at last, tanshinone IIA, a promising molecule derived from the roots of *Salvia miltiorrhiza* targeted against several neurological disorders (Subedi et Gaire, 2021).

Besides single components, exerting a protective skill towards proteotoxic disorders, we must consider the synergistic effect of the whole plant extract content and how this bioactive mixture should interface with UPS. Indeed, it was seen that active molecules alone are not effective as the natural mixture to prevent viability loss in cancerous cell lines (Baranowska et al., 2020; Terzo et al., 2018). Particular attention is being paid to the *Brassicaceae* family where a lot of biologically effective phytochemicals have been identified: glucosinolates (GLS), the major bioavailable constituent compound in Brassica tissues, and their myrosinase-processed products - isothiocyanates, thiocyanates, oxazolidine-2-thiones, indole-3-carbinols, and nitriles - have been intensively studied during the last years due to their strong anticancer properties (Barba et al., 2016; Terzo et al., 2018, Zhang et al., 2010).

Sicilian cultivars of Brassica, such as the *Brassica oleracea*, better known as black broccoli, aroused particular interest due to the ability of its fresh juice to determine viability dropping in human colon cancer and human melanoma cell lines (Terzo et al., 2018).

For all these reasons, the mutual biological effect of the plant juices towards neurological degenerative disorders should be deepened to provide new therapeutic weapons.

As we said before, the selection and characterization of new drug-like molecules, able to induce directly proteasome degradation, is not a simple process and requires a big economic investment. Production of new drugs is not a convenient activity and the best way to save

money and time is to redirect already approved drugs to other clinical purposes. As an example, pyrazolones, a class of compounds approved as antipyretic and analgesic medicals, are also able to induce an enhanced proteasome activity in ALS murine model (Trippier et al., 2014). In another work, aminopyrine, 4-aminoantipyrine, and nifenazone were selected between several pyrazolones because they reported an increased ability to stimulate the 20S proteasome in a fluorescent assay; furthermore, computational docking studies revealed a specific interaction of the former molecules with α-rings of 20S core particle, probably inducing an allosteric modification; at last viability assays (MTT) on differentiated SH-S5Y5 cells reported that aminopyrine and nifenazone protect neurons from Aβ toxicity when the proteasome is not inhibited by Bortezomib (A.M. Santoro et al., 2019).

Among repurposed old drugs, Chlorpromazine (CPZ), a phenothiazine previously used in schizophrenia or manic-depression, deserves a special mention because it is considered an allosteric proteasome activator: indeed, *in vitro* experiments exhibited that CPZ interacts with alpha subunits of 20S core particle promoting an open-gate conformation of the catalytic channel favoring the entrance of the substrate (Jones et al., 2017).

Targeting the proteasome to treat memory dysfunction and cognitive disorders in AD or related neurodegenerative pathologies is a very promising perspective but at the same time, it is very challenging and complex.

5. AIMS

Molecular mechanisms involved in Alzheimer's disease pathogenesis are still unclear and debated after decades of studies; for this reason, no effective therapeutic strategy, able to slow down or reverse the disease course, has been introduced yet.

This research project aimed to deepen and better understand the biochemical mechanisms underlying the involvement of the amyloidogenic pathway and Ubiquitin proteasome system (UPS) in AD and related neurodegenerative disorders to highlight unusual aspects of pathogenesis and open up new therapeutic perspectives.

In particular, our study is focused on the following peculiar aspects:

1) characterization of the interaction between ubiquitin and Aβ, to evaluate the importance of direct binding during protein clearance, such as in the poly-ubiquitin chain formation or by the insulin degrading enzyme (IDE) mediated degradation pathway;

2) development of an innovative and suitable real-time method for proteasome activity analysis finalized to the evaluation and selection of novel 26S proteasome enhancers;

3) deepening the peculiar hormetic effect of Aβ on cellular models and 26S proteasome degradation system;

4) assessment of the bioeffective properties of vegetal compounds, for example, *Brassica oleracea* extracts, toward cell viability and proteasome stimulation to identify new molecular mechanisms involved in neuroprotection.

6. RESULTS

6.1. Experimental materials and methods

In this chapter, I will discuss the materials and methods we applied in our experiments, explaining, in particular, aspects not already reported in the published paper: 1) an innovative technique based on real-time fluorescent measures for proteasome activity kinetics analysis; 2) the cultivation and extraction process of *Brassica Oleracea* juices at various stages of life; 3) the classical MTT assay for the assessment of cellular viability.

6.1.1 Development of a new real-time fluorescent method aimed at measuring the 20S proteasome activity *in vitro*

Several techniques have been developed over the years to finely measure the levels of proteasome activity; in particular, numerous *in vivo, in cell,* and *in vitro* procedures have been applied to better understand proteasome degradation mechanisms. These systems involve substrates of different nature, namely: 1) peptide-based substrates, often linked to a fluorophore; 2) protein-based substrates revealed through immunoblot analysis; 3) GFP fused substrates used for *in cell* and *in vivo* experiments (Thibaudeau and Smith 2019).

Our method collects fluorescence measurements continuously for 24 hours and the resulting real-time kinetics are compared to evaluate if a chosen compound is a proteasome activator or an inhibitor. To assess that, we bought from AAT Bioquest© the compound *(Suc-LLVY)2R110* (***Figure 7***)**,** a tetrapeptide linked to the fluorophore rhodamine 110; this molecule, once degraded by 20S chymotrypsin-like active site, provides a fluorescence emission (λ_{EM}=520nm) if excited at the proper wavelength (λ_{EX} =495nm).

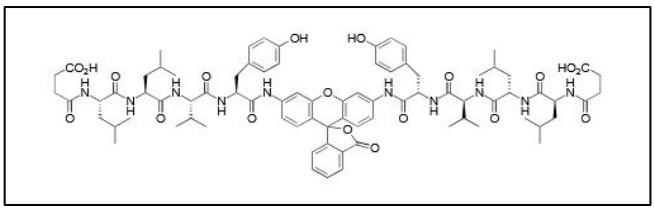

Figure 7. Molecular structure of (Suc-LLVY)2R110

Our proteasome activity assay, for the part relative to reagents, is adapted from Hugo et al. (2018) while the experimental procedure is completely innovative. To achieve our results, a real-time Applied Biosystems StepOne® system, previously used for real-time PCR analysis,

has been adapted: the 24 hours kinetics is performed at 37°C but it is preceded by 30 minutes at 4°C measurements to achieve a stable baseline where no reaction (or at very little extent) occurs. In this way it is possible, during the data analysis, to align and subtract efficiently all the baselines to distinguish even the smallest differences in enzymatic activity.

We used the cytosolic extract of SH-S5Y5 neuroblastoma cells as a proteasome testing model. Cell extracts were obtained as follows:
SH-S5Y5 cells were grown in DMEM medium (Pen/Strep), 10% FBS, in a T75 Flask. After cell confluence achievement (~8,5x10^6 cells), cells were trypsinized for 5 minutes, collected in a 15ml tube with an equal volume of DMEM medium (10% FBS) to inactivate trypsin activity, and centrifuged for 5 min 1500rpm. The supernatant was removed and washed three times with PBS in a 1,5ml tube. Then, cell pellets were resuspended in 690ul of proteasome lysis buffer (25mM HEPES, 250mM sucrose, 20mM MgCl2, 1mM EDTA, pH 7,4), lysed by three freeze-thaw cycles (5 minutes at -80°C freezer and 3 minutes at 37°C in a water bath, respectively). Then, cell lysates were centrifuged at 15,000 ×g for 30 minutes at 4°C to remove cell debris and the supernatant was placed in six 1,5ml tubes (6 x 115ul aliquots) and finally stored at -80°C.

Proteasome activity assay was measured through the Applied Biosystems StepOne RT-PCR system using MicroAmp® optical 48-wells reaction plate or strips: 2µl of the cytosolic extract samples were transferred in a microtube plate and the reaction is ready to be started after the addition of 20µl of proteasome activity buffer (150mM Tris, 30mM potassium chloride, 7.5mM MgOAc, 10mM MgCl2, 20µM Suc-LLVY-2R110 containing ATP 100uM, pH 7,4). Microtube plate reading was performed in real-time by Rhodamine 110 (R110) fluorescence emission analysis (Fluoresceine FAM filter: λ_{EX} =495nm and λ_{EM}=520nm). Data were collected by the StepOne software with a 96 cycle (24 hours kinetics, 15 minutes/cycle) method set at 37°C – preceded by a new 32min (8 minutes/cycle) 4°C step to obtain the baseline.

The data of 24 hours kinetics were analyzed by calculating the activity rate in the initial phase (0-60 minutes- exponential) and in a pre-plateau phase (9-19 hours- linear), expressed in ΔFu(Fluorescence Unit)/ Δt(sec). As demonstrated later (***Figure Met3*** e ***Figure Met4***), the proteasome activity in the initial phase, indicated as "P. Rate1" is ATP dependent while the other indicated as "P. Rate2" seems to be ATP independent.

To finely tune the method, several preliminary experiments have been done; in particular, the SDS effect and ATP addition at diverse concentrations were tested to improve the efficiency of the proteasome activity assay.

The addition of 0.02% SDS to assay buffer was seen to sensibly induce the opening of the latent 20S gate, especially in native gel-based proteasome activity measurements (Huang and Chen, 2019). Surprisingly, in our system, SDS addition not only does not improve 20S proteasome activity but, conversely, slows down and impairs the enzymatic process at as low as 0,005% (***Figure 8***).

ATP addition, otherwise, is a necessary condition to perform observable and reliable measurements: diverse concentrations (from 0 to 1mM) have been added to our proteasome activity buffer to define the optimal conditions. As reported in ***Figure 9*** and ***Figure 10***, the addition of ATP is required to achieve a significant assessable intensity: the maximum increase has been reached at ATP concentrations between 500µM and 1mM, indicating saturating levels over 500µM. ATP levels between 50µM and 100µM provide the optimal results halfway to be in the most favorable condition to discriminate possible proteasome enhancers or inhibitors of proteasome activity.

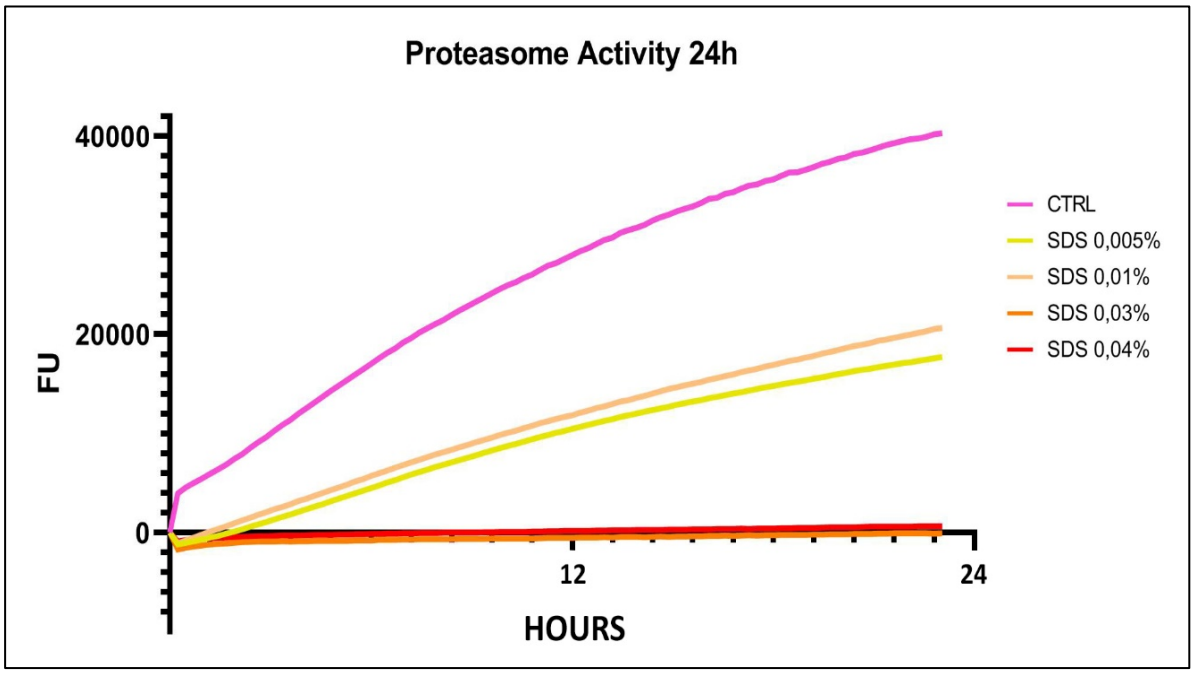

Figure 8. 24h proteasome activity kinetics measured in real-time: **CTRL** = SH-S5Y5 cytosolic extracts; **SDS**= Sodium Dodecyl sulfate at different concentration (0,005%; 0,01%; 0,03%; 0,04%);
note: addition of 0,02% SDS gave us not reliable measurements (data not reported).

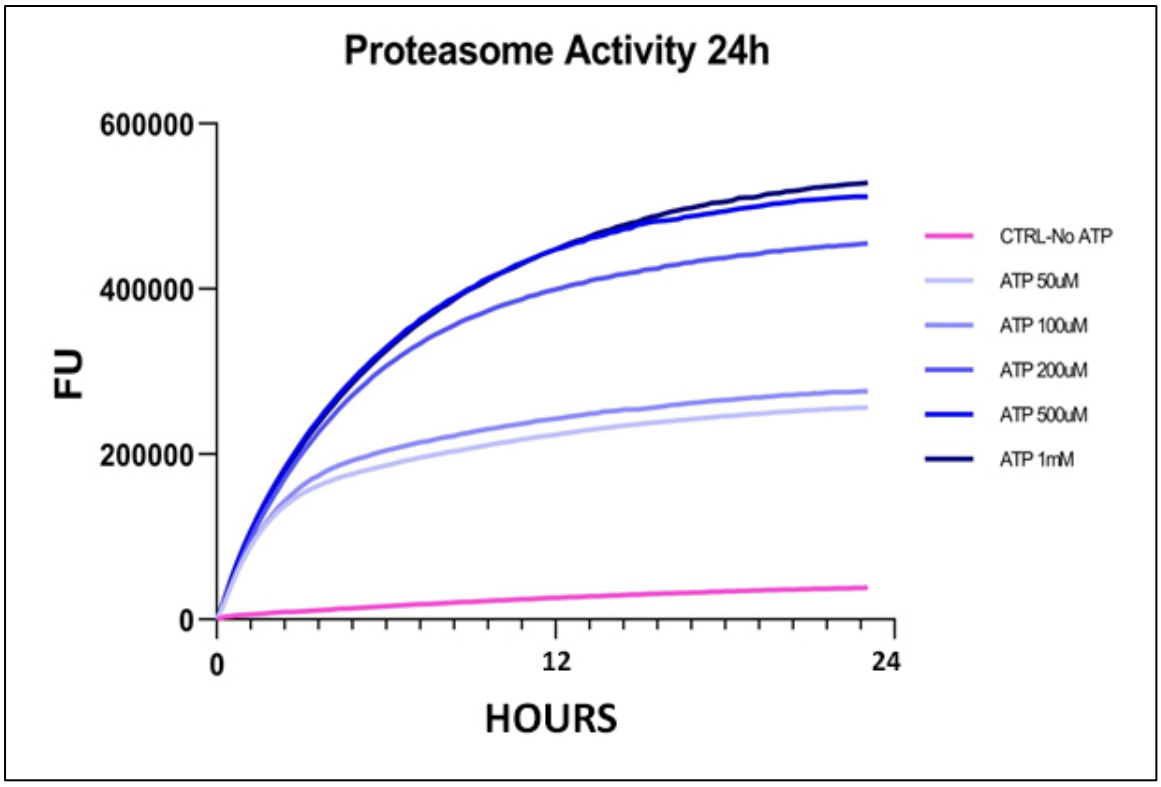

Figure 9. 24h proteasome activity kinetics followed in real-time: **CTRL** = SH-S5Y5 cytosolic extracts; **ATP=** Adenosine Triphosphate at different concentration (50µM-100µM-200µM-500µM-1mM).

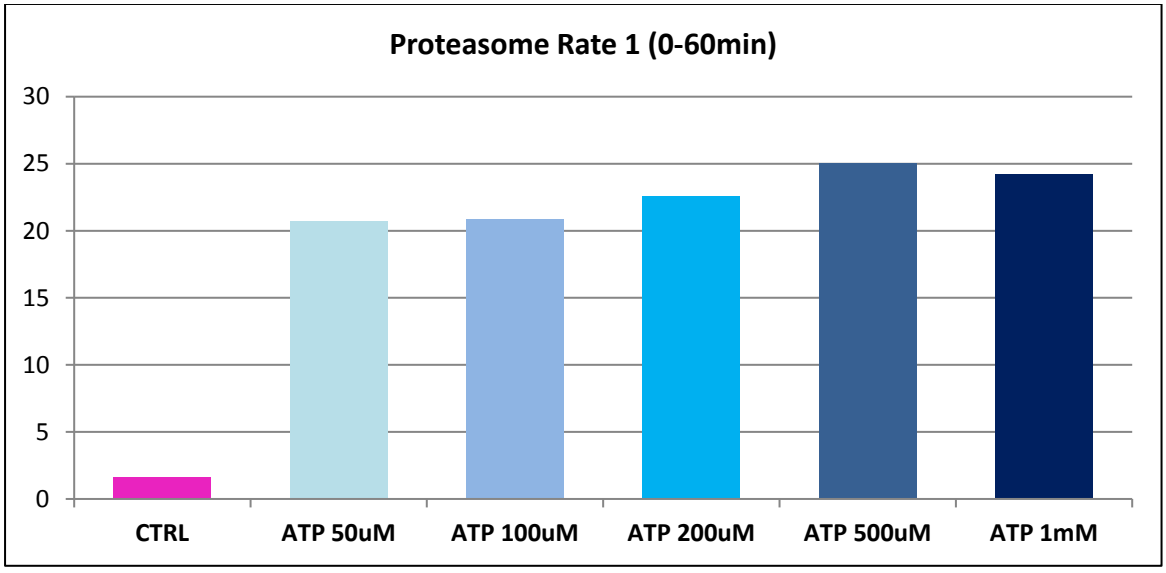

Figure 10. Proteasome rate activity 1 (ΔFU/ΔT) achieved during the first 60 minutes of 24h real-time kinetics: **CTRL** = SH-S5Y5 cytosolic extracts; **ATP=** Adenosine Triphosphate at different concentrations (50µM-100µM-200µM-500µM-1mM).

According to our evidence, this innovative real-time technique is very promising thanks to several reasons: at first, the control of temperature (baseline 4°C; activity 37°C) is a fundamental tool to program when the enzymatic reaction should start; moreover, the limited

amount of sample volume required (22µl), the high sensibility of fluorescence measurements and the absence of peculiar chemicals, such as SDS, provide a promising procedure for analyzing proteasome kinetics. An aspect to be explored concerns the use of SDS, often present in proteasome activity commercial kits due to its effect on the complete opening of the 20S channel gate and promotion of proteins degradation. The presence of SDS is suitable for candidate inhibitors testing, but it is not recommended for proteasome activators characterization, because the system is already fully activated. Therefore, our experimental system works in a more physiological environment than classical commercial analysis kits. For all the aforementioned reasons, our procedure should be implemented and taken into consideration for more reliable and affordable proteasome activity analyses.

6.1.2 Preparation of *Brassica oleracea* extracts

Crop cycle and morpho-biometric characterization of sprouts, microgreens, and baby leaves of *Brassica oleracea L. var. Italica Plenck*

Brassica oleracea testing materials were provided by Professor Ferdinando Branca and his research group at the Sicilian agricultural institute of Valdisavoja (IAS), located in Catania in via Valdisavoja 3, thanks to a collaboration recently started. *Brassica oleracea L. var. Italica Plenck*, a Sicilian cultivar of black broccoli grown on the slopes of Etna, has been characterized from the morphological and biometric point of view and its bioactive component profile has been compiled (data not shown). The seeds of black broccoli (BR365), from the Di3A germplasm bank of the University of Catania (UNICT), were properly cleaned, stored, and placed in alveolar containers arranged in a cold greenhouse in natural light conditions (from 4.6 to 9.2 MJ m -2 d -1), using the practice of organic cultivation. The containers were filled with Brill® semina bio-organic soil (Geotec, Italy) and irrigated according to ordinary techniques. The young seedlings were harvested in the three growth stages of the analyzed plant such as sprouts (seedlings with spread cotyledons without a seminal envelope, harvested after 7 days), microgreens (seedlings with the first true leaf, harvested after 15 days), and baby leaves (seedlings with 3-4 true leaves collected after 29 days); the collected samples were subjected to the washing, drying, and weighing phases. After 10 days from sowing, several treatments were carried out: 1) BTK ® 32 WG (Xeda, Italy) against *Pieris brassicae*; 2) *Bacillus thuringiensis var. kurstaki* at a concentration of

1.5g/l and Garlic 2.5 g/l against aphids; 3) lecithin, as a wetting agent. Young leaves of adult plants (AL) in the growing phase were collected from the adult black broccoli plant and were used to compare their biochemical and genetic profile to the above innovative products (S, MG, and BL). After harvesting, sprouts (S), microgreens (MG), baby-leaves (BL) were characterized for the main morphological descriptors, namely weight in grams of 10 samples, length of the hypocotyl in millimeters, length of cotyledons, the width of cotyledons, length of the stem, number of true leaves, leaf length and leaf width.

Juice extraction

Part of the samples of sprouts (S), microgreens (MG), baby leaves (BL), and growing leaves of an adult plant (AL) of black broccoli were weighed, placed inside a cold extractor (Hurom slow juicer) to separate the juice from fibrous part. The juice and fiber were stored inside falcon of 50 ml and their contents were weighed and refrigerated at -80 °C. After 48 hours, the falcons were placed inside the Heto Power Dry LL 3000 Freeze Dryer for 90 hours at -55 °C to obtain the freeze-dried samples. When the freeze-dried juice was obtained, a part of it was used for the characterization of biochemical components and, in the specific case, for the analysis of glucosinolate profile (GLSs); another part, was used for the characterization of genetic component that is the extraction and analysis of miRNAs (data not reported).

Extraction in water and methanol of freeze-dried Brassica juice bioactive components

To perform *in vitro* experiment, our group had to treat *Brassica Oleracea* freeze-dried powder, provided by Prof. Branca, in such a way to make available bioactive components coming from its distinct growth phase (S, MG, BL, and AL); the recovery of glucosinolates, isothiocyanates, and other bioeffective molecules was performed according to the extraction protocol, modified from Cools et al. (2012):

A. 150mg of the freeze-dried samples were suspended in 3ml of water (W) (boiling at 100°C for 15 minutes) or 3ml of methanol 70% (M) (boiling at 70°C for 10 minutes);
   note: for this operation 15ml falcon tubes capped with punctured parafilm to let the vapors exit.
B. centrifuge at 5000rpm/ 10 min/ 4°C

C. transfer the remaining supernatant in a tube on ice

D. filter sterilize the solution with 0,22μM filters

E. For the samples extracted in water, measure its volume and then aliquot and store at -80°C

F. For the samples extracted in methanol, evaporate under N_2 steam (on ice) and resuspend samples in the same volume of the H_2O extracted solution.

6.1.3 MTT Viability Assay

In preconditioning experiments, SH-S5Y5 cells were cultured in DMEM medium/ F10 nutrient mixture 50%/50% (10%FBS, Pen/Strep) in a T75 flask until they reached 90% confluence. Then, cells were trypsinized, counted on a Burker Chamber, and seeded in two 48 multiwell plates at a density of 25000 cells/well, and after one day, cells were ready to be treated. The experiment lasted 4 days and all treatments were diluted in DMEM medium/ F10 nutrient mixture 50%/50% (1%FBS, Pen/Strep) (200ul/well x4 replicates): the preconditioning step with SW was performed on the first day and required 48h; the third day, where needed, cells were pre-incubated with Carfilzomib for 1,5h and then treated with Aβ Toxic* for 24h. On the fourth day, the MTT assay was performed as described below.
3-(4,5-dimethylthiazol-2-yl)-2,5-diphenyl-2H-tetrazolium bromide (MTT) assay substrate was purchased from PanReac AppliChem© and the procedure was performed as follows:

1. Prepare MTT solution in a 15ml tube: dissolve 4-6mg of MTT in 2ml of PBS, mix thoroughly and add 8ml of culture medium without FBS
2. Remove medium from multiwell and add 100µl of MTT solution per well
3. Incubate the multiwell for 1h and a half at 37°C
4. Check if violet precipitate is formed and then remove supernatant
5. Add 100µl of DMSO and agitate plate for 15 minutes in the dark
6. Read at wavelength 595nm in a plate reader (569 filter spectrophotometer)

*Aβ 1-42 peptide (Sigma) was previously treated with HFIP overnight at 1mg/ml aliquoted in the amount for subsequent experiments, evaporated under nitrogen steam, then resuspended in DMSO at 5mM and stored at -80°C until before use. Aggregated toxic Aβ was prepared to add PBS 10mM (1X) to reach a final concentration of 600µm (205ul total volume). This solution was incubated at 50°C for 72h and then diluted in the medium before treatment at the final concentration of 15 µM.

6.2. RESEARCH PROJECT RESULTS

Effect of *Brassica oleracea* extracts on SH-S5Y5 cell viability

Due to the previously reported beneficial and anticancer properties of the *Brassicaceae* family, we decided to elucidate the role of bioactive molecules contained in the juice of *Brassica oleracea* after water- or methanol-based extractions from the samples collected at 4 distinct life stages, as reported in the methods chapter. At first, we checked the effect of the various *B. oleracea* extracts at low and high concentrations on the viability of SH-S5Y5 through the MTT assay; the results depicted in ***Figure 11*** exhibit that aqueous extracts of *B. oleracea* at the life stage of MG, BL, and AL exhibit a detrimental effect on neuroblastoma cell viability determining, at the low dose, a decrease of 16,5%, 15%, and 20% respectively while, at high dose, a higher efficacy is reported with 35,5%, 35,5%, and 22,5%. Conversely,

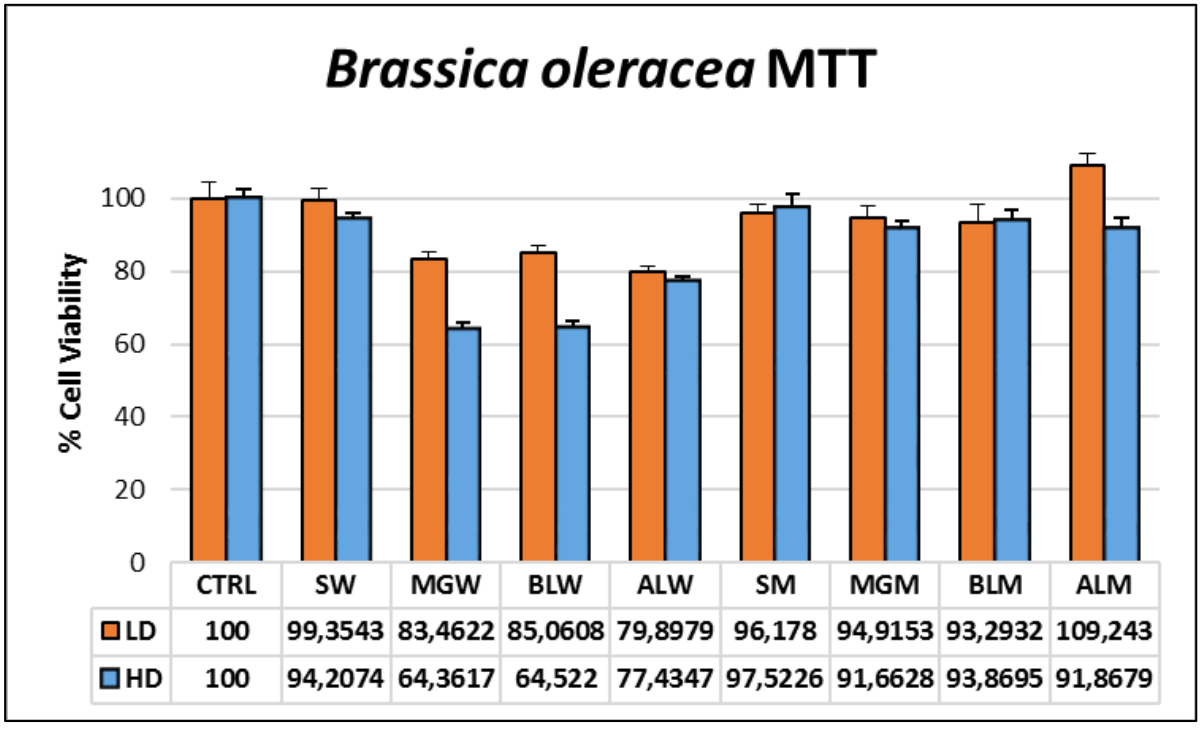

	CTRL	SW	MGW	BLW	ALW	SM	MGM	BLM	ALM
LD	100	99,3543	83,4622	85,0608	79,8979	96,178	94,9153	93,2932	109,243
HD	100	94,2074	64,3617	64,522	77,4347	97,5226	91,6628	93,8695	91,8679

Figure 11. MTT assays of SH-S5Y5 cells treated with Brassica oleracea extracts; **CTRL** represents SH-S5Y5 cells treated (150ul/well x4 replicates) for 24 hours with DMEM medium/ F10 nutrient mixture 50%/50% (1% fetal bovine serum (FBS), Pen/Strep). The other experimental points were treated with Brassica oleracea var. Italica extracts (1/90 v/v) at different life stages (**S**= Sprouts, **MG**= Micro Greens, **BL**=Baby-leaves, **AL**= Adult Leaf) if extracted with Water (**W**) or Methanol (**M**); MTT absorbance was measured at 568nm; values are expressed as mean value and error bars represent the standard error of the mean (SEM). The statistical ANOVA analysis, performed through *GraphPad Prisma* software, gave a statistically significant difference ($P < 0,0001$).
LD = Low Dose **(**Orange bars) = *B. oleracea* at dilution 1/90 v/v in medium.
HD = High Dose **(**Blue bars) = *B. oleracea* at dilution 1/22 v/v in medium.

on the other hand, MG, BL, and AL extracted in methanol show no significant decrease of MTT, but instead, ALW exhibit a 10% increase, meaning that no loss of viability is exerted by methanolic extracts, independently from the concentration applied. Only the aqueous extract of the *B. oleracea* sprouts (SW) and the methanolic one (SM), to a lesser extent, preserve almost completely the SH-S5Y5 cell viability. These results indicate that MGW, BLW, and ALW, in a tumor cell line, induce a cytotoxic effect confirming the anticancer activity of these mixtures. On the other side, SW, SM, and ALM should be taken into consideration for further experiments to better understand the mechanisms behind their bioeffective properties.

Aqueous extracts of *Brassica oleracea* enhance proteasome activity in SH-S5Y5 neuroblastoma cellular extracts

Proteasome activity measurement *in vitro* is an efficient and convenient way to predict the role of a peculiar treatment towards protein network regulation. As we discuss before, proteasome degradation impairment leads to proteotoxic diseases including neurodegenerative disorders while proteasome enhancement significantly improves cellular clearance pathways, preserving from degeneration.

Through a fluorescent 24 hours real-time assay, we measured the fluorescence intensity of each SH-S5Y5 neuroblastoma cytosolic extract sample to quantify their 20S chymotrypsin-like activity. So, as depicted in ***Figure 12***, we performed a 24h kinetics to test the ability of *B. oleracea* juice extracts of increasing or slow down the proteasome activity of neuroblastoma cellular extracts. Our results presented in ***Figure 13*** and ***Table 1*** show that, in the ATP-dependent degradation phase, all the aqueous extracts from black broccoli (MGW, BLW, SW, and ALW) exhibit a marked enhancing effect on substrate degradation while methanolic extracts present an ambivalent behavior that does not deserve any particular attention. Among all samples, SW provided the major activation boost with an increase of almost fifty percent in fluorescence intensity: thanks to this surprising evidence SW administration could be considered as a promising therapeutic strategy to improve the cell clearance efficiency of intrinsically disordered proteins, thus preventing the development of the diseases where aggregation-prone proteins play a central role.

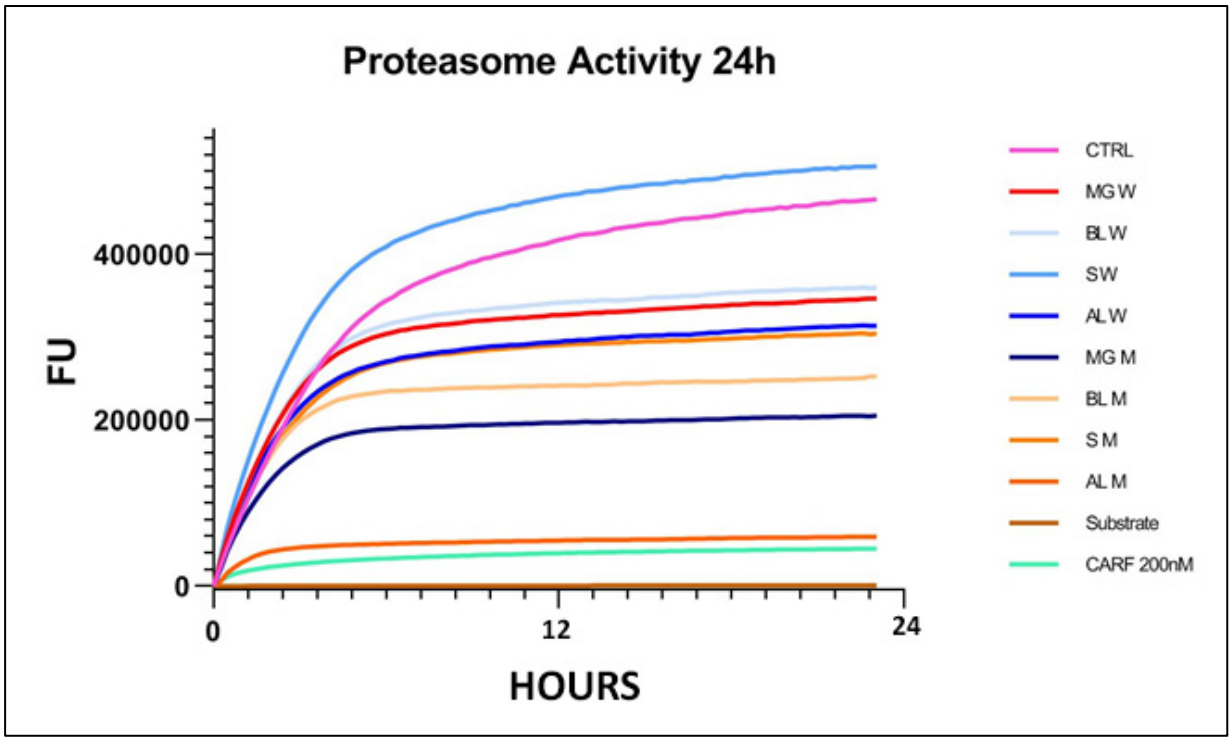

Figure 12. 24h proteasome activity kinetics followed in real-time: **CTRL** = SH-S5Y5 cytosolic extracts; **MG W, BL W, S W, AL W**= *Brassica oleracea var. Italica* aqueous extracts; **MG M, BL M, S M, AL M**= *Brassica oleracea var. Italica* methanolic extracts diluted 1/90 v/v in proteasome activity buffer; **Substrate** = LLVY-R110 proteasome substrate without SH-S5Y5 cytosolic extract; **CARF** = Carfilzomib 200nM.

Sample	P. Rate1	% P. Rate1	P. Rate2	% P. Rate2
CTRL	23,90	100,00	1,85	100,00
MG W	28,83	120,63	0,62	33,69
BL W	28,55	119,49	0,68	36,55
S W	35,07	146,76	1,44	77,71
AL W	27,67	115,80	0,65	34,92
MG M	20,98	87,78	0,24	12,88
BL M	26,15	109,44	0,22	11,95
S M	25,43	106,40	0,48	26,07
AL M	7,64	31,96	0,15	7,90
Substrate	0,00	0,00	0,01	0,47
CARF 200nM	4,58	19,17	0,19	10,20

Table 1. Overall table reporting the proteasome activity rates and their relative percentages of the 24h kinetics. Proteasome activity rates (**P. Rate**) are expressed in ΔFu (Fluorescence Unit)/ Δt (sec) while proteasome activity percentage rates **(% P. Rate**) are reported in % in respect to the control. **CTRL** = SH-S5Y5 cytosolic extracts; **MG W, BL W, S W, AL W**= *Brassica oleracea var. Italica* aqueous extracts; **MG M, BL M, S M, AL M**= *Brassica oleracea var. Italica* methanolic extracts diluted 1/90 v/v in proteasome activity buffer; **Substrate** = LLVY-R110 proteasome substrate without SH-S5Y5 cytosolic extract; **CARF** = Carfilzomib 200nM.

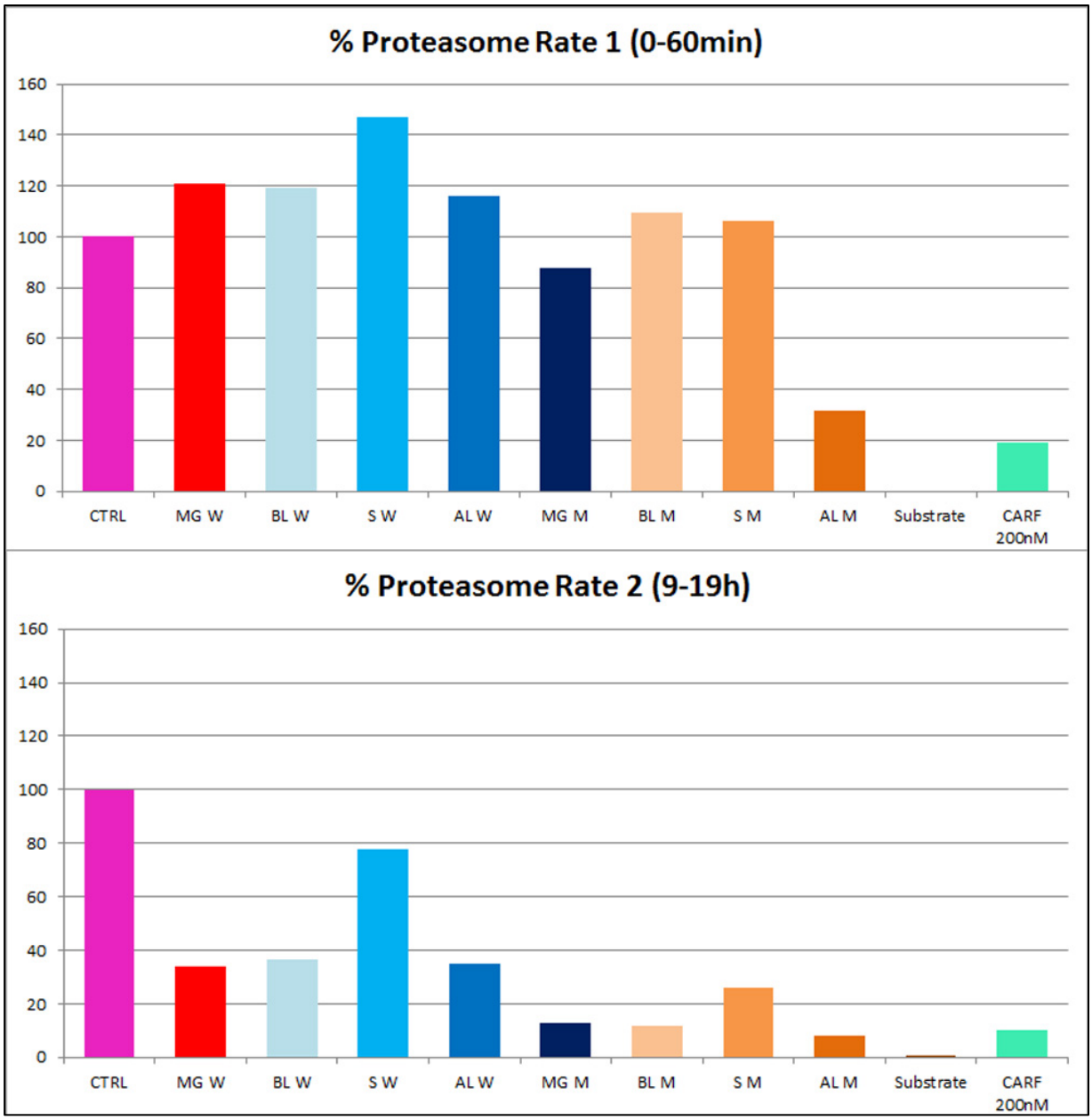

Figure 13. 24h proteasome activity kinetics followed in real-time: proteasome activity rates calculated in ΔFu (Fluorescence Unit)/ Δt (sec) and reported in % respect to the control. The upper panel refers to the 0-60minutes interval where the proteasome activity shape is an exponential straight line; the lower panel refers, instead, to proteasome rate2 calculated on a 9-19hours interval where the line gets back the shape of a straight line. **CTRL** = SH-S5Y5 cytosolic extracts; **MG W, BL W, S W, AL W**= *Brassica oleracea var. Italica* aqueous extracts; **MG M, BL M, S M, AL M**= *Brassica oleracea var. Italica* methanolic extracts diluted 1/90 v/v in proteasome activity buffer; **Substrate** = LLVY-R110 proteasome substrate without SH-S5Y5 cytosolic extract; **CARF** = Carfilzomib 200nM.

Sprouts aqueous extract of *Brassica oleracea* protects SH-S5Y5 neuroblastoma cells from aggregated amyloid beta toxicity.

The potentiality of Brassicaceae to ameliorate cellular pathologic conditions have been often reported in the literature; in particular, it was previously described that Brassica sprouts juice protects cells from $A\beta_{25-35}$ cytotoxicity in neuroblastoma cells (Masci et al., 2015) whereas, in another study, it prevents skin damage from ultraviolet (UV) radiation exposure (Talalay et al., 2007).

For these reasons and our previously reported results, SW activity has been further investigated under our experimental conditions, to confirm its beneficial biological effects. As reported in ***Figure 14***, during the preconditioning phase (48 hours), SW extract treatment ameliorated cell viability by more than 6 percentage points; furthermore, this preconditioning stage reduces almost totally the loss of viability caused by the Aβ toxic isoforms insult; as expected, at last, the addition of Carfilzomib reduced by cell viability 75 percentage points due to its proteasome inhibitory effect.

This evidence demonstrates that SW extracts protect cells from Aβ toxicity also through a proteasome degradation enhancement mechanism: SW preconditioning step avoids detrimental protein accumulating, aggregating, and bringing cells to death.

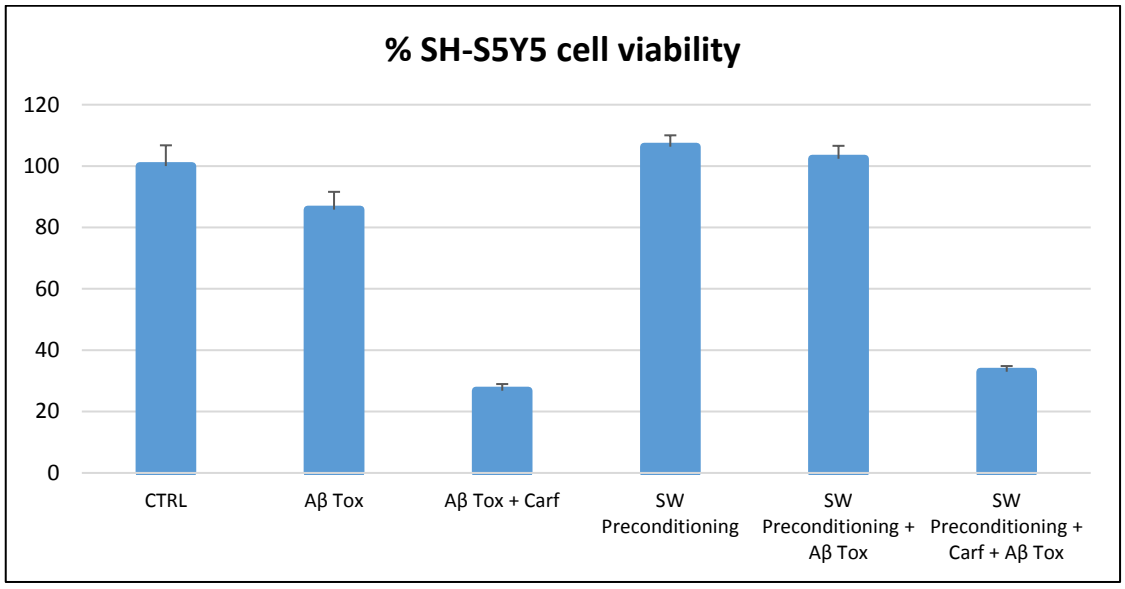

Figure 14. MTT viability assay of SH-S5Y5 cells treated with: **Aβ Tox** = aggregated Aβ 1-42 15µM, **Carf** = Carfilzomib 200nM, **SW**= *Brassica Oleracea* sprouts water extracts diluted 1/90 v/v and various combinations of them; **CTRL=** not treated SH-S5Y5 cells. The statistical analysis, performed through GraphPad Prisma software, gave a statistically significant difference ($P < 0,0001$).

Low concentrations of monomeric amyloid beta peptides enhance proteasome activity in SH-S5Y5 cytosolic extracts and protect SH-S5Y5 neuroblastoma cells from aggregated amyloid beta toxicity.

In physiological conditions, protein homeostasis is finely regulated and amyloid beta peptide isoforms are well balanced except if external or pathological perturbation occurs. As reported, Aβ exhibits a hormetic effect on the biological system: on the one hand, monomeric peptide shows, at low concentrations, a protective behavior toward pure rat cortical neurons via the activation of the PI-3-K pathway (Giuffrida et al., 2009); on the other hand, Aβ oligomers are mediators of pathology causing inflammation, proteasome impairment and neurotoxicity (Sengupta et al., 2016; Thibaudeau and Smith, 2019). Our experimental project has been developed looking for a connection between low and high Aβ concentrations, to deeply understand the molecular mechanism of UPS involvement in amyloid cascade.

At first, we evaluated the modulation of proteasome activity adding low to high Aβ monomeric peptides to our samples. Thanks to our innovative technique, able to detect also a small increase of activity, we were able to establish that nanomolar scale monomeric Aβ (0,001μM and 0,01μM in particular), both in the first phase of kinetics (***Figure 15*** and ***Figure 16*** *upper panel*) and in the second phase (***Figure 15*** and ***Figure 16*** *lower panel*), enhances the 20S chymotrypsin-like degradation.

Moreover, as expected, the treatment with the higher concentrations of Aβ (5μM to 60μM) slowed down, in a dose-dependent manner, the proteasome activity due to their higher aggregation rate (***Table 2***). Indeed, the higher concentration is the peptide, the higher the aggregation rate occurs, as demonstrated by a study by Morel et al. (2018) that went into detail about the aggregation kinetics of Aβ 1-40 and Aβ 1-42. Chlorpromazine (CPZ), a known proteasome activator for purified human 20S proteasome according to the literature (Jones et al., 2017), surprisingly exhibited an inhibitory effect towards human neuroblastoma cells cytosolic extracts in our measures.

This positive effect of monomeric Aβ peptide at low concentration, achieved with our innovative method, was further evaluated on SH-S5Y5 cell culture through an MTT viability assay: in the results reported in ***Figure 17***, the preconditioning phase with 1μM monomeric Aβ 1-42 peptide sensibly improved cell viability in 48 hours and reduces the toxic effects of aggregated Aβ isoforms.

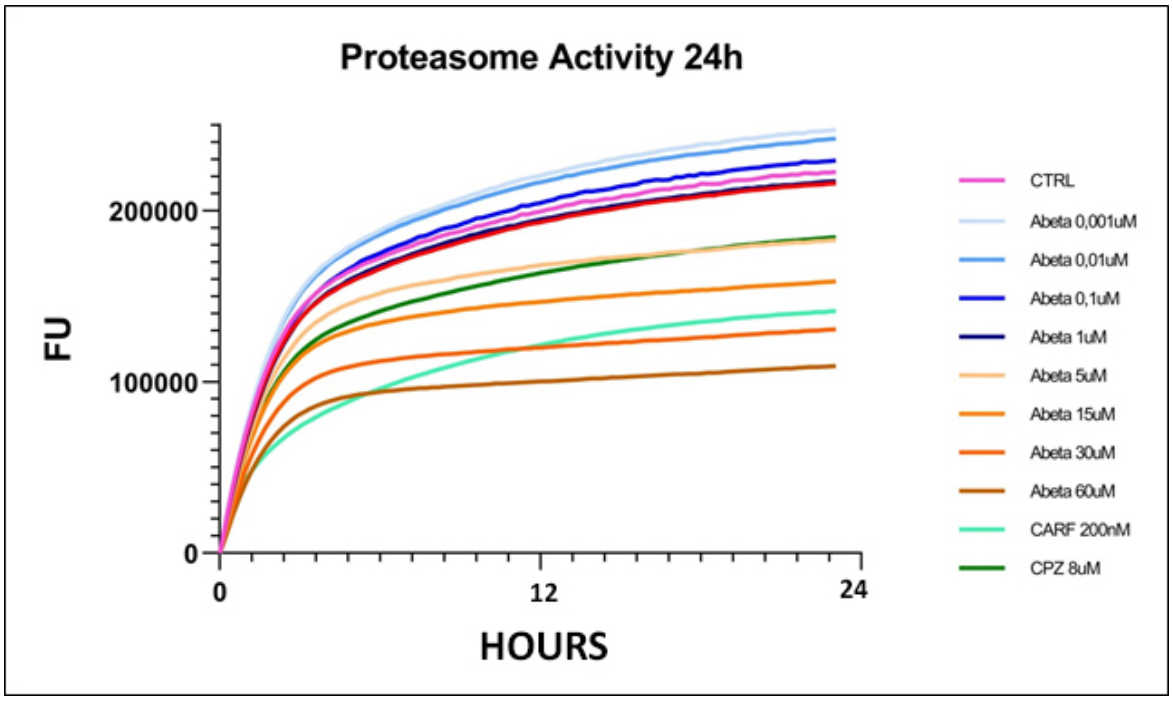

Figure 15. 24h proteasome activity kinetics followed in real time: **CTRL** = SH-S5Y5 cytosolic extracts, **Abeta** = monomeric Aβ 1-42 peptide (0,001μM- 0,01μM- 0,1μM- 1μM- 5μM- 15μM- 30μM- 60μM), **CARF** = Carfilzomib 200nM, **CPZ** = Chlorpromazine 8uM.

The most effective concentration discrepancy between proteasome activity assays (Aβ nanomolar range) and the preconditioning experiments (Aβ micromolar range) is due to the low cell membrane diffusivity of monomeric Aβ; indeed, only a little amount of it is uptaken into cells via a clathrin-independent endocytic pathway (Jin et al., 2015). For this aspect, we hypothesize that treating cells with a medium containing 1μM of monomeric Aβ, only a nanomolar fraction will be found intracellularly (further experiments will be performed to demonstrate our hypothesis). At last, as expected, proteasome inhibitor Carfilzomib treatment drops down cell viability.

We can speculate, finally, that monomeric Aβ peptide exhibits a neurotrophic effect towards SH-S5Y5 cells, not only via a classic receptor-based signaling cascade (Giuffrida et al., 2009) but also through a 26 proteasome degradation enhancement. This effect disappears during the amyloid cascade due to the deprivation of monomers that brings cells to a stressful and non-viable condition.

Sample	P. Rate1	% P. Rate1	P. Rate2	% P. Rate2
CTRL	19,28	100,00	0,83	100,00
Abeta 0,001uM	20,19	104,75	0,98	117,79
Abeta 0,01uM	20,10	104,29	0,90	108,92
Abeta 0,1uM	18,75	97,28	0,89	106,69
Abeta 1uM	18,14	94,09	0,80	96,11
Abeta 5uM	17,02	88,29	0,48	57,32
Abeta 15uM	15,82	82,09	0,36	43,07
Abeta 30uM	13,45	69,79	0,27	33,03
Abeta 60uM	11,31	58,69	0,22	26,33
CARF 200nM	11,89	61,68	0,74	89,70
CPZ 8uM	16,07	83,36	0,70	84,78

Table 2. Overall table reporting the proteasome activity rates and their relative percentages of the 24h kinetics. Proteasome activity rates (**P. Rate**) are expressed in ΔFu (Fluorescence Unit)/ Δt (sec) while proteasome activity percentage rates **(% P. Rate**) are reported in % in respect to the control.

CTRL = SH-S5Y5 cytosolic extracts; **Abeta** = monomeric Aβ 1-42 peptide (0,001μM- 0,01μM- 0,1μM- 1μM- 5μM- 15μM- 30μM- 60μM), **CARF** = Carfilzomib 200nM, **CPZ** = Chlorpromazine 8uM.

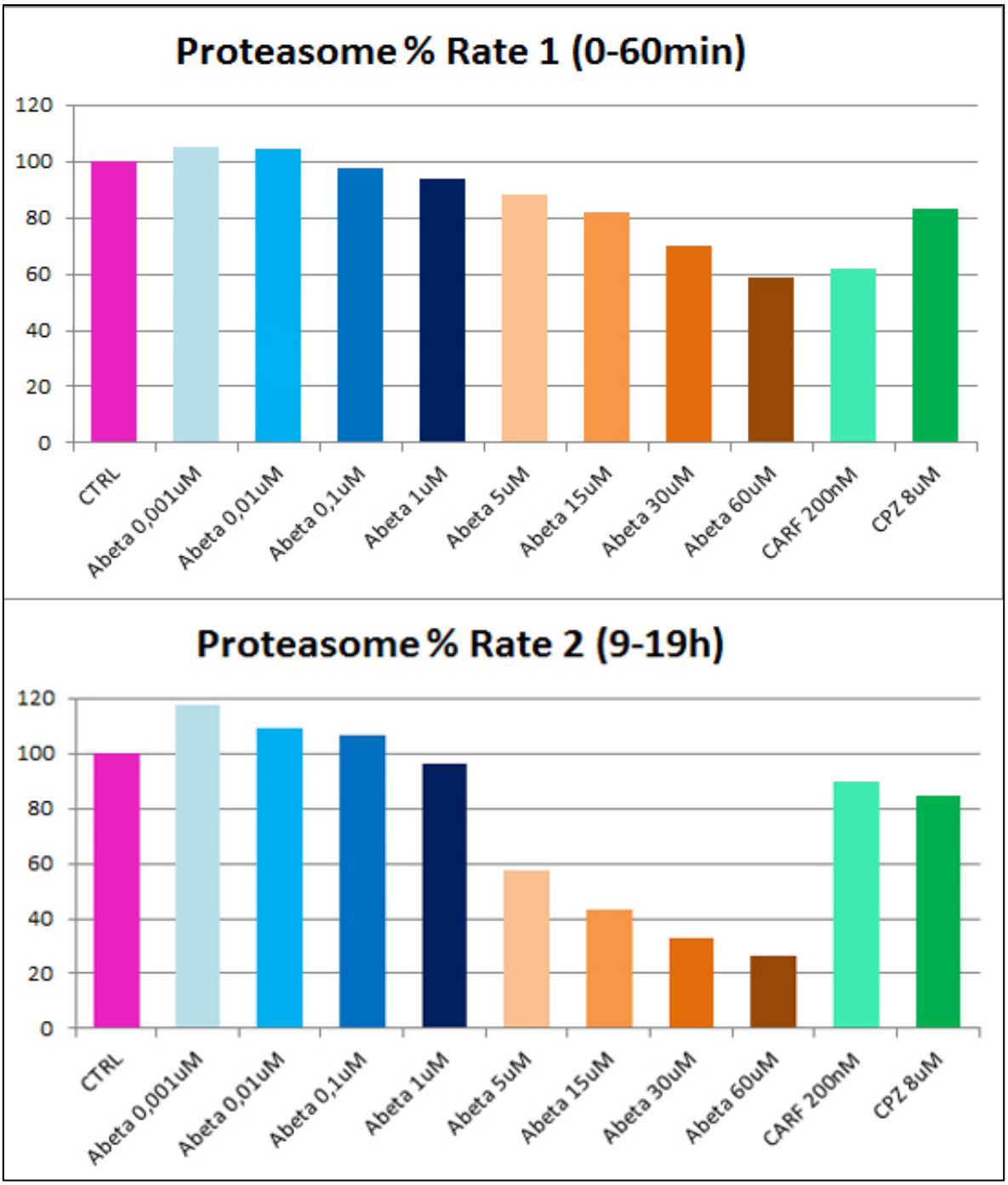

Figure 16. 24h proteasome activity kinetics followed in real-time: proteasome activity rates calculated in ΔFu (Fluorescence Unit)/ Δt (sec) and reported in % respect to the control. The upper panel refers to the 0-60minutes interval where the proteasome activity shape is an exponential straight line; the lower panel refers, instead, to proteasome rate2 calculated on the 9-19hours interval where the line gets back the shape of a straight line. **CTRL** = SH-S5Y5 cytosolic extracts, **Abeta** = monomeric Aβ 1-42 peptide (0,001μM- 0,01μM- 0,1μM- 1μM- 5μM- 15μM- 30μM- 60μM), **CARF** = Carfilzomib 200nM, **CPZ** = Chlorpromazine 8uM.

Freeze-dried **Aβ1-42** peptide was previously treated with HFIP overnight at 1mg/ml, evaporated under nitrogen steam, and then resuspended in DMSO at 7,1mM and stored at 80°C until before use.

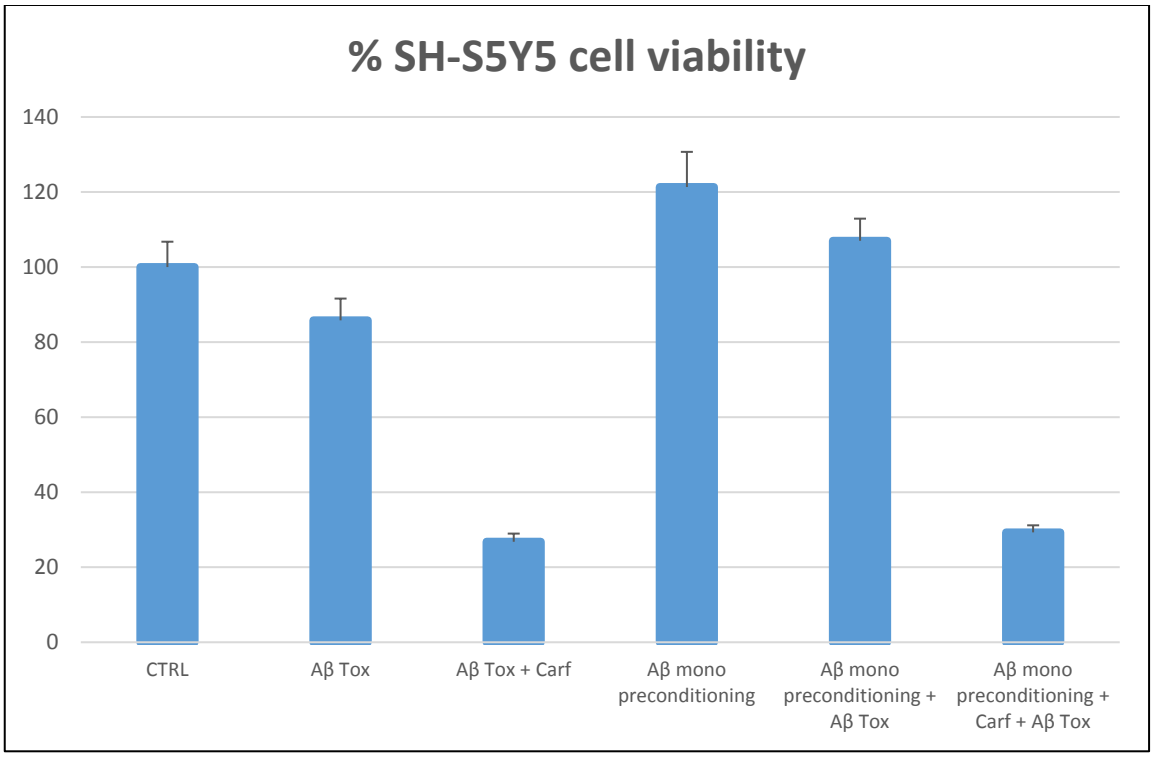

Figure 17. MTT viability assay of SH-S5Y5 cells treated with: **Aβ Tox*** = aggregated Aβ 1-42 15μM, **Carf** = Carfilzomib 200nM, **Aβ mono** = monomeric 1μM Aβ 1-42 peptide and various combinations of them; **CTRL=** not treated SH-S5Y5 cells. The statistical ANOVA analysis, performed through *GraphPad Prisma* software, gave a statistically significant difference ($P < 0{,}0001$).

*Monomeric Aβ was prepared by diluting an aliquot of DMSO dissolved Aβ stock solution (5mM) to the final concentration (1μM) in medium just before treatment.

7. DISCUSSION AND CONCLUSION

Our experiments highlighted the central role of amyloid beta in the modulation of the ubiquitin proteasome system, both in monomeric and aggregated form. Indeed, Aβ binds ubiquitin, a central UPS actor, in a non-covalent fashion through electrostatic/hydrophobic interactions between peculiar aminoacid residues of Aβ and a specific Ub domain. This binding was demonstrated also through an ELISA experiment in which Aβ and Ub were able to interact even in the presence of competition by the whole SH-S5Y5 cellular extract. Furthermore, it was observed that the resulting Aβ:Ub complex interferes with diverse clearance mechanisms, such as the poly-ubiquitin chain growth in ATP-dependent 26S proteasome degradation or the IDE-mediated degradation modality of amyloid beta peptide. From our experience, we can postulate that Aβ exhibits a hormetic effect towards cellular biological systems; indeed, at low concentration, Aβ can induce a duplex protective response: one represented by a receptor-mediated signaling cascade (Giuffrida et al., 2009) and the other, here demonstrated, based on a direct proteasome enhancement. Conversely, the treatment with a high concentration of Aβ and the subsequent formation of oligomers determines, also in this case, a possible dual detrimental effect: one is receptor-mediated (May et al., 2017) and the other is operated through an allosteric interaction with 20S proteasome that causes the gate channel closing (Thibaudeau, et al., 2018). According to this context, we could consider Aβ as a proteasome signaling molecule, able to induce proteasome activity at low concentration, probably advising cell proteostasis systems that something in the system is going wrong. In contrast, Aβ at high concentration tends to build up and aggregate in such a way that oligomers intracellularly impair 20S proteasome degradation ability, predisposing cells to apoptosis. Proteasome inhibition, thus, has been considered as a prerequisite of caspase activation and apoptosis activating; it is also true, however, that the proteasome inhibition, through a mechanism that involves HSP overexpression, decreases the levels of Caspase1 and Caspase8 preventing IFN-γ induced apoptosis in lens epithelial cells (LEC) (Awasthi & Wagner, 2005).

Moreover, to evaluate the 20S Proteasome activity modulation, a new real-time procedure has been developed to assess the 20S chymotrypsin-like protease activity in a neuronal cell-derived model. With this procedure, we screened several proteasome modulators and bio-effective extracts of *Brassica oleracea* sprouts juice. This has been evaluated as a proteasome enhancer, opening new therapeutic perspectives for AD and other neurodegenerative disorders affected by proteotoxic engulfment. However, the direct effect here observed on

proteasome activity can be further supported by the activation of other pathways. Indeed, proteasome activators could stimulate the overexpression of transcriptional factors, such as nuclear factor-erythroid 2 related factor 1 (Nrf1) and nuclear factor-erythroid 2 related factor 2 (Nrf2), which, in turn, were found to upregulate the expression of β-subunits of the 20S core particle (Masci et al., 2015; Hamazaki and Murata, 2020).

We, therefore, strengthen the concept that proteasome activation occurs not only via a receptor-based activation of a signaling cascade culminating with nuclear transcriptional factors overexpression, but also via a direct interaction between 26S proteasome complex, or ubiquitin, and Aβ monomers or bioeffective compounds,-like Brassica sprouts extracts.

For all the aforementioned reasons, we can confirm that 26S proteasome activity is a finely regulated process, responsible to maintain the absolute equilibrium required for physiological cellular proteostasis. The proteasome machinery is a crucial druggable system involved in many cellular physio-pathological processes. The establishment of specific molecular targets and modulating conditions can provide challenging strategies to counteract the AD amyloidogenic cascade involved in disease progression. By the way, the discovery of proteasome enhancers, derived from superfood and their bioavailable compounds introduced with diet, could be a very stimulating challenge, to improve lifestyle and dietary habits and finally define new medical guidelines for people affected by neurodegenerative disorders.

8. REFERENCE

1. Abbas, T. & Dutta, A. p21 in cancer: intricate networks and multiple activities. *Nat Rev Cancer* **9**, 400–414 (2009).
2. Adams, J. The proteasome: structure, function, and role in the cell. *Cancer Treatment Reviews* **29**, 3–9 (2003).
3. Adams, J. The development of proteasome inhibitors as anticancer drugs. *Cancer Cell* **5**, 417–421 (2004).
4. Aggarwal, B. B. Nuclear factor-κB: The enemy within. *Cancer Cell* **6**, 203–208 (2004).
5. Aki, M. *et al.* Interferon-gamma induces different subunit organizations and functional diversity of proteasomes. *J Biochem* **115**, 257–269 (1994).
6. Almond, J. B. & Cohen, G. M. The proteasome: a novel target for cancer chemotherapy. *Leukemia* **16**, 433–443 (2002).
7. Ao, L. *et al.* Development of Peptide-Based Reversing Agents for P-Glycoprotein-Mediated Resistance to Carfilzomib. *Mol. Pharmaceutics* **9**, 2197–2205 (2012).
8. Awasthi, N. & Wagner, B. J. Upregulation of Heat Shock Protein Expression by Proteasome Inhibition: An Antiapoptotic Mechanism in the Lens. *Investigative Ophthalmology & Visual Science* **46**, 2082–2091 (2005).
9. Bajorek, M. & Glickman, M. H. Keepers at the final gates: regulatory complexes and gating of the proteasome channel. *Cell Mol Life Sci* **61**, 1579–1588 (2004).
10. Balch, W. E., Morimoto, R. I., Dillin, A. & Kelly, J. W. Adapting proteostasis for disease intervention. *Science* **319**, 916–919 (2008).
11. Baldwin, A. S. Control of oncogenesis and cancer therapy resistance by the transcription factor NF-κB. *J Clin Invest* **107**, 241–246 (2001).
12. Baranowska, M. *et al.* Interactions between bioactive components determine antioxidant, cytotoxic and nutrigenomic activity of cocoa powder extract. *Free Radic Biol Med* **154**, 48–61 (2020).
13. Barba, F. J., Zhu, Z., Koubaa, M., Sant'Ana, A. S. & Orlien, V. Green alternative methods for the extraction of antioxidant bioactive compounds from winery wastes and by-products: A review. *Trends in Food Science & Technology* **49**, 96–109 (2016).
14. Barrio, S. *et al.* Spectrum and functional validation of PSMB5 mutations in multiple myeloma. *Leukemia* **33**, 447–456 (2019).
15. Baumeister, W. *et al.* Electron microscopy and image analysis of the multicatalytic proteinase. *FEBS Lett* **241**, 239–245 (1988).
16. Bingol, B. & Schuman, E. M. Activity-dependent dynamics and sequestration of proteasomes in dendritic spines. *Nature* **441**, 1144–1148 (2006).

17. Blum, J. S., Wearsch, P. A. & Cresswell, P. Pathways of antigen processing. *Annu Rev Immunol* **31**, 443–473 (2013).
18. Borissenko, L. & Groll, M. 20S proteasome and its inhibitors: crystallographic knowledge for drug development. *Chem Rev* **107**, 687–717 (2007).
19. Bredesen, D. E., Rao, R. V. & Mehlen, P. Cell death in the nervous system. *Nature* **443**, 796–802 (2006).
20. Buac, D. *et al.* From Bortezomib to other Inhibitors of the Proteasome and Beyond. *Current Pharmaceutical Design* **19**, 4025–4038.
21. Campos-Ramírez, A., Márquez, M., Quintanar, L. & Rojas-Ochoa, L. F. Effect of ionic strength on the aggregation kinetics of the amidated amyloid beta peptide Aβ (1-40) in aqueous solutions. *Biophys Chem* **228**, 98–107 (2017).
22. Carter, J. & Lippa, C. F. Beta-amyloid, neuronal death and Alzheimer's disease. *Curr Mol Med* **1**, 733–737 (2001).
23. Carvalho, M. I. *et al.* A Comparative Approach of Tumor-Associated Inflammation in Mammary Cancer between Humans and Dogs. *Biomed Res Int* **2016**, 4917387 (2016).
24. Chang, S. C. & Ding, J. L. Ubiquitination and SUMOylation in the chronic inflammatory tumor microenvironment. *Biochimica et Biophysica Acta (BBA) - Reviews on Cancer* **1870**, 165–175 (2018).
25. Chauhan, D. *et al.* A novel orally active proteasome inhibitor induces apoptosis in multiple myeloma cells with mechanisms distinct from Bortezomib. *Cancer Cell* **8**, 407–419 (2005).
26. Chen, D., Frezza, M., Schmitt, S., Kanwar, J. & Dou, Q. P. Bortezomib as the first proteasome inhibitor anticancer drug: current status and future perspectives. *Curr Cancer Drug Targets* **11**, 239–253 (2011).
27. Chondrogianni, N. & Gonos, E. S. Proteasome Function Determines Cellular Homeostasis and the Rate of Aging. in *Protein Metabolism and Homeostasis in Aging* (ed. Tavernarakis, N.) 38–46 (Springer US, 2010). doi:10.1007/978-1-4419-7002-2_4.
28. Ciechanover, A. Intracellular protein degradation: from a vague idea through the lysosome and the ubiquitin-proteasome system and onto human diseases and drug targeting. *Bioorg Med Chem* **21**, 3400–3410 (2013).
29. Ciechanover, A. & Kwon, Y. T. Degradation of misfolded proteins in neurodegenerative diseases: therapeutic targets and strategies. *Exp Mol Med* **47**, e147 (2015).
30. Coles, M., Bicknell, W., Watson, A. A., Fairlie, D. P. & Craik, D. J. Solution Structure of Amyloid β-Peptide(1−40) in a Water−Micelle Environment. Is the Membrane-Spanning Domain Where We Think It Is?,. *Biochemistry* **37**, 11064–11077 (1998).
31. Collins, G. A. & Goldberg, A. L. The Logic of the 26S Proteasome. *Cell* **169**, 792–806 (2017).

32. Cools, K. & Terry, L. A. Comparative study between extraction techniques and column separation for the quantification of sinigrin and total isothiocyanates in mustard seed. *J Chromatogr B Analyt Technol Biomed Life Sci* **901**, 115–118 (2012).
33. Crescenzi, O. *et al.* Solution structure of the Alzheimer amyloid beta-peptide (1-42) in an apolar microenvironment. Similarity with a virus fusion domain. *Eur J Biochem* **269**, 5642–5648 (2002).
34. Cuanalo-Contreras, K. & Moreno-Gonzalez, I. Natural Products as Modulators of the Proteostasis Machinery: Implications in Neurodegenerative Diseases. *International Journal of Molecular Sciences* **20**, 4666 (2019).
35. De la Peña, A. H., Goodall, E. A., Gates, S. N., Lander, G. C. & Martin, A. Substrate-engaged 26S proteasome structures reveal mechanisms for ATP-hydrolysis-driven translocation. *Science* **362**, eaav0725 (2018).
36. Demuro, A. *et al.* Calcium dysregulation and membrane disruption as a ubiquitous neurotoxic mechanism of soluble amyloid oligomers. *J Biol Chem* **280**, 17294–17300 (2005).
37. Diehl, J. A. & Ponugoti, B. Ubiquitin-Dependent Proteolysis in G1/S Phase Control and Its Relationship with Tumor Susceptibility. *Genes & Cancer* **1**, 717–724 (2010).
38. Dong, Y. *et al.* Cryo-EM structures and dynamics of substrate-engaged human 26S proteasome. *Nature* **565**, 49–55 (2019).
39. Dou, Q. P. & Zonder, J. A. Overview of proteasome inhibitor-based anti-cancer therapies: perspective on bortezomib and second generation proteasome inhibitors versus future generation inhibitors of ubiquitin-proteasome system. *Curr Cancer Drug Targets* **14**, 517–536 (2014).
40. Eggensperger, S. & Tampé, R. The transporter associated with antigen processing: a key player in adaptive immunity. *Biol Chem* **396**, 1059–1072 (2015).
41. Faller, P., Hureau, C. & Berthoumieu, O. Role of Metal Ions in the Self-assembly of the Alzheimer's Amyloid-β Peptide. *Inorg. Chem.* **52**, 12193–12206 (2013).
42. Fan, L. *et al.* New Insights Into the Pathogenesis of Alzheimer's Disease. *Frontiers in Neurology* **10**, 1312 (2020).
43. Giuffrida, M. L. *et al.* Beta-amyloid monomers are neuroprotective. *J Neurosci* **29**, 10582–10587 (2009).
44. Giżyńska, M. *et al.* Proline- and Arginine-Rich Peptides as Flexible Allosteric Modulators of Human Proteasome Activity. *J. Med. Chem.* **62**, 359–370 (2019).
45. Glickman, M. H. & Ciechanover, A. The ubiquitin-proteasome proteolytic pathway: destruction for the sake of construction. *Physiol Rev* **82**, 373–428 (2002).
46. Grasso, G. *et al.* The double faced role of copper in Aβ homeostasis: A survey on the interrelationship between metal dyshomeostasis, UPS functioning and autophagy in neurodegeneration. *Coordination Chemistry Reviews* **347**, (2017).
47. Groll, M. & Huber, R. Substrate access and processing by the 20S proteasome core particle. *Int J Biochem Cell Biol* **35**, 606–616 (2003).

48. Grune, T. *et al.* HSP70 Mediates Dissociation and Reassociation of the 26S Proteasome During Adaptation to Oxidative Stress. *Free Radic Biol Med* **51**, 1355–1364 (2011).
49. Gupta, N. *et al.* Clinical Pharmacology of Ixazomib: The First Oral Proteasome Inhibitor. *Clin Pharmacokinet* **58**, 431–449 (2019).
50. Gursky, O. & Aleshkov, S. Temperature-dependent beta-sheet formation in beta-amyloid Abeta(1-40) peptide in water: uncoupling beta-structure folding from aggregation. *Biochim Biophys Acta* **1476**, 93–102 (2000).
51. Haass, C. & Selkoe, D. J. Soluble protein oligomers in neurodegeneration: lessons from the Alzheimer's amyloid β-peptide. *Nat Rev Mol Cell Biol* **8**, 101–112 (2007).
52. Hamazaki, J. & Murata, S. ER-Resident Transcription Factor Nrf1 Regulates Proteasome Expression and Beyond. *Int J Mol Sci* **21**, E3683 (2020).
53. Hanahan, D. & Weinberg, R. A. The hallmarks of cancer. *Cell* **100**, 57–70 (2000).
54. Hartl, F. U., Bracher, A. & Hayer-Hartl, M. Molecular chaperones in protein folding and proteostasis. *Nature* **475**, 324–332 (2011).
55. Heink, S., Ludwig, D., Kloetzel, P.-M. & Krüger, E. IFN-γ-induced immune adaptation of the proteasome system is an accelerated and transient response. *PNAS* **102**, 9241–9246 (2005).
56. Hideshima, T. *et al.* Molecular mechanisms mediating antimyeloma activity of proteasome inhibitor PS-341. *Blood* **101**, 1530–1534 (2003).
57. Hilbich, C., Kisters-Woike, B., Reed, J., Masters, C. L. & Beyreuther, K. Aggregation and secondary structure of synthetic amyloid beta A4 peptides of Alzheimer's disease. *J Mol Biol* **218**, 149–163 (1991).
58. Holtzman, D. M., Morris, J. C. & Goate, A. M. Alzheimer's disease: the challenge of the second century. *Sci Transl Med* **3**, 77sr1 (2011).
59. Huang, L. & Chen, C. H. Proteasome regulators: activators and inhibitors. *Curr Med Chem* **16**, 931–939 (2009).
60. Hugo, M. *et al.* Early cysteine-dependent inactivation of 26S proteasomes does not involve particle disassembly. *Redox Biol* **16**, 123–128 (2018).
61. Jack, C. R. *et al.* Hypothetical model of dynamic biomarkers of the Alzheimer's pathological cascade. *Lancet Neurol* **9**, 119–128 (2010).
62. Jin, S. *et al.* Amyloid-β(1-42) Aggregation Initiates Its Cellular Uptake and Cytotoxicity. *J Biol Chem* **291**, 19590–19606 (2016).
63. Jones, C. L., Njomen, E., Sjögren, B., Dexheimer, T. S. & Tepe, J. J. Small Molecule Enhancement of 20S Proteasome Activity Targets Intrinsically Disordered Proteins. *ACS Chem Biol* **12**, 2240–2247 (2017).

64. Kanemitsu, H., Tomiyama, T. & Mori, H. Human neprilysin is capable of degrading amyloid beta peptide not only in the monomeric form but also the pathological oligomeric form. *Neurosci Lett* **350**, 113–116 (2003).
65. Karpowicz, P. *et al.* Interplay between Structure and Charge as a Key to Allosteric Modulation of Human 20S Proteasome by the Basic Fragment of HIV-1 Tat Protein. *PLOS ONE* **10**, e0143038 (2015).
66. Katsiki, M., Chondrogianni, N., Chinou, I., Rivett, A. J. & Gonos, E. S. The Olive Constituent Oleuropein Exhibits Proteasome Stimulatory Properties In Vitro and Confers Life Span Extension of Human Embryonic Fibroblasts. *Rejuvenation Research* **10**, 157–172 (2007).
67. Kaundal, M., Zameer, S., Najmi, A. K., Parvez, S. & Akhtar, M. Betulinic acid, a natural PDE inhibitor restores hippocampal cAMP/cGMP and BDNF, improve cerebral blood flow and recover memory deficits in permanent BCCAO induced vascular dementia in rats. *European Journal of Pharmacology* **832**, 56–66 (2018).
68. Keller, J. N., Hanni, K. B. & Markesbery, W. R. Impaired proteasome function in Alzheimer's disease. *J Neurochem* **75**, 436–439 (2000).
69. Kisselev, A. F., Songyang, Z. & Goldberg, A. L. Why does threonine, and not serine, function as the active site nucleophile in proteasomes? *J Biol Chem* **275**, 14831–14837 (2000).
70. Kudriaeva, A., Kuzina, E. S., Zubenko, O., Smirnov, I. V. & Belogurov Jr., A. Charge-mediated proteasome targeting. *The FASEB Journal* **33**, 6852–6866 (2019).
71. Kuperstein, I. *et al.* Neurotoxicity of Alzheimer's disease Aβ peptides is induced by small changes in the Aβ42 to Aβ40 ratio. *EMBO J* **29**, 3408–3420 (2010).
72. LaFerla, F. M., Green, K. N. & Oddo, S. Intracellular amyloid-beta in Alzheimer's disease. *Nat Rev Neurosci* **8**, 499–509 (2007).
73. Lambert, M. P. *et al.* Vaccination with soluble Aβ oligomers generates toxicity-neutralizing antibodies. *Journal of Neurochemistry* **79**, 595–605 (2001).
74. Lau, J. L. & Dunn, M. K. Therapeutic peptides: Historical perspectives, current development trends, and future directions. *Bioorganic & Medicinal Chemistry* **26**, 2700–2707 (2018).
75. Lovell, M. A. A potential role for alterations of zinc and zinc transport proteins in the progression of Alzheimer's disease. *J Alzheimers Dis* **16**, 471–483 (2009).
76. Malgieri, G. & Grasso, G. The clearance of misfolded proteins in neurodegenerative diseases by zinc metalloproteases: An inorganic perspective. *Coordination Chemistry Reviews* **260**, 139–155 (2014).
77. Marshall, R. S. & Vierstra, R. D. Dynamic Regulation of the 26S Proteasome: From Synthesis to Degradation. *Front Mol Biosci* **6**, 40 (2019).
78. Masci, A. *et al.* Neuroprotective Effect of Brassica oleracea Sprouts Crude Juice in a Cellular Model of Alzheimer's Disease. *Oxidative Medicine and Cellular Longevity* **2015**, e781938 (2015).

79. May, L. M. *et al.* G-Protein-Coupled Inwardly Rectifying Potassium (GIRK) Channel Activation by the p75 Neurotrophin Receptor Is Required for Amyloid β Toxicity. *Front Neurosci* **11**, 455 (2017).
80. McAlary, L., Plotkin, S. S. & Cashman, N. R. Emerging Developments in Targeting Proteotoxicity in Neurodegenerative Diseases. *CNS Drugs* **33**, 883–904 (2019).
81. Mitch, W. E. & Goldberg, A. L. Mechanisms of Muscle Wasting — The Role of the Ubiquitin–Proteasome Pathway. *http://dx.doi.org/10.1056/NEJM199612193352507* https://www.nejm.org/doi/10.1056/NEJM199612193352507(2009).
82. Morel, B., Carrasco, M. P., Jurado, S., Marco, C. & Conejero-Lara, F. Dynamic micellar oligomers of amyloid beta peptides play a crucial role in their aggregation mechanisms. *Phys. Chem. Chem. Phys.* **20**, 20597–20614 (2018).
83. Murakami, A. Modulation of protein quality control systems by food phytochemicals. *J Clin Biochem Nutr* **52**, 215–227 (2013).
84. Murata, S., Takahama, Y., Kasahara, M. & Tanaka, K. The immunoproteasome and thymoproteasome: functions, evolution and human disease. *Nat Immunol* **19**, 923–931 (2018).
85. Myeku, N. *et al.* Tau-driven 26S proteasome impairment and cognitive dysfunction can be prevented early in disease by activating cAMP-PKA signaling. *Nat Med* **22**, 46–53 (2016).
86. Naoi, M., Shamoto-Nagai, M. & Maruyama, W. Neuroprotection of multifunctional phytochemicals as novel therapeutic strategy for neurodegenerative disorders: antiapoptotic and antiamyloidogenic activities by modulation of cellular signal pathways. *Future Neurology* **14**, FNL9 (2019).
87. Nunan, J. & Small, D. H. Regulation of APP cleavage by alpha-, beta- and gamma-secretases. *FEBS Lett* **483**, 6–10 (2000).
88. O'Nuallain, B., Shivaprasad, S., Kheterpal, I. & Wetzel, R. Thermodynamics of Abeta(1-40) amyloid fibril elongation. *Biochemistry* **44**, 12709–12718 (2005).
89. Papaevgeniou, N. *et al.* 18α-Glycyrrhetinic Acid Proteasome Activator Decelerates Aging and Alzheimer's Disease Progression in Caenorhabditis elegans and Neuronal Cultures. *Antioxid Redox Signal* **25**, 855–869 (2016).
90. Pickering, A. M. & Davies, K. J. A. Differential roles of proteasome and immunoproteasome regulators Pa28αβ, Pa28γ and Pa200 in the degradation of oxidized proteins. *Arch Biochem Biophys* **523**, 181–190 (2012).
91. Potts, B. C. & Lam, K. S. Generating a Generation of Proteasome Inhibitors: From Microbial Fermentation to Total Synthesis of Salinosporamide A (Marizomib) and Other Salinosporamides. *Marine Drugs* **8**, 835–880 (2010).
92. Raiss, C. C. *et al.* Functionally different α-synuclein inclusions yield insight into Parkinson's disease pathology. *Sci Rep* **6**, 23116 (2016).

93. Regitz, C., Fitzenberger, E., Mahn, F. L., Dußling, L. M. & Wenzel, U. Resveratrol reduces amyloid-beta (Aβ1–42)-induced paralysis through targeting proteostasis in an Alzheimer model of Caenorhabditis elegans. *Eur J Nutr* **55**, 741–747 (2016).
94. Roeten, M. S. F., Cloos, J. & Jansen, G. Positioning of proteasome inhibitors in therapy of solid malignancies. *Cancer Chemother Pharmacol* **81**, 227–243 (2018).
95. Santoro, A. M. *et al.* Pyrazolones Activate the Proteasome by Gating Mechanisms and Protect Neuronal Cells from β-Amyloid Toxicity. *ChemMedChem* **15**, 302–316 (2020).
96. Seals, D. F. & Courtneidge, S. A. The ADAMs family of metalloproteases: multidomain proteins with multiple functions. *Genes Dev.* **17**, 7–30 (2003).
97. Sengupta, U., Nilson, A. N. & Kayed, R. The Role of Amyloid-β Oligomers in Toxicity, Propagation, and Immunotherapy. *EBioMedicine* **6**, 42–49 (2016).
98. Shah, C. *et al.* Efficacy and safety of carfilzomib in relapsed and/or refractory multiple myeloma: systematic review and meta-analysis of 14 trials. *Oncotarget* **9**, 23704–23717 (2018).
99. Shen, C. L. & Murphy, R. M. Solvent effects on self-assembly of beta-amyloid peptide. *Biophysical Journal* **69**, 640–651 (1995).
100. Shin, E.-C., Sung, P. S. & Park, S.-H. Immune responses and immunopathology in acute and chronic viral hepatitis. *Nat Rev Immunol* **16**, 509–523 (2016).
101. Sinha, S. *et al.* Purification and cloning of amyloid precursor protein beta-secretase from human brain. *Nature* **402**, 537–540 (1999).
102. Smith, D. G., Cappai, R. & Barnham, K. J. The redox chemistry of the Alzheimer's disease amyloid beta peptide. *Biochim Biophys Acta* **1768**, 1976–1990 (2007).
103. Smith, D. M. *et al.* Docking of the proteasomal ATPases' carboxyl termini in the 20S proteasome's alpha ring opens the gate for substrate entry. *Mol Cell* **27**, 731–744 (2007).
104. Su, Y. & Chang, P. T. Acidic pH promotes the formation of toxic fibrils from beta-amyloid peptide. *Brain Res* **893**, 287–291 (2001).
105. Subedi, L. & Gaire, B. P. Tanshinone IIA: A phytochemical as a promising drug candidate for neurodegenerative diseases. *Pharmacological Research* **169**, 105661 (2021).
106. Tai, H.-C. *et al.* The Synaptic Accumulation of Hyperphosphorylated Tau Oligomers in Alzheimer Disease Is Associated With Dysfunction of the Ubiquitin-Proteasome System. *The American Journal of Pathology* **181**, 1426–1435 (2012).
107. Talalay, P. *et al.* Sulforaphane mobilizes cellular defenses that protect skin against damage by UV radiation. *Proc Natl Acad Sci U S A* **104**, 17500–17505 (2007).
108. Terzo, M. N. *et al.* Evaluation of a sicilian black broccoli extract on in vitro cell models. *Acta horticulturae* (2018).
109. Thibaudeau, T. A., Anderson, R. T. & Smith, D. M. A common mechanism of proteasome impairment by neurodegenerative disease-associated oligomers. *Nat Commun* **9**, 1097 (2018).

110. Thibaudeau, T. A. & Smith, D. M. A Practical Review of Proteasome Pharmacology. *Pharmacol Rev* **71**, 170–197 (2019).
111. Trippier, P. C. *et al.* Proteasome Activation is a Mechanism for Pyrazolone Small Molecules Displaying Therapeutic Potential in Amyotrophic Lateral Sclerosis. *ACS Chem. Neurosci.* **5**, 823–829 (2014).
112. Tseng, B. P., Green, K. N., Chan, J. L., Blurton-Jones, M. & LaFerla, F. M. Abeta inhibits the proteasome and enhances amyloid and tau accumulation. *Neurobiol Aging* **29**, 1607–1618 (2008).
113. Tundo, G. R. *et al.* The proteasome as a druggable target with multiple therapeutic potentialities: Cutting and non-cutting edges. *Pharmacol Ther* **213**, 107579–107579 (2020).
114. Vassar, R. *et al.* Beta-secretase cleavage of Alzheimer's amyloid precursor protein by the transmembrane aspartic protease BACE. *Science* **286**, 735–741 (1999).
115. Walsh, D. M., Klyubin, I., Fadeeva, J. V., Rowan, M. J. & Selkoe, D. J. Amyloid-beta oligomers: their production, toxicity and therapeutic inhibition. *Biochem Soc Trans* **30**, 552–557 (2002).
116. Wilquet, V. & De Strooper, B. Amyloid-beta precursor protein processing in neurodegeneration. *Curr Opin Neurobiol* **14**, 582–588 (2004).
117. Yao, T. & Cohen, R. E. A cryptic protease couples deubiquitination and degradation by the proteasome. *Nature* **419**, 403–407 (2002).
118. Yeo, I. J. *et al.* A dual inhibitor of the proteasome catalytic subunits LMP2 and Y attenuates disease progression in mouse models of Alzheimer's disease. *Sci Rep* **9**, 18393 (2019).
119. Yin, K.-J. *et al.* Matrix metalloproteinases expressed by astrocytes mediate extracellular amyloid-beta peptide catabolism. *J Neurosci* **26**, 10939–10948 (2006).
120. Yoshiike, Y. *et al.* New insights on how metals disrupt amyloid beta-aggregation and their effects on amyloid-beta cytotoxicity. *J Biol Chem* **276**, 32293–32299 (2001).
121. Zhang, B., Wang, X., Yang, Y. & Zhang, X. Extraction and identification of isothiocyanates from broccolini seeds. *Nat Prod Commun* **6**, 65–66 (2011).
122. Zhao, X. & Yang, J. Amyloid-β Peptide Is a Substrate of the Human 20S Proteasome. *ACS Publications* https://pubs.acs.org/doi/pdf/10.1021/cn100067e (2010) doi:10.1021/cn100067e.
123. Zhao, X. & Yang, J. Amyloid-β peptide is a substrate of the human 20S proteasome. *ACS Chem Neurosci* **1**, 655–660 (2010).
124. Zhou, H.-J. *et al.* Design and Synthesis of an Orally Bioavailable and Selective Peptide Epoxyketone Proteasome Inhibitor (PR-047). *J. Med. Chem.* **52**, 3028–3038 (2009).

9. PUBLISHED PAPERS

Ubiquitin binds the Amyloid β peptide and interferes with its clearance pathways

By

F. Bellia[a], V. Lanza[a], S. García-Viñuales[a], I. M. M. Ahmed[a], A. Pietropaolo[b], C. Iacobucci[c], G. Malgieri[d], G. D'Abrosca[d], R. Fattorusso[d], **V. G. Nicoletti**[e], D. Sbardella[f], G. R. Tundo[f], M. Coletta[f], L. Pirone,[g] E. Pedone,[g] **D. Calcagno,**[h] G. Grasso,*[h] D. Milardi[a*]

[a]*Consiglio Nazionale delle Ricerche, Istituto di Biostrutture e Bioimmagini, Via P. Gaifami 18, 95126 Catania, Italy;*
[b]*Dipartimento di Scienze della Salute, Universita` degli Studi Magna Graecia di Catanzaro, Viale Europa, 88100, Catanzaro, Italy;*
[c]*Department of Pharmaceutical Chemistry & Bioanalytics, Institute of Pharmacy, Martin Luther University Halle-Wittenberg, 06120 Halle/Saale, Germany;*
[d]*Department of Environmental, Biological and Pharmaceutical Sciences and Technologies, University of Campania "Luigi Vanvitelli", Via Vivaldi 43, 81100 Caserta, Italy;*
[e]*Dipartimento di Scienze Biomediche e Biotecnologiche (BIOMETEC), sez. Biochimica medica, Università di Catania, Via Santa Sofia 97, 95124 Catania, Italy;*
[f]*Dipartimento di Scienze Cliniche e Medicina Traslazionale, Università di Roma Tor Vergata, Via Montpellier 1, 00133, Roma, Italy;*
[g]*Consiglio Nazionale delle Ricerche, Istituto di Biostrutture e Bioimmagini, Via Mezzocannone, 16, Naples I-80134 Italy;*
[h]*Dipartimento di Scienze Chimiche, Università di Catania, V.le Andrea Doria 6, 95125 Catania, Italy; Italy;*
E-mail:grassog@unict.it; danilo.milardi@cnr.it

Abstract

Several lines of evidence point to a compromised proteostasis associated to a reduction of the Ubiquitin Proteasome System (UPS) activity in patients affected by Alzheimer's Disease (AD) and suggest that the amyloid β peptide (Aβ) is an important player in the game. Inspired also by many reports, underlining the presence of ubiquitin (Ub) in the amyloid plaques of AD brains, here we set out to test whether Ub may bind the Aβ peptide and have any effect on its clearance pathways. By using an integrated array of MALDI-TOF/UPLC-HRMS, fluorescence, NMR, SPR, Microscale Thermophoresis (MST) and molecular dynamics studies, we consistently demonstrated that Aβ40 binds Ub with a 1:1 stochiometry and K_d in the high micromolar range. In particular, we show that the N-terminal domain of Aβ peptide (through residues D1, E3 and R5) interacts with the C-terminal tail of Ub (involving residues K63 and E64), inducing the central region of Aβ (^{14}HQKLVFFAEDVGSNK^{28}) to adopt a mixed α-helix/β-turn structure. ELISA assays, carried out in neuroblastoma cell lysates, suggest that Aβ competitively binds Ub also in the presence of the entire pool of cytosolic Ub binding proteins. Ub-bound Aβ has a lower tendency to aggregate into amyloid-like fibrils and is more slowly degraded by the Insulin degrading Enzyme (IDE). Finally, we observe that the water soluble fragment Aβ1-16 significantly inhibits Ub chain growth reactions. These results evidence how the non-covalent interaction between Aβ peptides and Ub may have relevant effects on the regulation of the upstream events of the UPS and pave the way to future *in vivo* studies addressing the role played by Aβ peptide in the malfunction of proteome maintenance occurring in AD.

Introduction

Alzheimer's disease (AD), the most common form of dementia worldwide, is an age-related, fatal neurodegenerative disorder. A hallmark of AD is the presence of extracellular proteinaceous deposits (senile plaques) in the brain of affected people. The prevalent component of senile plaques is the β-amyloid (Aβ).[1] Although a firm relationship between the occurrence of different Aβ aggregates in the AD brain and the severity of the disease has not been established yet, Aβ misfolding and self-assembly are widely believed to be crucial pathogenic events in AD (amyloid hypothesis)[2–4]. Unfortunately, all clinical trials of amyloid-targeting drugs have failed so far[5,6] suggesting that the amyloid hypothesis needs to be reconsidered. Intriguingly, several reports put in evidence that transgenic mice models of AD show an intracellular Aβ immunoreactivity[7] which occurs before cognitive loss and massive amyloid plaques deposition and that may be more closely associated with the disease progress.[8] Therefore, studies focusing on the interplay between Aβ amyloid growth and protein clearance in the cell represent a promising arena for the design of more effective AD therapies.[9]

The removal of misfolded and potentially toxic cytosolic proteins is mostly regulated by the ubiquitin proteasome system (UPS).[10] The first component of the UPS is Ubiquitin (Ub), a small protein composed of 76 amino acids, with a compact globular structure characterized by a mixed parallel/anti-parallel β-sheet packing against an α-helix.[11] Degradation of misfolded proteins by the UPS occurs first by labeling a lysine residue of the substrate with a (poly)ubiquitin tag (ubiquitinylation) which is specifically identified and degraded by the proteasome.[12] When the UPS is not efficient, the removal of toxic protein assemblies gets slower and, in turn, the disease may progress more rapidly.

Consistently with this hypothesis, many reports suggest that UPS malfunction plays a significant role in Aβ accumulation and, in turn, in AD progress[13] However, the effects of Aβ on proteasome function are still under debate. In particular if, on one hand, Aβ peptide has been observed to be a proteasome inhibitor by its own,[14–21] on the other hand some studies have outlined how distinct Aβ peptide assemblies may inhibit or even activate different proteasome particles[22] The controversial role of Aβ in affecting proteasome function as well as the presence of Ub-positive proteinaceous aggregates in the senile plaques of AD patients[23] suggests that UPS malfunction observed in AD could be then more likely linked to a failure of its upstream components (*i.e.*, ubiquitinylation)[24]

Ubiquitinylation needs the coordinated activity of three distinct types of enzyme: i) an ATP-consuming Ub-activating enzyme (E1); ii) a Ub-conjugating enzyme (E2) and a Ub

ligase (E3).[25] Further, the fact that these processes are largely governed by low-affinity interactions between Ub and the various Ub-writing enzymes (*i.e.*, E1, E2 and E3)[26] envisages the possibility that an excess of Aβ might inhibit, as a decoy effect, these processes through non covalent binding to Ub.

To test this hypothesis, here we use a battery of experimental (NMR, SPR, cross-linking XL ESI-MS, MALDI-TOF MS) and *in silico* (MD) approaches to fully characterize the interactions of Ub with the Aβ amyloid peptide in terms of stoichiometry, affinity and binding sites. Next, we employ an ELISA assay to evaluate if the interaction of Aβ with Ub is detectable in cell lysates too, thus supporting the significance of this study in a biological context. These experiments are also paralleled by ESI-MS studies addressing Aβ hydrolysis by the Insulin Degrading Enzyme (IDE), a protease which is known to be involved in the physiological amyloid clearance[27] The effects of Ub on Aβ amyloid aggregation and Ub chain growth reactions are finally investigated.

Results and Discussion

NMR analysis of Ub in complex with Aβ40.

In an attempt to assess if Ub binds Aβ, we first analyzed Ub/Aβ interactions in solution by NMR spectrocopy. Free ^{15}N-^{13}C labeled Ub was characterized by means of a standard set of triple and double resonance experiments that constituted the reference spectra. There are two naturally occurring forms of Aβ peptide: Aβ42 and Aβ40. Although Aβ42 is known to be more prone to form amyloid aggregates, Aβ40 is produced more abundantly in the cell (Aβ40:Aβ42 molar ratio is 9:1) and thus may be more conveniently used to investigate interactions with Ub.[28] Unlabeled Aβ40 was then added as single aliquot of known amount to the sample and a new set of spectra was recorded. The translational diffusion coefficient, chemical shift and intensity variations of the different nuclei in the presence and absence of Aβ were evaluated. The translational diffusion coefficient measured for Ub in absence of the peptide is (1.33±0.12) x 10^{-10} m^2 s^{-1}, consistent with the values reported in the literature.[29] The same coefficient measured in the presence of Aβ40 is (1.28±0.18) x 10^{-10} m^2 s^{-1}. These coefficients allow us to rule out protein–protein aggregation phenomena mediated by Aβ40 within the NMR spectroscopic concentration range investigated and are in agreement with the interaction between the two molecules. The analysis of Ub HSQC after sub-stoichiometric Aβ40 addition shows that the overall Ub fold is maintained, although a number of peaks are perturbed. As proteins-ligand interactions correspond often to a redistribution of the protein internal dynamics[30–33] intensity changes of the amide cross-peaks in the 2D [^1H,^{15}N]-HSQC spectra represent sensitive probes of exchange and/or relaxation rates variations of each protein residue upon interaction (see Fig. S1 in the Electronic Supporting Information). Perturbation of signal intensities with respect to the reference spectra as a function of ligand addition thus provide useful dynamic and conformational information about the binding event. Mapping the differences in normalized signal intensities onto the Ub structure (Fig. 1 upper panel) outlines a region influenced by the interaction with Aβ40, which involves the residues belonging to the C-terminal tail and the β sheet of the molecule, leading to a loss in intensity of their HSQC cross-peaks (Fig. 1 lower panel). The residues composing the helix appear not to be involved in the interaction as their cross-peaks are less influenced by the presence of the peptide in solution.

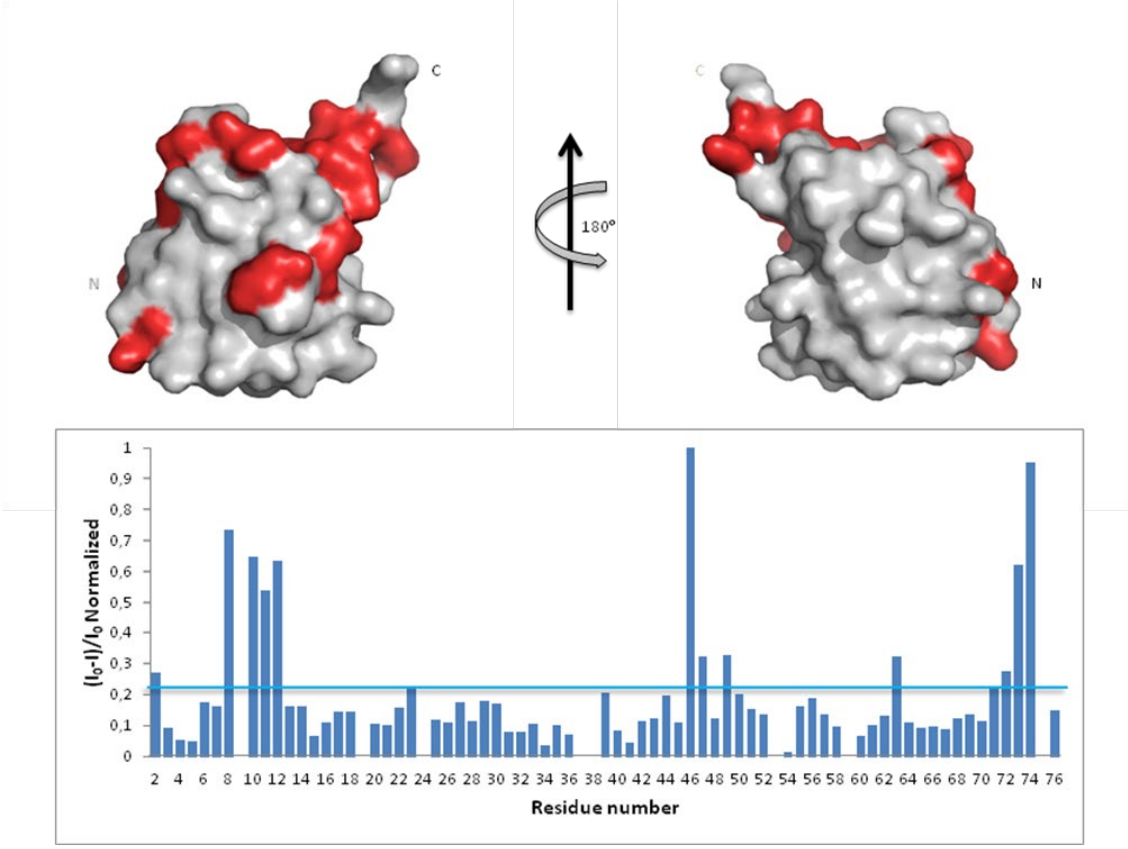

Figure 1. Upper panel: mapping onto the Ub structure of the intensity variations of the ^{1}H and ^{15}N amide cross-peaks after the addition of Aβ40 defines a neat region of the peptide interaction. The residues whose peaks were reduced in intensity are reported in red. Lower panel: ^{1}H and ^{15}N amide cross-peaks intensity variations of the Ub HSQC spectrum after the addition of 30 μM Aβ40 reported as a function of protein residue numbers.

Molecular modeling of Ub/Aβ complexes

NMR analysis provides molecular details about the Ub residues directly involved in the interaction with Aβ. These data are used as a starting point to describe, at an atomistic level, the Ub-bound conformation of Aβ by molecular modeling. Upon Aβ40 interacts with Ub, three main binding poses may be disclosed (Fig. 2A). The first binding pose is featured by a network of salt-bridges involving the N-terminal section of Aβ40, with residues D1, E3 and K28 facing the Ub K6 residue (Fig. 2Aa). This interaction triggers hydrophobic contacts between the Ub central region and Aβ40, which adopts mainly turn conformations with a short 3_{10} helix involving the ^{16}KLV^{18} segment. At variance with the latter binding surface, in the second binding pose, the N-terminal domain of Aβ40 faces the Ub C-terminal region. Herein, Aβ40 residues D1, E3 and R5 contact Ub residues K63 and E64, perturbing the typical salt-bridge network featuring the free Ub structure (Fig. 2Ab). The central region of Aβ40 is less prone to interact with Ub owing to the intramolecular interactions building an α-helix in the ^{14}HQKLVFFAEDVGSNK^{28} segment. In the third binding pose, the Aβ40 charged N-terminal amine of D1 faces residue E64 of Ub (Fig. 2Ac). Even in this binding pose, the salt-bridge between K63 and E64 is affected by the N-terminal amine group. Furthermore, D23 contacts R42 which is close to R72, perturbing the typical network of the charged arginine residues of Ub structure. The central region of Aβ40 is involved in a loop, forming small β-turn, which involve the segments ^{16}KL^{17} and ^{35}MV^{36}. On the whole, the Aβ40 N-terminal domain interacts with both the N- or C-terminal region of Ub triggering subtle variations in the Aβ central domain which folds in α-helical structures resembling those observed elsewhere for membrane – bound Aβ peptides.[34] Notably, molecular modeling suggests that the Ub binding induces significant structural constraints along the region encompassing the hydrophobic Phe residues of Aβ.

Cross-linking experiments. Chemical cross-linking/mass spectrometry (XL-MS) is a well-established tool that allows gaining insights into protein conformations and protein-protein interactions[35–38] It relies on creating distance constraints between cross-linked amino acid side chains that can further be used to derive protein structures. Cross-linking can involve two residues belonging to a common protein or to different proteins of a supramolecular complex. In this study disuccinimidyl dibutyric urea (DSBU)[39] has been used as homobifunctional cross-linker. Its succinimidyl ester (NHS-ester) head groups can react with nucleophilic side chains of Lys, Ser, Thr, and Tyr, and with the N-terminus of proteins fixing their spatial arrangement. The cross-linked proteins and protein assemblies can be subsequently studied by mass spectrometry (MS) following a bottom-up approach. Such a process allows to

unambiguously identify the cross-linked amino acid, proving their proximity in the native structure of the protein assembly.[40] Cross-linking experiments of Ub in the presence of Aβ40 have been performed at pH 8 and DSBU has been employed as a reagent for covalently bridging Lys, N-termini, Ser, Thr, and Tyr, which lie within a Cα-Cα distances range of 27 Å. Cross-linked samples were submitted to a proteomic analysis following a bottom-up approach and data were scrutinized with MeroX software. Several intra- and inter-molecular crosslinks have been identified for the Ub/Aβ40 complex. Thirteen unique intramolecular Ub cross-links (Table S1 in Electronic Supporting Information) were mapped onto its X-ray structures (PDB code 1UBQ, 1.8 Å resolution)[11] The relevant Euclidean Cα-Cα distances measured fall within the range of 6.2 to 20.2 Å with an average of 15.3 Å and are fully consistent with the known 3D arrangement of Ub. Intra-molecular Aβ40 cross-links were not considered for deriving structural information. In fact, it is not possible to distinguish between inter- and intra-molecular cross-links of Aβ40 as oligomeric Aβ40 aggregates may be present in solution during the cross-linking reaction. Four intermolecular cross-links were found between Ub and Aβ40. Interestingly, they exclusively involve the N-terminal region of Aβ40. In particular, Aβ40 D1 was found to be connected to K48 and K63 of Ub. The other two bridges were found between S8 or Y10 of Aβ40 and K48 and K63 of Ub. The targeted residues (S8 or Y10) of Aβ40 could not be assigned unambiguously. These cross-links were mapped onto the three 3D structure models of Ub/ Aβ40 complex disclosed by theoretical calculations (Fig. 2B). In all three binding poses the Euclidean Cα-Cα distances measured are < 27 Å, in agreement with the distances that DSBU can connect. Interestingly, the overall surface of Ub predicted to interact with Aβ40 is confirmed. However, the cross-links involving K63 partially tunnel the protein chains in pose “a” and can be explained only by an high Aβ40 flexibility. Conversely, all cross-links are fully consistent with the calculated binding poses “b” and “c” (Fig. 2A). These results mainly support the proposed binding poses “b” and “c” suggesting a structural organization of the Ub/Aβ40 complex where the N-terminal part of Aβ40 is in close proximity to the salt-bridge between K63 and E64 in Ub. The binding of Aβ42 with Ub disclosed through molecular simulations features lesser non-covalent interactions than those detected in the binding of Aβ40 with Ub. In particular, the salt-bridge network involving D1, E3 and K28 residues and the K6 residue of Ub is herein replaced by a salt-bridge interaction involving D11 or D7 with K6. Furthermore, the salt-bridge interaction between K63 and E64 of Ub remains unperturbed in the presence of Aβ42 and no charged residue of Aβ42 contact R42 or R72 of Ub (see Fig. S2 of the Electronic Supporting Information).

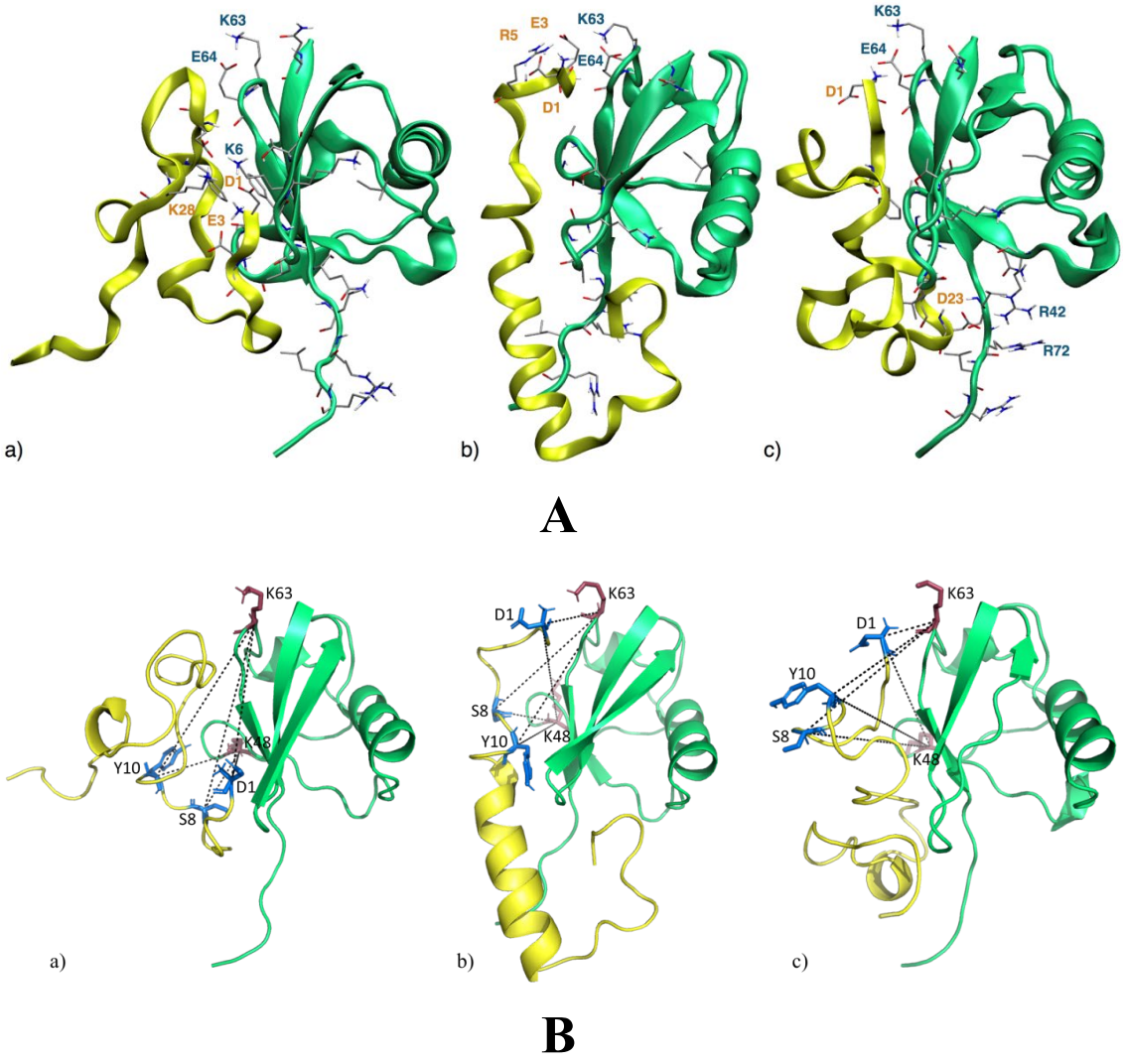

Figure 2. Panel A. The three lowest energy binding modes for the Aβ40/Ub complex. Aβ40 sections are shown by yellow ribbons, Ub sections are shown by green ribbons. The residues of Ub interacting with Aβ40 are shown by solid sticks and those involved in salt-bridge interactions are also labeled. The internal energies of the Aβ40/Ub complex in the three binding poses a) -c) are -4490 kcal/mol, -4404 kcal/mol and -4271 kcal/mol, respectively. Panel B. DSBU cross-links mapped onto the three lowest energy binding modes for the Aβ40/Ub complex. Aβ40 sections are shown in yellow, Ub sections are shown in green. The cross-linked residues of Aβ40 are shown by blue solid sticks and cross-linked residues of Ub are reported as red solid sticks. All the measured Cα-Cα Euclidean distances are shorter than 27 Å as required by the DSBU cross-linker.

Measurement of dissociation constants (Kd) of the Aβ40/Ub complex.

The majority of known Ub binding partners are characterized by affinities in the micro-molar range (2 μM<K_D<200 μM).[41] Here, to evaluate the binding affinity Aβ to Ub, we

performed SPR analysis on immobilized Aβ. Ub solutions were prepared by dissolving the protein in PBS 10mM (pH 7.4)/Tween 20 (0,05%) and the injections were carried out in serial configuration for 5 minutes at 20 µl/min. Ubiquitin solutions were prepared dissolving the protein in PBS 10mM (pH 7.4)/Tween 20 (0,05%) and the injections were carried out in serial configuration for 5 minutes at 30 µl/min. Different concentration solutions of ubiquitin (43 µM, 86 µM, 171 µM, 343 µM, 755 µM) were prepared and after each injection a regeneration step was achieved using NaCl 2M/NaOH 10mM (30 µl/min for 3 minutes). Resulting sensograms, obtained after reference subtraction, were extracted with MP-SPR Navi Data viewer analyzed through the Trace Drawer™ software and kinetic parameters of the interaction between ubiquitin and $A\beta_{40}$ were calculated. Panel A of Fig 3 represents the overlay between experimental curves and fitted ones, while in Fig. S3 of the Electronic Supporting Information the fitting residual values graph is reported. The fitting model adopted was "OneToOne", which describes one monovalent ligand binding to one target. In this case, the following equation can be assumed to describe the biomolecular interactions:

$dY/dt = (k_a * c - k_d) * Y$

where Y is the recorded signal ($Y(t=0) = 0$), c is the concentration of ligand in the bulk liquid, t is the time in second, k_a [1/(M*s)] is the association rate constant and k_d (1/s) is the dissociation rate constant. Fitting parameters are reported in Table S4 in the Electronic Supporting Information, where B_{max} represents the maximum signal, dependent on e.g. the number of receptors. All four fittings converge to the same kinetic parameters and reveal that Aβ binds Ub with a $K_D = 3.56 \times 10^{-4}$ M. In order to confirm that the Kd value obtained by SPR is not due to artifacts intrinsically linked to the SPR approach (immobilization of the Aβ40 on a solid substrate), it could be advantageous to evaluate the Ub/Aβ binding constants by an independent technique. Microscale thermophoresis (MST) is a technology for the biophysical analysis of interactions between biomolecules. Microscale thermophoresis is based on the detection of a temperature-induced change in fluorescence of a target as a function of the concentration of a non-fluorescent ligand. Normalized fluorescence (Fnorm) is used to quantify binding via MST: Fnorm = F1/F0 where F1 is the fluorescence measured several seconds after the IR-laser has been turned on, when the traces of unbound and bound state can be discriminated, while F0 refers to the initial fluorescence. Plotting these values against the ligand concentration results in a typical binding isotherm providing the affinity constant value of the interaction.

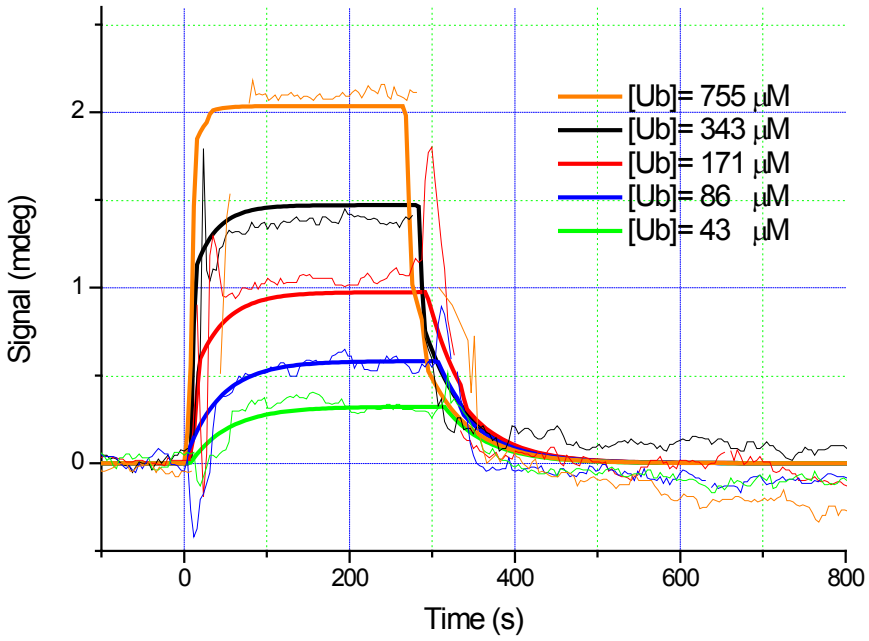

A

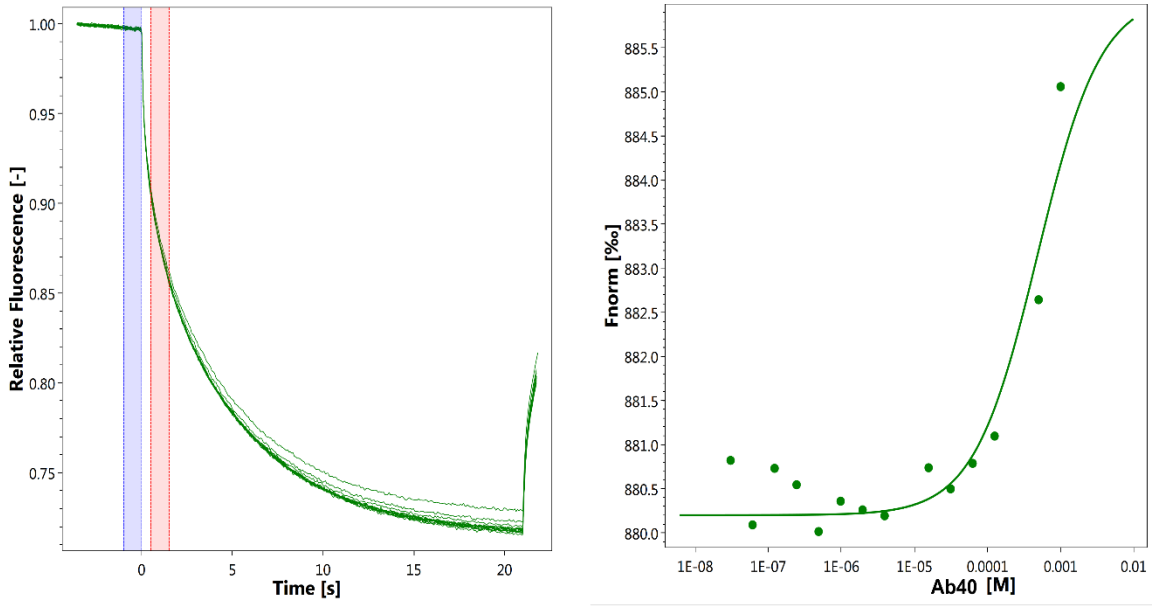

B

Figure 3. Panel A): Sensograms (thin lines) and fitted curves (bold lines) of ubiquitin interacting with immobilized Aβ40. Five concentrations of ubiquitin were injected: 43 µM (green lines)- 86 µM (blue lines)- 171 µM (red lines)- 343 µM (black lines)- 755 µM (orange lines). Panel B): MST traces (left) of titrations of Aβ40 against Ubiquitin; F0 (blue bar) and F1 (red bar) correspond to the fluorescence of unbound state and bound state respectively. Plot of normalized fluorescence (right) obtained from Ub binding experiment versus Aβ40 at different concentrations (from 1 mM to 20 nM).

First, we carried out MST experiments to measure Kd for Ub binding to Aβ40 (see Fig. 3 panel B). Next, to rule out any possible bias due to amyloid aggregation, we analysed also $A\beta_{1\text{-}16}$, a short soluble fragment that is thought to encompass the residues of the amyloid peptide involved in Ub interaction. (see Fig. S4 in the electronic Supporting Information). We found that Ub is able to bind both the molecules with a comparable Kd (Kd Aβ40 = 4.8×10^{-4} M and Kd $A\beta_{1\text{-}16}$, = 3.4×10^{-4} M) in agreement with SPR data.

Aβ competitively binds Ub in whole cell extracts.

SPR analysis has demonstrated that Aβ binds Ub with a binding affinity which is comparable with those observed for many other Ub binding proteins.[40] Therefore, our next step was to confirm if Aβ may competitively bind Ub also in the presence of the complete pool of cellular Ub binding partners. To this aim, we investigated the interaction of Ub with Aβ peptide in the presence of whole cell extracts from previously differentiated SHSY5Y neuroblastoma cells. Enzyme-linked immunosorbent assay (ELISA) is a convenient method widely employed to analyze protein-protein interactions in complex biological mixtures. Here, we employ an ELISA inhibition procedure, using alternatively Ub or Aβ40 as the solution binding partner to demonstrate that Aβ maintains its ability to bind Ub also in the presence of all natural cytosolic Ub binding partners (Fig. 4). Aβ peptide binding to Ub-coated well surface shows an overwhelming increase of the signal over the control. In this case, the presence of cell lysate reduced the Aβ40 binding to Ub by about 50%, thus demonstrating that Ub binds Aβ, albeit with a reduced signal intensity, also in the presence of the complete pool of cellular Ub binding partners. In a second control experiment, Ub binding to Aβ40 peptide immobilized on the well surface of ELISA plate shows a significantly increased signal too (Fig. S5 of Electronic Supporting Information). As in the previous experiment, the binding is counteracted by the presence of cell lysate thus demonstrating that Aβ may competitively bind Ub also in the presence of all cytosolic components.

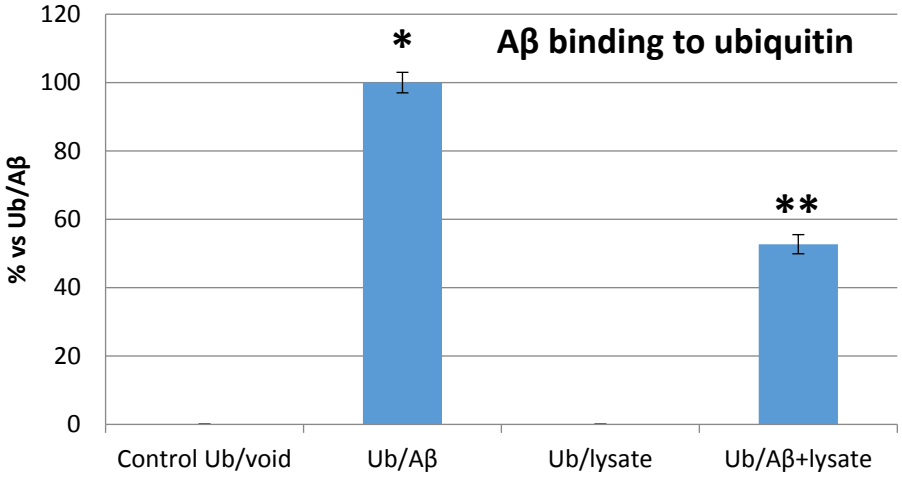

Figure 4. Inhibition ELISA histograms for different Aβ solutions (Ub/void: buffer; Ub/Aβ: 10 μM Aβ in buffer solution; Ub/Lys: whole cell lysates; Aβ/Ub+Lys: 10 μM Aβ in cell lysate) added to Ub-coated microwells (panel C). Significant differences from control values were indicated by ($p<0.05$) * (vs. control) ** (vs. lysate competition) (one-way ANOVA with Tukey's post hoc test). Normalized data are reported as percentages considering as 100% the signal referring to the Ub/Aβ solution.

The proteolytic activity of IDE versus Aβ40 is altered by Ubiquitin.

Once established that Aβ may bind Ub in the cytosol, it is important to evaluate how this interaction may interfere with the physiological peptide clearance. The cellular homeostasis of Aβ is regulated by several proteases and degrading systems[42] among which IDE gives a particularly important contribution to the clearance of amyloidogenic peptides[43] including Aβ, amylin and insulin[44–47]. Thus, any substance that somehow interacts with Aβ under physiological conditions could reasonably affect its IDE-mediated hydrolysis. In this context, the dose-dependent effect of Ub on the IDE-catalyzed hydrolysis of Aβ has been evaluated through a proteomic approach based on Ultra Performance Liquid Chromatography (UPLC) coupled with High Resolution Mass Spectrometry (HRMS). The enzymatic degradation of the amyloid peptide produced nine peptide fragments within 60 min of reaction (Table S3 of Electronic Supporting Information). As previously described,[48] in the early stage of the IDE-mediated hydrolysis, the main targeted regions encompass the hydrophobic Phe residues, the vicinal His residues, and, to a lesser extent, Asn27 and Met35 (Fig. 5A). By means of the LC-MS analysis, all complementary peptide fragments adjacent to each cleavage site have been detected. The total amount of the full length substrate (*i.e.*, Aβ40) clearly decreases over the reaction time (Fig. 5B), such that after 20 min of reaction the concentration of Aβ40 is 28%

relative to the initial value and drops down to 5% after 30 min. Such a trend is maintained when Ub was added in the reaction mixture but, noteworthy, the rate of decrease is affected by Ub in a dose-dependent manner (Fig. 5B). When the Ub:Aβ40 molar ratio is 0.5:1, the residual substrate is 32% after 30 minutes with respect to the starting condition. Finally, 56% of Aβ40 is still present after 60 min of reaction at the highest Ub:Aβ40 molar ratio tested (3:1). Although the documented interaction between IDE and Ub[49] does not rule out the possibility that Ub itself might somewhat affect IDE proteolytic activity, data reported in Fig. 5 represent a clear evidence in favor of an inhibitory effect by the non-covalent interaction between Ub and Aβ40 on the IDE-mediated hydrolysis of Aβ40, in accordance to the other methodological approaches adopted throughout this paper. In order to elucidate the regions of the Aβ sequence mainly involved in the interaction with Ub, the amount of all the peptide fragments was reported as function of the Ub:Aβ40 molar ratio (Fig. 5C). In the absence of Ub (green bars) and in samples collected after 60 min reaction, the chromatographic peaks having the higher intensity are those related to the complementary peptides $A\beta_{1-19}$ and $A\beta_{20-40}$, whereas $A\beta_{1-20}$, $A\beta_{21-40}$, $A\beta_{14-40}$ and $A\beta_{15-40}$ are barely detectable. Increasing amounts of Ub had a very small effect on the concentration of $A\beta_{1-20}$ and $A\beta_{21-40}$; only a slight increase was observed for $A\beta_{1-19}$, whilst the concentration of $A\beta_{14-40}$, $A\beta_{15-40}$ and $A\beta_{20-40}$ was greatly affected by the presence of Ub in a dose-dependent manner. In particular, the formation of $A\beta_{15-40}$ (and even more of $A\beta_{14-40}$) is activated by the presence of Ub, whereas the formation of $A\beta_{20-40}$ is greatly inhibited proportionally to the concentration of Ub. The opposite trend, relative to the amounts of these peptide fragments formed at the various peptide:Ub ratios, is evident in Fig. 5D.

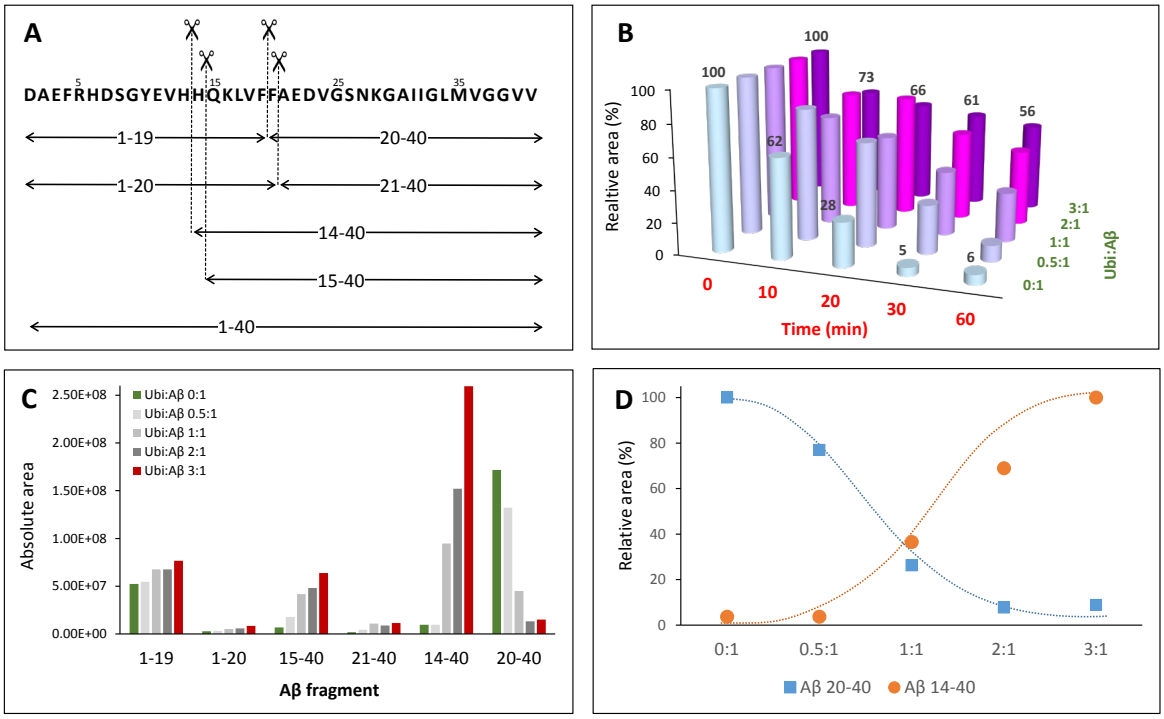

Figure 5. Dose-dependent effect of ubiquitin on the hydrolysis of Aβ40 catalysed by IDE. (A) Schematic of the IDE-induced hydrolytic pattern of Aβ40 at 37°C after 1h reaction. (B) Relative amounts of Aβ40 (with respect to the initial one) as a function of the reaction time and of the Ub:Aβ40 molar ratio. Amounts of all the digestion peptide fragments (C) or only Aβ14-40 and Aβ20-40 (D) as a function of the Ub:Aβ40 molar ratio.

The non-covalent interaction between Aβ and Ub has a clear site-specific effect on the IDE-mediated hydrolysis of Aβ. The trend related to the formation of the peptide fragments suggests that Ub somehow inhibits the cleavage at the Phe19-Phe20 peptide bond. Such an effect of Ub on the degradation pathway of Aβ is in accordance with molecular models, described above (see Fig. 2), showing significant structural restraints in Aβ regions encompassing the central hydrophobic cluster (14-28 residues) occurring upon Ub binding. The strong activation of the enzymatic hydrolysis at His13-His14 and His14-Gln15 might be considered a natural consequence of the inhibition involving the vicinal Phe residues. Indeed, $A\beta_{14\text{-}40}$ and $A\beta_{15\text{-}40}$ are also processed by IDE to form $A\beta_{20\text{-}40}$; therefore, their own Ub-dependent accumulation is reasonably considered a consequence of the effect of Ub on the formation of $A\beta_{20\text{-}40}$. Noteworthy, the crossing point between the Ub-induced increase of $A\beta_{14\text{-}40}$ and the concomitant decrease of $A\beta_{20\text{-}40}$ is reached when the Ub:Aβ molar ratio is 1:1. This evidence indeed strongly supports the 1:1 stoichiometry of the Ub:Aβ complex supported by all other experiments (NMR, XL-MS, SPR and modeling). The 1:1 Ub:Aβ adduct has also been observed by MALDI-TOF measurements (Fig. 6). The molecular weight of the 1:1 adduct was detected in all samples containing both the amyloid peptide and Ub (Fig. 6, left

graph). Moreover, the higher the Ub:Aβ molar ratio, the higher the absolute intensity of the mono-charged peak detected in linear mode, as a direct consequence of the amount of the complex formed. As a further confirmation of the peak attribution, these peaks drop down in the presence of IDE and proportionally to reaction time, regardless of the Ub:Aβ molar ratio (Fig. 6, right graphs). This trend can only be ascribed to a Ub-related inhibition of Aβ hydrolysis by IDE. These results, coupled also with the finding that Aβ is a proteasome inhibitor (see Fig. S6 of the Electronic Supporting Information) support the hypothesis that excess Aβ may significantly affect protein clearance pathways.

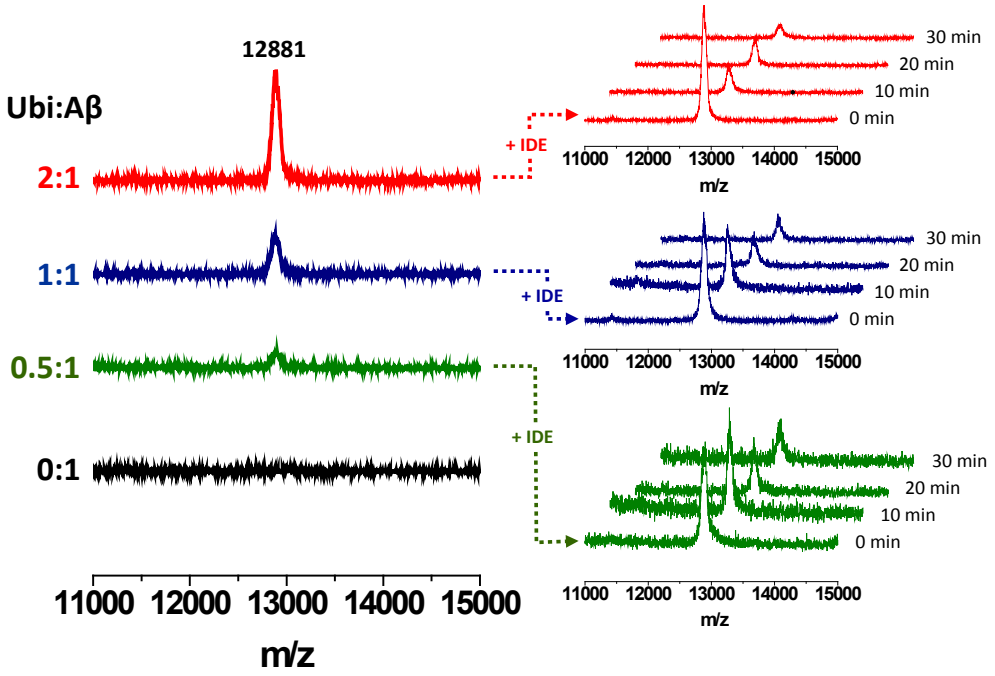

Figure 6. Formation of Ub-Aβ adducts as a function of the Ub:Aβ molar ratio (left graphs) revealed by MALDI-TOF measurements and time-dependent variation of their intensities in the presence of IDE (right graphs).

Ubiquitin interferes with Aβ amyloid growth.

It is known that Aβ aggregation starts intracellularly,[50] likely during abnormal interactions with lipid membranes.[51–53] In order to investigate if the interaction between the amyloid peptide and ubiquitin modifies the well-known propensity of Aβ to aggregate into amyloid-like fibers, the amyloid aggregation of Aβ was monitored by using a switch-on fluorescent dye (ThT). The experimental data obtained by the kinetic measurements were properly fitted to the theoretical aggregation models (Fig. 7) in order to calculate the kinetic parameters of

the aggregation process (Table S2 of Electronic Supporting information). The amyloid-like aggregation of Aβ follows a sigmoidal trend, as previously reported.[54] The lag phase of the self-induced aggregation of Aβ lasts 19.2 h. Such a value significantly increases in the presence of Ub, even when the Ub:Aβ molar ratio is 0.2:1. The lengthening of the lag phase is proportional to amount of Ub added and t_{lag} becomes more than 60 h when Ub:Aβ molar ratio is 3:1. The maximal fluorescent gain (F_{max}-F_0), proportional to the extent of fibril formation, has an opposite trend with respect to the concentration of Ub. F_{max}-F_0 value is significantly affected by Ub when Ub:Aβ molar ratio is equal or higher than 0.2:1. F_{max}-F_0 value is 2.2 at the highest ratio tested (3:1). These data demonstrate that Ub delays the amyloid-type aggregation of Aβ in a dose-dependent manner and considerably reduces the extent of the fibril formation. Such an effect might be ascribed to a direct or indirect influence on the Aβ sequence covering the LVFF motif, which is involved on the mechanism of the amyloid aggregation and is a common target of many inhibitors of the Aβ aggregation.[55] This hypothesis congruently matches the results of the IDE-mediated hydrolysis of Aβ in the presence of Ub.

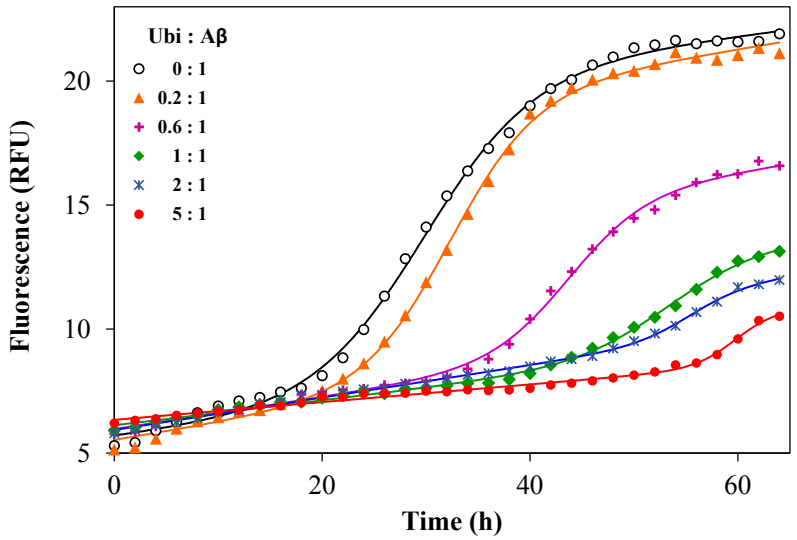

Figure 7. Representative kinetic profiles of the aggregation of Aβ40 in the presence of Ubiquitin, being the Ub:Aβ ratio ranging from 0:1 to 3:1. Solid lines represent the fitted curves for each kinetic profile, whose related parameters are reported in Table S2.

$Aβ_{1-16}$ inhibits Ub chain growth reactions in tube tests.

In the cell, Ub chain growth is initiated by the Ub-activating enzyme E1, which adenylates the C-terminus of ubiquitin in an ATP-dependent fashion to form a high energy thioester bond by a cysteine residue. Then, E1 hands the activated Ub over to a conjugating enzyme (E2), forming an E2–Ub complex in proximity of the target protein. The final ubiquitinylation of

the substrate occurs through the action of specific E3 ubiquitin ligases. Unanchored (or free) Ub chains (*i.e.*, Ub chains that are not linked to any substrate) are normally considered very useful tools to study ubiquitinylation processes. A number of protocols have been developed to produce K48 and K63-linked free Ub chains in tube tests,[56] which may be thus considered as an helpful method to single out the capacity of adverse factors in affecting the Ub-conjugation machinery.[56] Due to its significant affinity for Ub, it is plausible that Aβ may interfere with the complex cascade of events leading to poly-ubiquitinylation. To address this issue, we have carried out the poly-ubiquitinylation reactions in the presence of increasing concentration of Aβ. First, we tried to use the full length Aβ40 peptide, but the simultaneous formation of high molecular weight oligomeric species during the ubiquitinylation reactions masked any possible effect. Then we used a soluble Aβ1-16 peptide, a fragment that contains all the peptide residues that previous experiments consistently identified as Ub binding sites. The $A\beta_{\mathbf{1\text{-}16}}$ peptide has been added to **a** ratio 1:0,5, 1:1 and 1:2 with respect to Ub in both reactions mixtures (Fig. 8). Western Blot (WB) analysis has shown the dose- dependent inhibitory effects of $A\beta_{1\text{-}16}$ peptide on both Lys48- and Lys-63-linked ubiquitin chain elongation, being already evident at a ratio 1:1 of Ub/ $A\beta_{1\text{-}16}$. These data have further demonstrated that the interaction of Ub and Aβ hinders the regions close to the lysine 63 and 48.

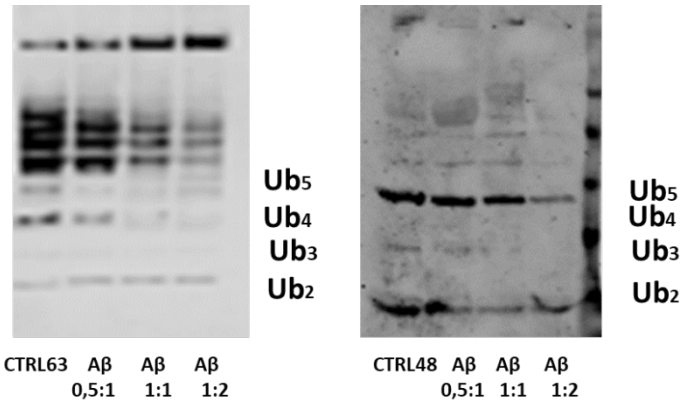

Figure 8. The WB analysis of Ub reactions in presence of Aβ1-16 peptide, with ratio 0,5:1, 1:1 and 1:2 respect to Ub concentration.

Conclusions

Although accumulation of extracellular amyloid plaques in the brain is widely considered a hallmark of AD, a direct relationship between amyloid load and cognitive decline has never been unequivocally demonstrated. On the other hand, it is becoming increasingly evident that an abnormal rise of intracellular Aβ levels may be better correlated to neuronal loss and disease progression. Unfortunately, our knowledge of the intracellular chemistry of Aβ is largely incomplete and there is urgent need for a more detailed description of the role played by Aβ in the pathological failure of cytosolic protein clearance supervisors like UPS and IDE.

Here, we show that Aβ has a relatively significant affinity for Ub. It forms 1:1 protein-protein complexes mostly involving the C-terminal tail and the β1/β2 loop of Ub. Next, consistently with many reports showing that Ub is often recognized by binding proteins through the hydrophobic surface encompassing residues Leu8, Ile44, His 68 and Val 70,[57] non-covalent interactions involving the central hydrophobic cluster of Aβ40 and the Ub Ile44 were also observed. The residue D1 of the peptide was found to be linked to K48 and K63 residues of Ub. These two Ub residues resulted also to be in contact with residues S8 and Y10 of Aβ40. The N-terminal segment of Aβ40 (residues D1 E3 and R5) interacts with the Ub C-terminal domain and in particular with residues Lys63 and Glu64. Consistently with the observation that Lys48 and Lys63 residues are buried upon interaction with the N-terminal domain of Aβ, we have also observed that the water soluble fragment $A\beta_{1\text{-}16}$ significantly inhibits Ub chain growth in tube tests. Noteworthy, Aβ/Ub interaction reminds non covalent contacts between Ub and Ub binding domains (UBDs) which are important players in Ub chain growth and signaling. For example, most of the known UBDs are predominantly α-helical and bind the Ile44 hydrophobic patch of Ub[58] Moreover, most of the UBDs exhibit binding affinities (K_d) in the range between 2 and 200 μM.[41] Next, $A\beta_{40}$ may assume an α-helical structure in its central hydrophobic cluster (residues 14-20) upon interaction with Ub. Beside these hydrophobic contacts, salt bridges connecting the D1 residue of Aβ40 with K63 and K48 of Ub are also evident. This coupled electrostatic/hydrophobic interaction likely explains the evident binding affinity of Aβ for Ub and may explain why the peptide is a competitive Ub binding protein. Furthermore, while on one side upon Aβ binding Ub exhibits a compromised ability to recognize its physiological Ub binding partners, on the other side it significantly influences peptide secondary structure and ability to self-assemble into amyloid-like aggregates and to be degraded by IDE. The reduced propensity of Aβ40 to aggregate into amyloid fibrils is ascribable to the increased α-helical content observed in Ub-bound peptide. This ability of Ub to mold poorly structured peptides has been already observed in previous reports.[30] Remarkably, Ub/Aβ interactions have also a site-specific effect on the IDE-mediated degradation process of the

amyloid peptide with possible consequences on the toxicity of the hydrolyzed Aβ fragments.[59] Conclusively, these results evidence how the non-covalent interaction between Aβ40 and Ub may have important consequences in the regulation of the upstream events of the UPS and in IDE-mediated clearance pathways. These results may hopefully pave the way to future studies addressing the multifaceted role played by the altered Aβ homeostasis occurring in AD.

Acknowledgements

This work was financially supported by the Italian MiUR (PRIN 20157WZM8A).

Author Contribution:

F.B. performed IDE-mediated hydrolysis studies; V.L. and S.G.V. performed polyubiquitination reactions; I.M.M.A. performed MALDI-TOF studies, A.P. performed molecular simulations; C.I. performed cross-linking studies; G.M., G.D.A and, R.F. performed NMR studies; V.G.N. performed ELISA assays; D.S. and G.R.T. contributed to cell studies, M.C. wrote the paper, D.C. performed SPR experiments; L.P. and E.P. performed MST experiments; G.G. analyzed SPR data and designed the research; D.M. designed the research and wrote the paper.

References

1D. J. Selkoe, *Neuron*, 1991, **6**, 487–498.

2E. Terzi, G. Hölzemann and J. Seelig, *Biochemistry*, 1997, **36**, 14845–14852.

3B. A. Yankner, L. K. Duffy and D. A. Kirschner, *Science*, 1990, **250**, 279–282.

4J. A. Hardy and G. A. Higgins, *Science*, 1992, **256**, 184.

5I. Benilova, E. Karran and B. De Strooper, *Nature neuroscience*, 2012, **15**, 349.

6K. P. Kepp, *Progress in neurobiology*, 2016, **143**, 36–60.

7O. Wirths and T. A. Bayer, *Life sciences*, 2012, **91**, 1148–1152.

8C. Schmitz, B. P. Rutten, A. Pielen, S. Schäfer, O. Wirths, G. Tremp, C. Czech, V. Blanchard, G. Multhaup and P. Rezaie, *The American journal of pathology*, 2004, **164**, 1495–1502.

9G. Grasso, A. M. Santoro, V. Lanza, D. Sbardella, G. R. Tundo, C. Ciaccio, S. Marini, M. Coletta and D. Milardi, *Coordination Chemistry Reviews*, 2017, **347**, 1–22.

10 A. Ciechanover and Y. T. Kwon, *Experimental & molecular medicine*, 2015, **47**, e147.

11 S. Vijay-Kumar, C. E. Bugg and W. J. Cook, *Journal of molecular biology*, 1987, **194**, 531–544.

12 C. M. Pickart and D. Fushman, *Current opinion in chemical biology*, 2004, **8**, 610–616.

13 D. A. Nijholt, T. R. de Graaf, E. S. van Haastert, A. O. Oliveira, C. R. Berkers, R. Zwart, H. Ovaa, F. Baas, J. J. Hoozemans and W. Scheper, *Cell death and differentiation*, 2011, **18**, 1071.

14 L. Gregori, C. Fuchs, M. E. Figueiredo-Pereira, W. E. Van Nostrand and D. Goldgaber, *Journal of Biological Chemistry*, 1995, **270**, 19702–19708.

15 L. Gregori, J. F. Hainfeld, M. N. Simon and D. Goldgaber, *Journal of Biological Chemistry*, 1997, **272**, 58–62.

16 M. L. Salon, L. Pasquini, M. B. Moreno, J. M. Pasquini and E. Soto, *Experimental neurology*, 2003, **180**, 131–143.

17 S. Song, S.-Y. Kim, Y.-M. Hong, D.-G. Jo, J.-Y. Lee, S. M. Shim, C.-W. Chung, S. J. Seo, Y. J. Yoo and J.-Y. Koh, *Molecular cell*, 2003, **12**, 553–563.

18 S. Oh, H. S. Hong, E. Hwang, H. J. Sim, W. Lee, S. J. Shin and I. Mook-Jung, *Mechanisms of ageing and development*, 2005, **126**, 1292–1299.

19 C. G. Almeida, R. H. Takahashi and G. K. Gouras, *Journal of Neuroscience*, 2006, **26**, 4277–4288.

20 B. P. Tseng, K. N. Green, J. L. Chan, M. Blurton-Jones and F. M. LaFerla, *Neurobiology of aging*, 2008, **29**, 1607–1618.

21 X. Zhao and J. Yang, *ACS chemical neuroscience*, 2010, **1**, 655–660.

22 A. V. Morozov, A. A. Kulikova, T. M. Astakhova, V. A. Mitkevich, K. M. Burnysheva, A. A. Adzhubei, P. A. Erokhov, M. B. Evgen'ev, N. P. Sharova and V. L. Karpov, *Journal of Alzheimer's Disease*, 2016, **54**, 763–776.

23 J. Lowe, A. Blanchard, K. Morrell, G. Lennox, L. Reynolds, M. Billett, M. Landon and R. J. Mayer, *The Journal of pathology*, 1988, **155**, 9–15.

24 A. Ciechanover and P. Brundin, *Neuron*, 2003, **40**, 427–446.

25 A. Hershko and A. Ciechanover, *Annual Review of Biochemistry*, 1998, **67**, 425–479.

26 J. D. Wright, P. D. Mace and C. L. Day, *Trends in Biochemical Sciences*, 2016, **41**, 924–937.

27 G. R. Tundo, D. Sbardella, C. Ciaccio, G. Grasso, M. Gioia, A. Coletta, F. Polticelli, D. Di Pierro, D. Milardi and P. Van Endert, *Critical reviews in biochemistry and molecular biology*, 2017, **52**, 554–582.

28 M. F. Sciacca, V. Romanucci, A. Zarrelli, I. Monaco, F. Lolicato, N. Spinella, C. Galati, G. Grasso, L. D'Urso and M. Romeo, *ACS chemical neuroscience*, 2017, **8**, 1767–1778.

29 G. Arena, R. Fattorusso, G. Grasso, G. I. Grasso, C. Isernia, G. Malgieri, D. Milardi and E. Rizzarelli, *Chemistry – A European Journal*, **17**, 11596–11603.

30 V. Lanza, A. Travaglia, G. Malgieri, R. Fattorusso, G. Grasso, G. Di Natale, V. Zito, G. Arena, D. Milardi and E. Rizzarelli, *Chemistry–A European Journal*, 2016, **22**, 17767–17775.

31 T. Ebendal, *Journal of neuroscience research*, 1992, **32**, 461–470.

32 J. S. Elam, S. T. Thomas, S. P. Holloway, A. B. Taylor and P. J. Hart, *Advances in protein chemistry*, 2002, **60**, 151–219.

33 L. Aloe, L. Bracci-Laudiero, S. Bonini, L. Manni and L. Aloe, *Allergy*, 1997, **52**, 883–994.

34 S. Vivekanandan, J. R. Brender, S. Y. Lee and A. Ramamoorthy, *Biochemical and biophysical research communications*, 2011, **411**, 312–316.

35 A. Sinz, *Mass spectrometry reviews*, 2006, **25**, 663–682.

36 J. Rappsilber, *Journal of structural biology*, 2011, **173**, 530–540.

37 A. Leitner, T. Walzthoeni, A. Kahraman, F. Herzog, O. Rinner, M. Beck and R. Aebersold, *Molecular & Cellular Proteomics*, 2010, mcp–R000001.

38 C. Iacobucci, S. Reale and F. De Angelis, *ChemBioChem*, 2013, **14**, 181–183.

39 M. Q. Müller, F. Dreiocker, C. H. Ihling, M. Schäfer and A. Sinz, *Analytical chemistry*, 2010, **82**, 6958–6968.

40 C. Iacobucci and A. Sinz, *Analytical Chemistry*, 2017, **89**, 7832–7835.

41 K. Sokratous, L. V. Roach, D. Channing, J. Strachan, J. Long, M. S. Searle, R. Layfield and N. J. Oldham, *J. Am. Chem. Soc.*, 2012, **134**, 6416–6424.

42 R. J Baranello, K. L Bharani, V. Padmaraju, N. Chopra, D. K Lahiri, N. H Greig, M. A Pappolla and K. Sambamurti, *Current Alzheimer Research*, 2015, **12**, 32–46.

43 L. A. McCord, W. G. Liang, E. Dowdell, V. Kalas, R. J. Hoey, A. Koide, S. Koide and W.-J. Tang, *Proceedings of the National Academy of Sciences*, 2013, **110**, 13827–13832.

44 F. Bellia and G. Grasso, *Journal of mass spectrometry*, 2014, **49**, 274–279.

45 F. Bellia, A. Pietropaolo and G. Grasso, *Journal of Mass Spectrometry*, 2013, **48**, 135–140.

46 G. R. Tundo, E. Di Muzio, C. Ciaccio, D. Sbardella, D. Di Pierro, F. Polticelli, M. Coletta and S. Marini, *The FEBS journal*, 2016, **283**, 3755–3770.

47 G. Tundo, C. Ciaccio, D. Sbardella, M. Boraso, B. Viviani, M. Coletta and S. Marini, *PloS one*, 2012, **7**, e34376.

48 V. Lanza, F. Bellia and E. Rizzarelli, *Coordination Chemistry Reviews*, 2018, **369**, 1–14.

49 G. Grasso, E. Rizzarelli and G. Spoto, *Biochimica et Biophysica Acta (BBA)-Proteins and Proteomics*, 2008, **1784**, 1122–1126.

50 S. Oddo, A. Caccamo, L. Tran, M. P. Lambert, C. G. Glabe, W. L. Klein and F. M. LaFerla, *J. Biol. Chem.*, 2006, **281**, 1599–1604.

51 S. A. Kotler, P. Walsh, J. R. Brender and A. Ramamoorthy, *Chemical Society Reviews*, 2014, **43**, 6692–6700.

52 M. F. M. Sciacca, C. Tempra, F. Scollo, D. Milardi and C. La Rosa, *Biochimica et Biophysica Acta (BBA) - Biomembranes*, 2018, **1860**, 1625–1638.

53 F. Scollo, C. Tempra, F. Lolicato, M. F. Sciacca, A. Raudino, D. Milardi and C. La Rosa, *The journal of physical chemistry letters*, 2018, **9**, 5125–5129.

54 G. I. Grasso, G. Arena, F. Bellia, E. Rizzarelli and G. Vecchio, *Journal of inorganic biochemistry*, 2014, **131**, 56–63.

55 V. Oliveri, S. Zimbone, M. L. Giuffrida, F. Bellia, M. F. Tomasello and G. Vecchio, *Chemistry–A European Journal*, 2018, **24**, 6349–6353.

56 C. M. Pickart and S. Raasi, in *Methods in Enzymology*, Academic Press, 2005, vol. 399, pp. 21–36.

57 D. Komander and M. Rape, *Annual Review of Biochemistry*, 2012, **81**, 203–229.

58 J. H. Hurley, S. Lee and G. Prag, *Biochemical Journal*, 2006, **399**, 361–372.

59 A. Zhang, W. Qi, T. A. Good and E. J. Fernandez, *Biophysical journal*, 2009, **96**, 1091–1104.

Supplementary information

Chemicals. Aβ40 (HFIP treated) was purchased from Bachem. $A\beta_{1\text{-}16}$ was purchased form Genscript. PBS (phosphate buffer saline), Tween 20, ubiquitin, and other chemicals were purchased from Sigma-Aldrich. Carboxy-methyl-dextrane functionalized gold sensor slide (CMD3D) was obtained from Bionavis Company.

IDE-dependent hydrolysis. Aβ40 (Genscript) was properly treated in order to enrich the sample of monomer species according an experimental procedure previously reported.[1] The amyloid peptide (2 μM) was then incubated in phosphate buffer (1 mM, pH 7.4) with Ub (1-6 μM) IDE (5 nM). Time-course experiments were carried out for 1 or 2 hours. The reaction of each sample aliquots was stopped by adding TFA (1 %).

LC-MS measurements. Ultra-High Performance Liquid chromatography (UHPLC) analyses were performed using a Ultimate 3000 (Thermo Electron Corporation, USA), and Q-Exactive hybrid quadrupole-Orbitrap mass spectrometer (Thermo Electron Corporation, USA) was coupled to the LC system for the high resolution detection of the amyloid peptide fragments. Capillary temperature and voltage were 300 °C and 2 kV, respectively. The chromatographic analyses were performed with solvents A (H_2O:CH_3CN 5:95, 0.01% TFA) and B (H_2O:CH_3CN 20:80, 0.01% TFA) on a Easy Spray Accucore® C4 (75 μm × 150 mm, 2.6-μm particle size) column, at a flow rate of 300 nl/min. Peak detection for quantitative evaluation was carried out using the extracted ion chromatogram (XIC) related to the most abundant charged species detected for each peptide fragment. MS and MS–MS (HCD) spectra were used for identification and unambiguous assignment of the peptide fragments (see Table S1).

MALDI-TOF measurements. MALDI-TOF MS experiments were performed using an AB SCIEX MALDI-TOF/TOF 5800 Analyzer (AB SCIEX, Foster City, CA) equipped with a nitrogen UV laser (λ = 337 nm) pulsed at a 20 Hz frequency. The mass spectrometer operated in the linear mode was also, which consisted of an accelerating potential of 25 kV, a grid percentage of 93% and an extraction delay of 800 ns. Mass spectra were recorded with the laser intensity set just above the ionization threshold (4500 in arbitrary units) to avoid fragmentation and labile group losses, to maximize the resolution, and to result in a strong analyte signal with minimal matrix interference. Mass spectra were obtained by accumulation 800–1000 laser shots and processed using Data Explorer 4.11 software (Applied Biosystems). A saturated solution of sinapinic acid in water/acetonitrile 70:30 with 0.1% TFA was used as the matrix with the sample concentration ranging from 0.2 to 1 μM. Experimental spectra were analysed using Data Explorer software.

Aβ aggregation assay. The monomerized Aβ peptide (20μM) was suspended in phosphate buffer 10 mM (pH 7.4), along with ThT (40 μM) and ubiquitin (from 4 μM to 60 μM); they were then incubated in a black 96-well plate (Nalge-Nunc, Rochester, NY) for 65 hours at 37 °C in the Varioskan plate reader (Thermo Scientific). The kinetics of amyloid aggregation was followed by measuring the ThT fluorescence emission at 480 nm with an excitation wavelength of 450 nm. All the measurements were carried out in triplicate and the experimental data were fitted to equation (1):

$$\boldsymbol{F(t) = F_0 + mt + \frac{F_{max} - F_0}{1 + e^{-\frac{t - t_{1/2}}{k}}}} \quad (1)$$

in which F_0 and F_{max} are the initial and final fluorescence emissions of amyloid aggregation process, respectively; $1/k$ is the elongation rate constant and $t_{½}$ is the time at which the amplitude of ThT emission is 50% of the $F_{max} - F_0$ value. The lag time (t_{lag}) is defined as the intercept between the time axis and the tangent of the curve with slope k from the midpoint of the fitted sigmoidal curve; this parameter was calculated from the fitted parameters by using the following equation:

$$\boldsymbol{t_{lag} = t_{1/2} - 2k} \quad \textbf{(2)}$$

The kinetic parameters of any set of measurements were expressed as mean ± SD (Table S2).

Cross-linking MS. Cross-linking experiments were conducted in duplicate and the identified cross-links were combined. All chemicals were obtained from Sigma Aldrich (Taufkirchen, Germany). HPLC solvents were purchased from VWR (Darmstadt, Germany), Milli-Q water was produced by a TKA Pacific system with X-CAD dispenser from Thermo Electron LED GmbH (Thermo Fisher Scientific, Niederelbert, Germany). Cross-linking reactions. Ub stock solution was diluted to give a final protein concentration of 10 μM (20 mM HEPES at pH 8.0). 1 uL of a freshly prepared stock solution of Aβ40 in DMSO was added to 49 uL of Ub solution to a final Aβ40 concentrations of 10 μM. The protein solution was incubated for 30 min at 37° C or on ice and 0.5 ul of DSBU in DMSO were added to a final concentration of 1 mM. The final concentration of DMSO was 3%vv. The reaction was incubated for for 30 minutes at 37° C or 1 hour on ice and it was stopped with Tris buffer (final concentration 20 mM).

Enzymatic in-solution digestion. Protein solutions were subjected to in-solution digestion with trypsin/GluC mixture according to an existing protocol.[2]

Nano-HPLC/Nano-ESI-Orbitrap-MS/MS measurements. Peptide mixtures were analyzed by LC/MS/MS on an UltiMate 3000 RSLC nano-HPLC system (Thermo Fisher Scientific) coupled to

an Orbitrap Q-Exactive Plus mass spectrometer (Thermo Fisher Scientific), equipped with Nanospray Flex ion source (Thermo Fisher Scientific). Fragmentation was performed by HCD (30 ± 3% NCE); data were acquired in data-dependent MS/MS mode. Each high-resolution full scan (R = 140,000 at m/z 200) in the Orbitrap was followed by high-resolution HCD product ion scans (R = 17,500 at m/z 200) within 5 s, starting with the most intense signal in the mass spectrum (isolation window of 2 Th). A with maximum accumulation times of 250 ms was employed. Dynamic exclusion (exclusion duration 60s) was enabled.

Identification of Cross-Linked Products. Cross-linked products were automatically annotated with MeroX and manually validated. Mass deviations of 3 and 10 ppm were applied for precursor and product ions. A 5% FDR cut-off and a signal-to-noise ratio of ≥ 2 were applied. Lys, Ser, Thr, and Tyr were considered as potential cross-linking sites for DSBU. Oxidation of Met and carbamidomethylation of cysteines were set as variable modifications. Three missed cleavage sites were considered for each amino acid [Lys and Arg].

NMR analysis. Two samples were prepared for the NMR characterization. 100 μM or 60μM final concentration of ^{15}N-^{13}C labeled human-Ubiquitin (Ub) (CortecNet, Voisins le Bretonneux France) was dissolved in 500 μL of 10 mM phosphate buffer (90% H2O, 10% 2H2O, pH 7.0). Aβ40 unlabeled was added to both solutions as a single aliquot of known amount of lyophilized peptide. The final peptide concentration was in both cases 30 μM. Freshly prepared sample were used immediately. NMR experiments were acquired on each sample at 298 K on a Bruker Avance III HD 600 MHz equipped with cryoprobe at the Department of Environmental, Biological and Pharmaceutical Sciences and Technologies of the University of Campania – Luigi Vanvitelli (Caserta, Italy). Chemical shifts were calibrated indirectly by using external references. Data were processed with the TopSpin 3.5 software (Bruker) and analysed by using CARA software (computer aided resonance assignment - cara.nmr.ch). A standard set of triple resonance NMR experiments were collected as previously reported[4] to enable sequence-specific backbone and Cα resonances assignment. The pulsed-field gradient spin-echo DOSY experiment was used to measure the translation diffusion coefficient. The intensity variations of the amide cross-peaks were evaluated using the equation: $\Delta I = (I - I_0)/I_0$, where I_0 and I are the amide cross-peak intensities in absence and in presence of Aβ40 respectively.

Molecular simulations. Aβ40 and Aβ42 underwent 75 ns of parallel tempering simulations in explicit solvent, after an equilibration of 2 ns of MD in explicit solvent. GROMACS 5.0.4 package was used.[5]

Parallel tempering simulations were used in order to boost the sampling of flexible protein domains, avoiding any dependence on the starting coordinates. The overall charge of the system was neutralized by adding three sodium ions. Periodic boundary conditions were applied. The AMBER99SB[6] force field was used for the biomolecules and counter ions, and the TIP3P force field was used for water molecules[7]. Electrostatic interactions were calculated using the Particle Mesh Ewald method.[8] A cutoff (0.9 nm) was used for the Lennard-Jones interactions. The time-step was set to 2 fs. All bond lengths were constrained to their equilibrium values using the SHAKE[9] algorithm for water and the LINCS[10] algorithm for the peptide. We simulated 64 replicas distributed in the temperature range 300-400 K following a geometric progression. All replicas were simulated in NVT ensemble using a stochastic thermostat with a coupling time of 0.1 ps.[11] A thermostat that yields the correct energy fluctuations of the canonical ensemble is crucial in parallel tempering simulations.[12] Exchanges were attempted every 0.1 ps. The method of Daura and Van Gunsteren[13] was used in post-processing phase to cluster the resulting trajectories, with a cutoff of 4 Å calculated on the backbone atoms as implemented in the clustering utility provided in the GROMACS package[5]. The former protocol has been successful in a wealth of studies.[14–19] Docking simulations have been performed using HADDOCK interface.[20] The three main Aβ40 clusters found through PT simulations were docked to the Ub structure whose starting coordinates were considered from the X-ray structure of the complex between the UBA1 enzyme and Ub (pdb code: 3CMM). The following residues of Ub were considered as active residues, since observed through NMR experiments to interact with Aβ40. Those involve Q2, L8, G10, K11, T12, I23, A46, G47, Q49, K63, L71, R72 ,L73, R74. The binding surface of Aβ40 was considered as active surface. Structures underwent rigid body energy minimization, semirigid simulated annealing in torsion angle space, with a final clusterization of the results.

Surface Plasmon Resonance. To assess the interaction between ubiquitin and Aβ40 a multi-parametric SPR instrument (Bionavis SPR Navi 210A) was used. Covalent Aβ40 immobilization was obtained by amine coupling of the lysine-free amino groups and terminal amines of the peptide, as described elsewhere.[21] CMD3D sensor was mounted onto the sensor slide holder and then onto the SPR Navi 210A instrument, previously equilibrated with the running buffer, PBS 10mM (pH 7.4). The flow cell temperature was set to 22C°. Activation of CMD3D sensor was performed immediately previous Aβ injection through the reaction between EDC (0,2M)/NHS (0,05M) and matrix carboxyl groups to achieve reactive succinimide ester groups that can react with primary amines. Lyophilized amyloid beta 1-40 (HFIP treated) was dissolved in pure DMSO to a final concentration of 1,6mM and stored in freezer at -20 C°. To avoid amyloid beta aggregation the injection solutions were prepared immediately before immobilization step diluting the peptide stock solution in sodium acetate

buffer (10mM, pH 4); in particular two amyloid beta injections were performed at 5 μM for 10 minutes at 15 μl/min and two injections at 10 μM was performed for 15 minutes at 15 μl/min. Immobilization was performed in parallel configuration in the channel 1 while in the channel 2 (reference channel) only running buffer was injected. At the end of the immobilization step ethanolamine-HCl 1M (pH 8,5) was injected in serial mode for 10 minutes at 15 μl/min to deactivate all the residual active sites on the surface. After deactivation step the final immobilization angular delta (Δθ) was 0,27 degrees. Analysis of the binding curves was carried out by the Tracedrawer software®. Residual values between the fitted curves and the experimental ones are reported in figure S1. Fitting parameters are reported in Table S4.

Microscale Thermophoresis (MST). MST experiments were performed on a Monolith NT 115 system (Nano Temper Technologies, Munchen, Germany) using 100% LED and 20% IR-laser power. The labelling of Ab40 and Ab1-16 (10 μM) was performed in labelling buffer with NT-647-NHS reactive dye (30 μM) (Nanotemper), which reacts efficiently with the primary amines of the proteins to form a stable dye protein conjugates. The labeling reaction was carried out for 30 min at RT. A 16-point serial dilution (1:1) was prepared for ubiquitin at the final concentration ranged from 1 mM to 30 nM in PBS tween 0.05%. The samples were filled into Standard capillaries and measurements were conducted at 25 °C. An equation implemented by the software MO-S002 MO Affinity Analysis, provided by the manufacturer, was used for fitting normalized fluorescence values at different concentrations of ligands.[21]

Lys63 and Lys48 self-polyubiquitination reactions in Tube Tests. Lys63-linked polyUb reactions were performed at pH 7.4 (T = 37 °C) in small volumes (40 μL) of a ligation buffer (50 mM TRIS, 5 mM MgCl2, 100 μM DTT, and 2 mM ATP) containing Ub (10 μM), UBE1 (500 nM), and UbcH13/Uev (50 nM). Lys48 polyUb chain synthesis was carried out by mixing Ub (10 μM), UBE1 (100 nM), and E2-25K (1 μM) in the same experimental conditions as those used for Lys63 polyUb reactions. All reactions were carried out at different $A\beta_{1\text{-}16}$ to Ub molar ratios and constant Ub concentration. The reactions were quenched after 3-hour incubation with addition of 10 μL of the sample loading buffer containing 8% (w/v) SDS, 24% (v/v) glycerol, 0.015% Coomassie Blue G, and were size-fractioned by SDS-polyacrylamide gel electrophoresis. Samples were then electro-transferred onto a nitrocellulose membrane (GE Healthcare, Lifescience). The membranes were blocked with Odyssey blocking buffer for 1 hour and then incubated overnight at 4°C with K48-linkage specific polyubiquitin antibody. The membrane was washed thrice for 5 minutes with PBS-T (PBS-0.05% Tween-20) and then incubated with IRDye 800–labeled secondary antibody (1:12,000) from

Molecular Probes (Eugene, OR) for 30 minutes. Membrane visualization was done using the LI-COR Odyssey IR Imaging System (LI-COR Biosciences, Lincoln).

ELISA assay (Enzyme-Linked-ImmunoSorbent-Assay). To perform a protein/interaction experiment was also used an Indirect ELISA approach. High binding plates (Ultracruz, Santacruz) were coated with Ubiquitin or Abeta, alternatively. The peptides were diluted to a final concentration of 10 μM in carbonate/bicarbonate buffer, pH 9,6, and distributed to the selected wells of the plate for coating reaction (overnight 4°C). The remaining protein-binding sites in the well were blocked by covering the surface with 100 / 200 μL blocking buffer (PBS-T) for 2hrs. The second protein/peptide solution (20 μM in PBS 100 uL pH 7,4) was then added to the selected wells. The sealed plate was incubated for 2 hrs at room temperature. After washing and a further step of unspecific site blocking, 100 μL of the appropriately diluted primary monoclonal antibodies, anti Aβ (Mouse anti-Aβ [1-16], Invitrogen) or anti Ubiquitin (Mouse anti-Ubiquitin VU-1, Life sensor) alternatively, were added to each well, and sealed plate incubated overnight at 4°C. Each step was interrupted by washing steps with PBS/Tween. Incubation for 1 hour at 37°C with the appropriately diluted HRPO conjugated secondary anti mouse antibody (Invitrogen) to each well, was followed by detection. The addition of TMB substrate solution (50 μL, 20 minutes) to each well resulted in the development of colored product. After stopping the enzymatic reaction the plate was read at 450 nm by a plate reader (Multiskan Ascent). Neuroblastoma SHSY5Y cell cultures were grown until 80% confluency and differentiated by classic retinoic acid treatment before mechanical harvesting and homogeneization in PBS. A 30 min 12000 rpm centrifugation preceded the recovery of supernatant cytoplasmic material used in the ELISA experiments.

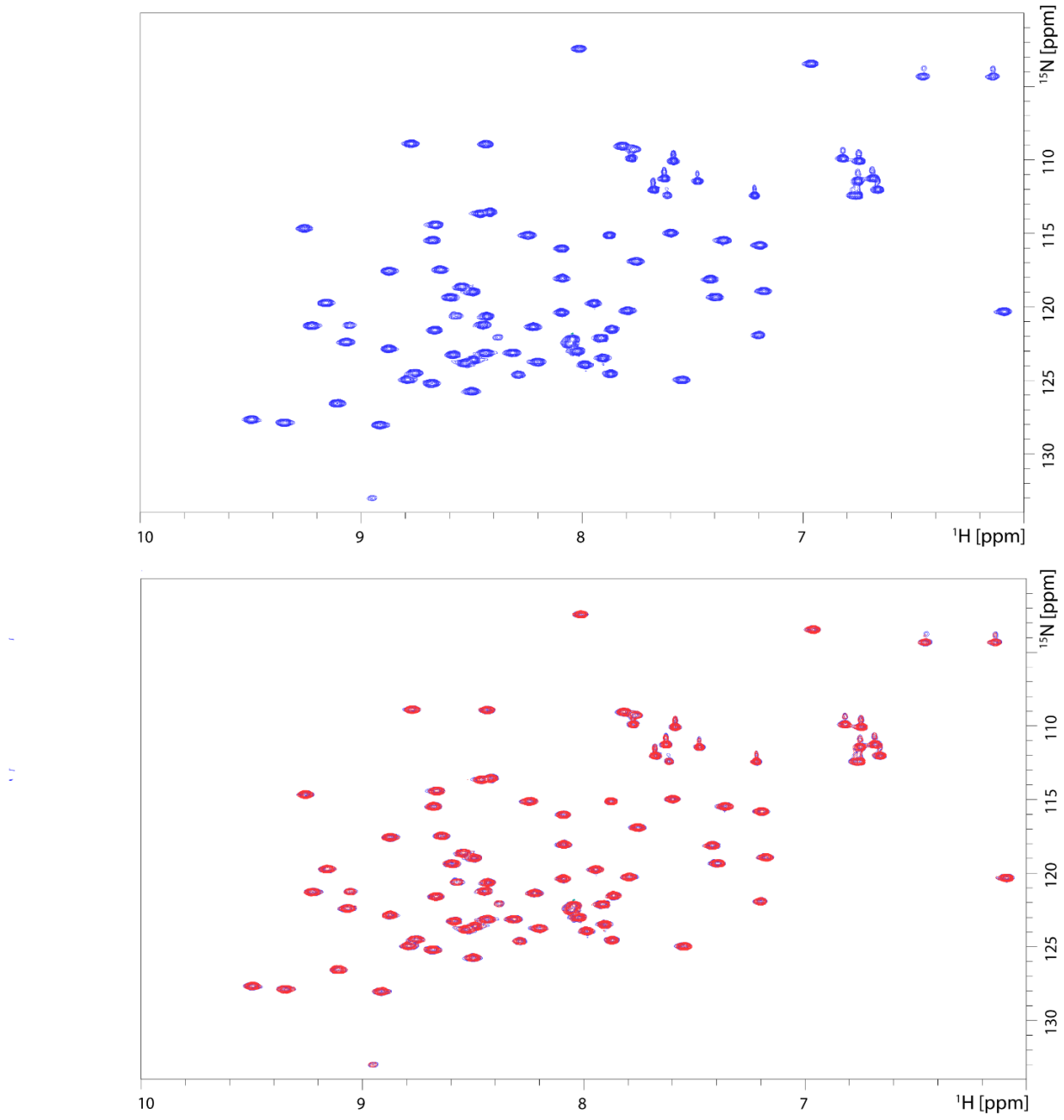

Figure S1. Upper panel: ^{1}H-^{15}N HSQC spectrum of ^{15}N-^{13}C-labeled Ubiquitin. Lower panel: superimposition of the ^{1}H-^{15}N HSQC spectra of ^{15}N-^{13}C-labeled Ubiquitin in absence (blue) and in presence (red) of substoichiometric amount of unlabeled Aβ40 (2:1 Ubiquitin:Aβ40 ratio). All the spectra were acquired as reported in Materials and Methods section.

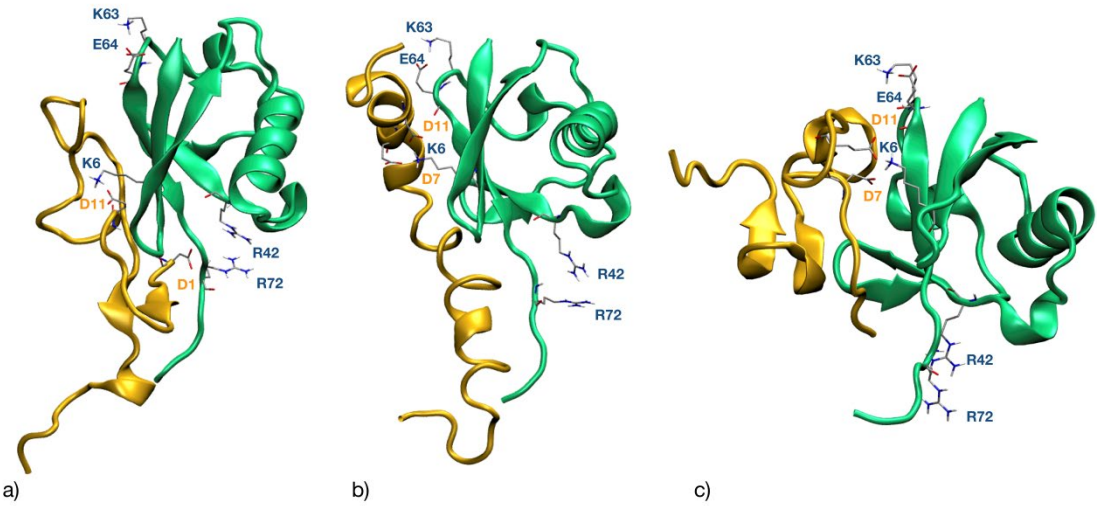

Figure S2. The three lowest energy binding modes for the Aβ42/Ub complex. Aβ42 sections are shown by orange ribbons, Ub sections are shown by green ribbons. The residues of Ub interacting with Aβ42 are shown by solid sticks and those involved in salt-bridge interactions are also labeled. The internal energies of the Aβ42/Ub complex in the three binding poses a)-c) are -4195 kcal/mol, -4140 kcal/mol, -4178 kcal/mol.

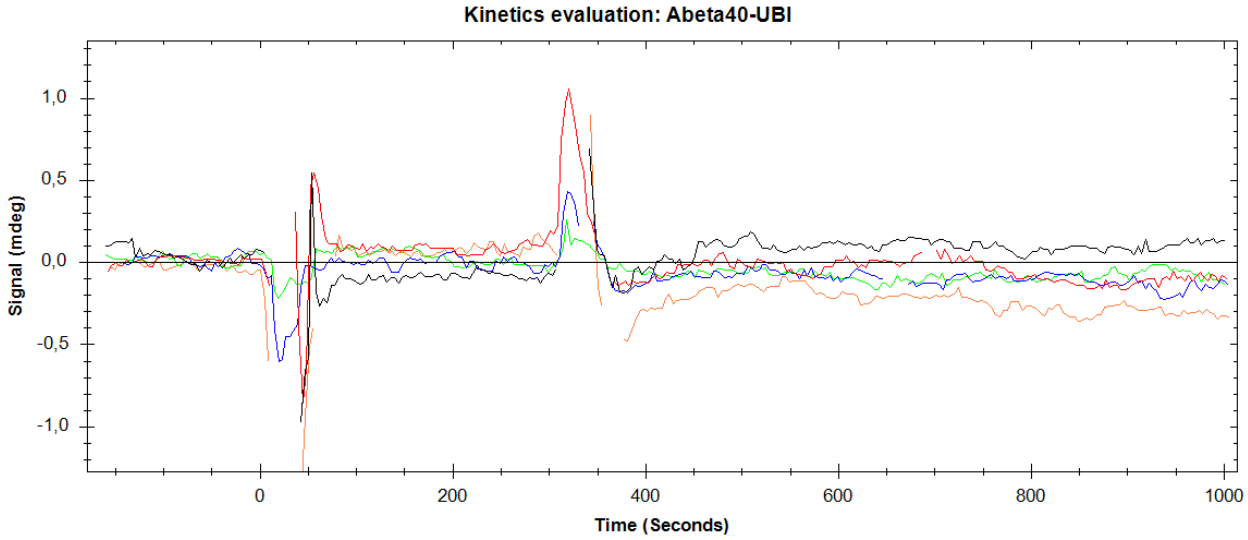

Figure S3. Residual values between the fitted curves and the experimental ones of the interaction between immobilized Aβ40 and ubiquitin at increasing concentration: 43 µM (green line)- 86 µM (blue line)- 171 µM (red line)- 343 µM (black line)- 755 µM (orange line).

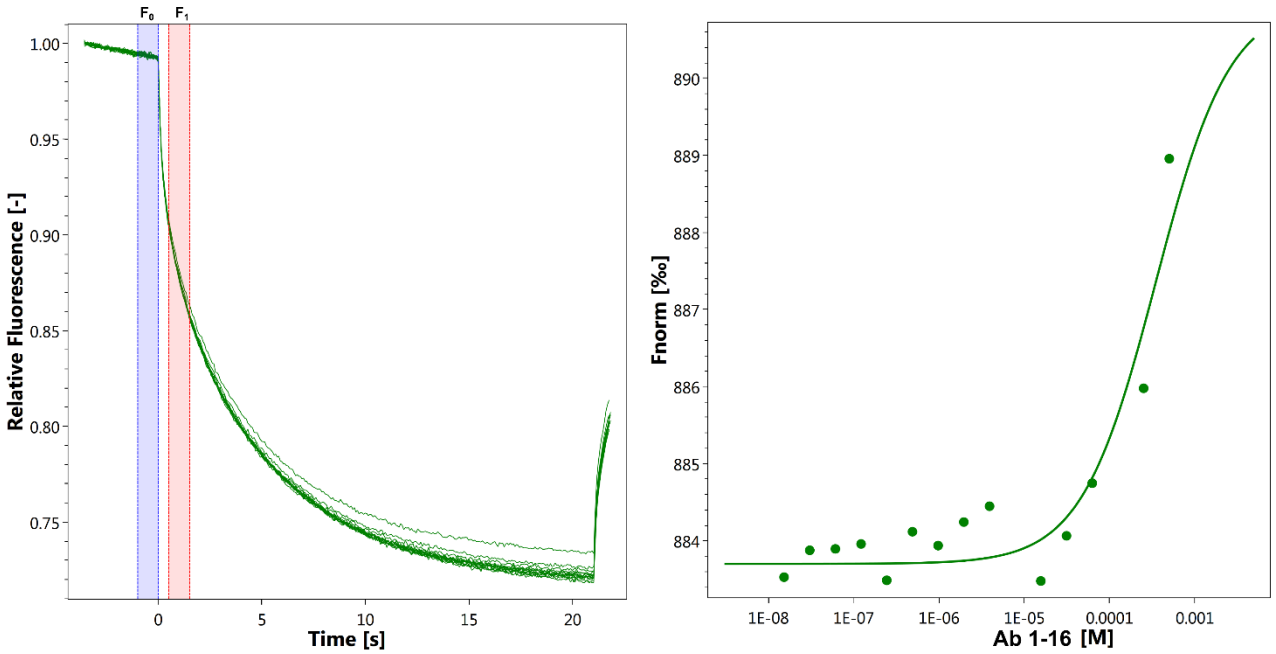

Figure S4. MST traces (left) of titrations of $A\beta_{1\text{-}16}$ against Ubiquitin; F0 and F1 correspond to the fluorescence of unbound state and bound state respectively. Plot of normalized fluorescence (right) obtained from Ubiquitin binding experiment versus $A\beta_{1\text{-}16}$ at different concentrations (from 1 mM to 20 nM).

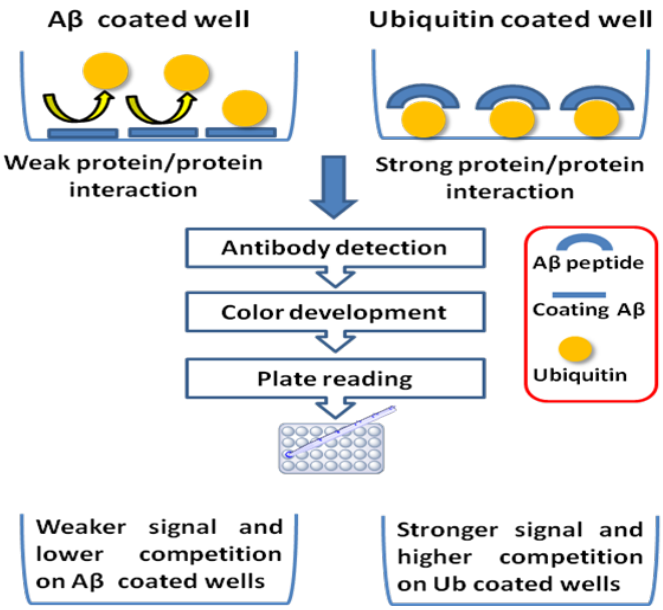

A

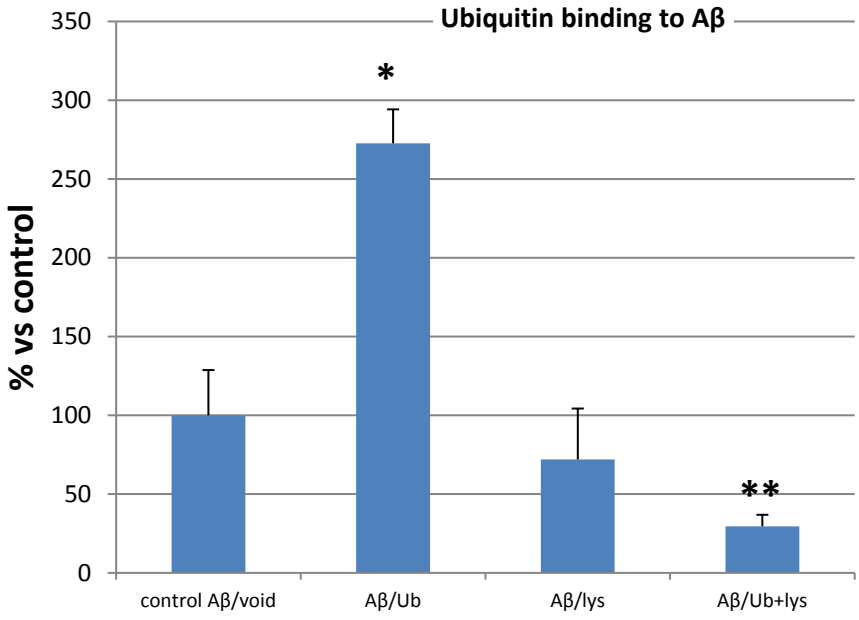

B

Figure S5. Flowchart of the two different ELISA assays. The Aβ peptides covalently linked on the surface in the microwells or in solution are shown as blue bars or semicircles, respectively. The graph schematically explains the two situations occurred in the ELISA experiments (panel A). Inhibition ELISA histograms for different Ub solutions (control Aβ/void: buffer; Aβ/Ub: 10 μM Ub in buffer solution; Aβ/Lys: whole cell lysates; Aβ/Ub+Lys: 10 μM Ub in cell lysate) added to Aβ-coated microwells (panel B). Significant differences from control values were indicated by ($p<0.05$) * (vs. control) ** (vs. lysate competition) (one-way ANOVA with Tukey's post hoc test). Normalized data are reported as percentages considering 100% the signal referring to the control Aβ/void.

Effect of Aβ40 on the proteasome activity

The inhibitory effect of Aβ40 on the proteasome activity was evaluated by using $A\beta_{16\text{-}28}$ as the substrate of proteasome 20S. Aβ40 is not appreciably degraded by proteasome within 30 min at 37°C (data not shown), whereas $A\beta_{16\text{-}28}$ drops down to 33% of the starting concentration within the same incubation time (Figure S4, 0:1 sample). Aβ40 clearly inhibits the proteasome mediated-clearance of $A\beta_{16\text{-}28}$ in a dose-dependent manner. When the larger [Aβ40]/[$A\beta_{16\text{-}28}$] molar ratio was used (3:1), the $A\beta_{16\text{-}28}$ is not significantly degraded. This experiment demonstrates the inhibitory effect of Aβ40 on the proteasome activity.

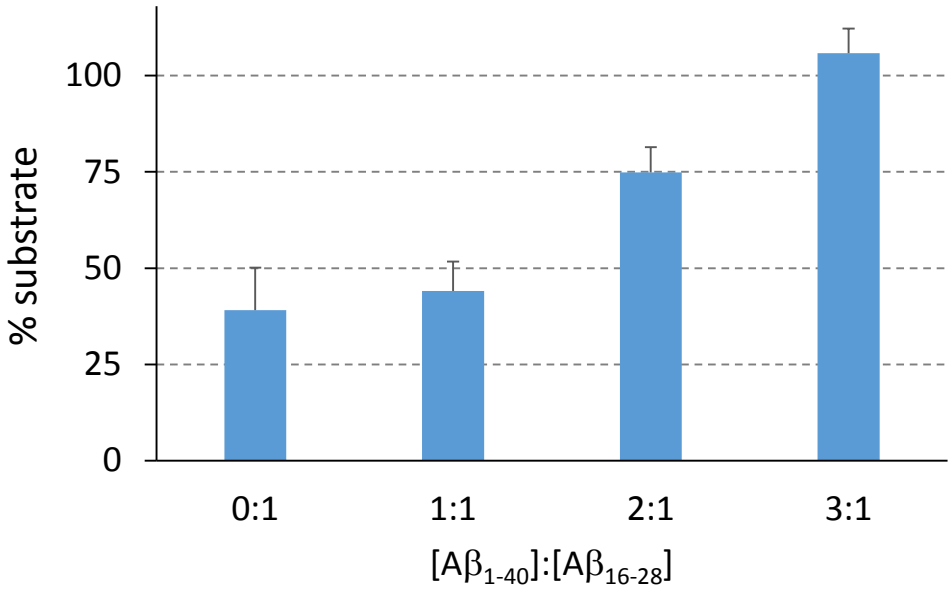

Figure S6. Dose dependent effect of the Aβ40 on the degradation of $A\beta_{16\text{-}28}$ (2 µM) catalysed by yeast proteasome 20S (2 nM) in Tris buffer 1 mM pH 8, at 37 °C for 30 min. Samples were analysed by means of nanoLC-HRMS. The peak area of the XIC related to the main m/z species of the substrate ($A\beta_{16\text{-}28}$) was referred to that one obtained before starting the reaction with proteasome. Such values (% substrate) were reported as a function of the Aβ40 concentration (expressed as a ratio between the Aβ40 and $A\beta_{16\text{-}28}$ concentrations).

Table S1. Intramolecular unique cross-links in Ub

10 µM Ub, 10 µM Aβ, 20 mM HEPES, pH 8,			
Entry	**Site (1)**	**Site (2)**	**Cα-Cα distance**
1	K27	K48	15.9
2	S20	K63	12.5
3	K48	K63	17.9
4	K48	S20	18.3
5	S65	K48	13.9
6	K63	K29	16.7
7	K63	K33	19.6
8	K48	K27	15.9
9	K29	K33	6.2
10	K27	S20	14.0
11	K48	K29	20.2
12	S20	K29	14.2
13	S65	K27	14.0

Table S2. Fitted kinetic parameters related to the aggregation of $A\beta_{1-40}$ in the presence of Ub, being the Ubi:Aβ ratio ranging from 0:1 ($A\beta_{1-40}$ alone) to 3:1. All results are expressed as mean ± standard deviation (SD).

Ubi:Aβ	**0:1**	**0.2:1**	**0.6:1**	**1:1**	**2:1**	**3:1**
F_{max}-F_0	13.0 ± 0.9	11.6 ± 0.8	6.5 ± 0.5	4.2 ± 0.4	2.0 ± 0.2	2.2 ± 0.3
t_{lag}	19.2 ± 0.9	23.9 ± 0.8	51.3 ± 0.9	44.4 ± 0.8	50.0 ± 0.9	63.7 ± 0.8

Table S2. List of the peptide fragments formed by the action of IDE on Aβ40 within 60 min at 37°C.

RT	**m/z (exp.)**	**z**	**m/z (theor.)**	**Δ (ppm)**	**Aβ peptide sequence**
13.18	849.8667	2	849.8669	-0.3	^{1}DAEFRHDSGYEVHH^{14}
16.12	772.0374	3	772.0387	-1.8	^{1}DAEFRHDSGYEVHHQKLVF^{19}
16.75	674.3915	1	674.3911	0.6	^{34}LMVGGVV^{40}
17.35	791.4163	2	791.4178	-1.9	^{15}QKLVFFAEDVGSNK^{28}
17.73	821.0607	3	821.0615	-1.0	^{1}DAEFRHDSGYEVHHQKLVFF^{20}
20.36	943.5054	2	943.5068	-1.4	^{21}AEDVGSNKGAIIGLMVGGVV^{40}
20.94	1017.0392	2	1017.0410	-1.8	^{20}FAEDVGSNKGAIIGLMVGGVV^{40}
21.11	1082.7954	4	1082.7949	0.4	^{1}DAEFRHDSGYEVHHQKLVFFAEDVGSNKGAIIGLMVGGVV^{40}
21.72	929.1727	3	929.1744	-1.8	^{14}HQKLVFFAEDVGSNKGAIIGLMVGGVV^{40}
22.26	883.4869	3	883.4881	-1.3	^{15}QKLVFFAEDVGSNKGAIIGLMVGGVV^{40}

Table S4 - Kinetic parameters obtained from the fitting of the SPR curves reported in Figure 1. Data were calculated using the "OneToOne" fitting model.

[Ub] (μM)	Bmax ([Signal (mdeg)])	ka (1/(M*s))	kd (1/s)	KD (μM)	Chi2 ([Signal (mdeg)]^2)
43	3	5,33E+01	1,90E-02	3,56E-04	0
86	3	5,33E+01	1,90E-02	3,56E-04	0
171	3	5,33E+01	1,90E-02	3,56E-04	0
343	3	5,33E+01	1,90E-02	3,56E-04	0
755	3	5,33E+01	1,90E-02	3,56E-04	0

References

1 V. Oliveri, F. Bellia and G. Vecchio, *ChemPlusChem*, **80**, 762–770.
2 M. Götze, J. Pettelkau, R. Fritzsche, C. H. Ihling, M. Schäfer and A. Sinz, *J. Am. Soc. Mass Spectrom.*, 2015, **26**, 83–97.
3 M. Palmieri, L. Russo, G. Malgieri, S. Esposito, I. Baglivo, A. Rivellino, B. Farina, I. de Paola, L. Zaccaro, D. Milardi, C. Isernia, P. V. Pedone and R. Fattorusso, *Journal of Inorganic Biochemistry*, 2014, **131**, 30–36.
4 B. Hess, C. Kutzner, D. van der Spoel and E. Lindahl, *J Chem Theory Comput*, 2008, **4**, 435–447.
5 V. Hornak, R. Abel, A. Okur, B. Strockbine, A. Roitberg and C. Simmerling, *Proteins*, 2006, **65**, 712–725.
6 W. L. Jorgensen, J. Chandrasekhar, J. D. Madura, R. W. Impey and M. L. Klein, *The Journal of Chemical Physics*, 1983, **79**, 926–935.
7 U. Essmann, L. Perera, M. L. Berkowitz, T. Darden, H. Lee and L. G. Pedersen, *The Journal of Chemical Physics*, 1995, **103**, 8577–8593.
8 S. Miyamoto and P. A. Kollman, *Journal of Computational Chemistry*, **13**, 952–962.
9 B. Hess, *J. Chem. Theory Comput.*, 2008, **4**, 116–122.
10 G. Bussi, D. Donadio and M. Parrinello, *The Journal of Chemical Physics*, 2007, **126**, 014101.
11 E. Rosta, N.-V. Buchete and G. Hummer, *J. Chem. Theory Comput.*, 2009, **5**, 1393–1399.
12 X. Daura, K. Gademann, B. Jaun, D. Seebach, W. F. van Gunsteren and A. E. Mark, *Angewandte Chemie International Edition*, **38**, 236–240.
13 G. Pandini, C. Satriano, A. Pietropaolo, F. Gianì, A. Travaglia, D. La Mendola, V. G. Nicoletti and E. Rizzarelli, *Front. Neurosci.*, , DOI:10.3389/fnins.2016.00569.
14 A. Travaglia, A. Pietropaolo, R. Di Martino, V. G. Nicoletti, D. La Mendola, P. Calissano and E. Rizzarelli, *ACS Chem. Neurosci.*, 2015, **6**, 1379–1392.
15 A. Travaglia, D. La Mendola, A. Magrì, A. Pietropaolo, V. G. Nicoletti, G. Grasso, G. Malgieri, R. Fattorusso, C. Isernia and E. Rizzarelli, *Inorg. Chem.*, 2013, **52**, 11075–11083.
16 I. Naletova, V. G. Nicoletti, D. Milardi, A. Pietropaolo and G. Grasso, *Metallomics*, 2016, **8**, 750–761.
17 G. Grasso, A. Magrì, F. Bellia, A. Pietropaolo, D. La Mendola and E. Rizzarelli, *Journal of Inorganic Biochemistry*, 2014, **130**, 92–102.
18 G. Grasso, V. Lanza, G. Malgieri, R. Fattorusso, A. Pietropaolo, E. Rizzarelli and D. Milardi, *Chemical Communications*, 2015, **51**, 15724–15727.
19 S. J. de Vries, M. van Dijk and A. M. J. J. Bonvin, *Nature Protocols*, 2010, **5**, 883–897.
20 G. Grasso, P. Mielczarek, M. Niedziolka and J. Silberring, *International Journal of Molecular Sciences*, 2014, **15**, 16787–16799.
21 G. Smaldone, L. Pirone, A. Capolupo, L. Vitagliano, M. C. Monti, S. Di Gaetano and E. Pedone, *International journal of biological macromolecules*, 2018, **115**, 469–475.